INFORMATION TO USERS

This manuscript has been reproduced from the microfilm master. UMI films the text directly from the original or copy submitted. Thus, some thesis and dissertation copies are in typewriter face, while others may be from any type of computer printer.

The quality of this reproduction is dependent upon the quality of the copy submitted. Broken or indistinct print, colored or poor quality illustrations and photographs, print bleedthrough, substandard margins, and improper alignment can adversely affect reproduction.

In the unlikely event that the author did not send UMI a complete manuscript and there are missing pages, these will be noted. Also, if unauthorized copyright material had to be removed, a note will indicate the deletion.

Oversize materials (e.g., maps, drawings, charts) are reproduced by sectioning the original, beginning at the upper left-hand corner and continuing from left to right in equal sections with small overlaps.

Photographs included in the original manuscript have been reproduced xerographically in this copy. Higher quality 6" x 9" black and white photographic prints are available for any photographs or illustrations appearing in this copy for an additional charge. Contact UMI directly to order.

Bell & Howell Information and Learning
300 North Zeeb Road, Ann Arbor, MI 48106-1346 USA
800-521-0600

DISSERTATION

SOLVATION DYNAMICS IN BINARY MIXTURES

Submitted by

Bradley M. Luther

Department of Chemistry

In partial fulfillment of the requirements

for the Degree of Doctor of Philosophy

Colorado State University

Fort Collins, Colorado

Spring 2000

COLORADO STATE UNIVERSITY

February 29, 2000

WE HEREBY RECOMMEND THAT THE DISSERTATION PREPARED UNDER OUR SUPERVISION BY BRADLEY M. LUTHER ENTITLED "SOLVATION DYNAMICS IN BINARY MIXTURES" BE ACCEPTED AS FULLFILING IN PART REQUIREMENTS FOR THE DEGREE OF DOCTOR OF PHILOSPHY.

Committee on Graduate Work

Adviser

Department Head

ABSTRACT OF DISSERTATION

SOLVATION DYNAMICS IN BINARY MIXTURES

The solvation dynamics of two binary mixtures are examined. Fluorescence upconversion spectroscopy is used to determine the solvation response function of the mixtures with ~ 250 femtosecond time resolution. The first mixture, dimethylsulfoxide(DMSO)-water, is a strongly interacting, hydrogen bonding mixture. It is shown that the DMSO-water mixtures display dramatic changes in their solvation response functions as compared to the pure solvents. These changes include both the inertial and diffusional response. The magnitude of the inertial response is seen to diminish when the solvents are mixed. The diffusional response maximizes at 33% DMSO, which corresponds to a 2DMSO-1water complex. Quasi-elastic neutron scattering is also included for water in the above mixtures. The second mixture is benzene-acetonitrile. This mixture is non-associating and involves both a nonpolar and strongly polar solvent. The solvation response function is seen to be sensitive to the mixing of the pure solvents, affecting both the inertial and diffusive portions of the solvation response function. The addition of acetonitrile to benzene is seen to increase the magnitude of the inertial response of the mixtures. At high benzene concentrations the diffusive portion shows a slow component that is attributed to translational diffusion of the acetonitrile.

Bradley M. Luther
Chemistry Department
Colorado State University
Fort Collins, CO 80523
Spring 2000

ACKNOWLEDGEMENTS

I would like to thank all of the people who I have worked with through the years (in no particular order). This includes the little people (Kyle and Joel). Ian, for entertaining me for a while. Micah, for the good times (moo) and the food poisoning. Ruth, for her encouragement. Dale, for providing the Vegas line. Actually, I forgot Debi, who taught me about flies in the laser. Liz, I couldn't have done it without your money. DJ Langdon, for being his cool self.

My dad always told me that I have to thank my mom for birthing me. So, thanks to my parents for the impossible to say.

To my beautiful wife, Corinno Luther, for being so patient, helping me, and putting up with me through this whole process. You are my inspiration. ILYSMBBL

Thanks to Nancy, for your guidance and being a really accessible and cool advisor. Thanks to Dr. Ladanyi, who I couldn't have done this without. I appreciate all of your help and comments.

I'd like to thank Dr. Skaf for preprints of his work and Dr. Herwig for his collaboration on the neutron scattering experiments.

Table of Contents

LIST OF TABLES

LIST OF FIGURES

Chapter One

Introduction to Solvation Dynamics

I. Solvation and Chemical Reactions

The most important step in any reaction is to bring together reactants in a way that will lead to the formation of products. Solvation is simply the process of dissolving a compound known as the solute into another compound known as the solvent. The importance of this simple process is ubiquitous in chemistry, as it is the most common way to bring reactants together. Without this important first step much of chemistry as we know it would not exist.

One of the most important ways in which solvents affect reactions is through their influence on the rates of reactions. Solvents can influence reaction rates in two ways. The first is due to the effects that solvents have on the equilibrium properties of the reaction. These include stabilization or destabilization of the products, reactants, and activated complexes involved in the reaction, and most importantly the free energy of activation of the reaction. The second way solvents influence reactions is due to non-equilibrium or dynamical effects. Both of these effects are seen in the Arrhenius expression for the rate of a reaction,

$$k = A \exp[-Ea / (RT)] \qquad 1.1$$

where k is the rate constant of the reaction, Ea is the activation energy, R is the gas constant, T is the temperature, and A is the dynamical frequency factor. The frequency factor gives a measure of the rate at which steps important for the formation of the activated complex occur. These steps can be as simple as the rate of collisions for a simple bi-molecular reaction or very complicated for more involved reactions.

In the case of electron transfer reactions, the pioneering work of Marcus sets the stage [1]. Since the early work of Marcus it has been well known that fluctuations of the solvatation energy can provide the necessary energy for a reaction to reach its activated state, and this was shown in the Marcus relationship for the activation energy for an electron transfer reaction,

$$Ea = [\,(\Delta G + \lambda_t)^2\,] / (4\lambda_s) \qquad 1.2$$

where λ_s is the solvent reorganizational energy, λ_t is the total reorganizational energy (solvent and reactants), and ΔG is the driving force of the reaction. From equation 1.2 it can be seen that the relative sizes of ΔG and λ_t can influence the rate at which reactions proceed. In general electron transfer reactions can be classified into three categories, normal, activationless, and inverted. Figure 1.1 shows the relationship between the product and reactant wells as a function of the reaction coordinate Q, which is a function of all the nuclear coordinates of the reactants, products and the solvent. It can be

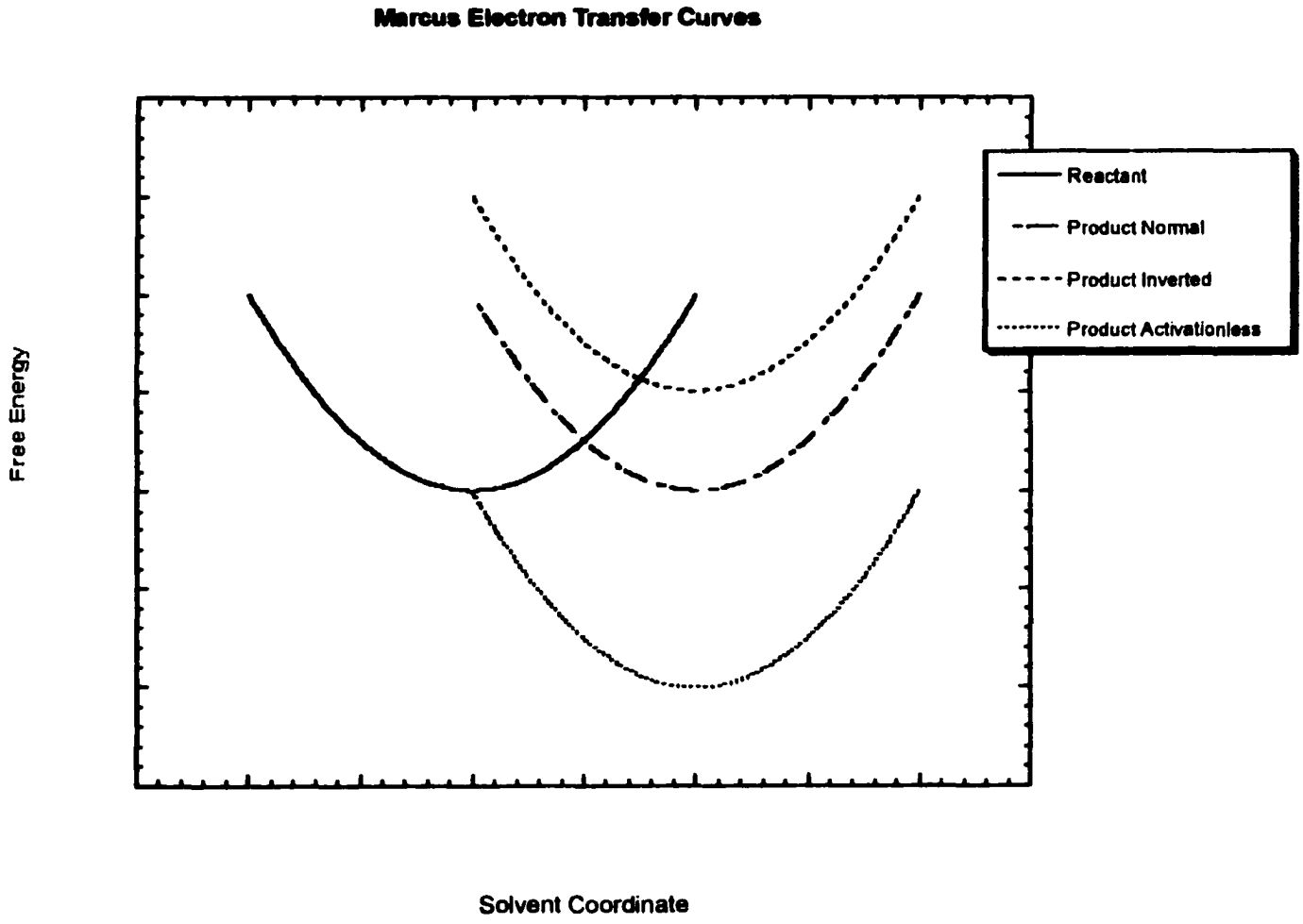

Figure 1.1
Free Energy curves as a function of the solvent coordinate for the three Marcus regimes. The activationless regime electron transfer rate is very sensitive to solvation dynamics.

seen here that in the case of the activationless regime there is strong coupling of the reactant and product wells. In this regime the frequency factor plays an important role in the reaction kinetics and can be the rate determing step in some cases. In these cases the Arrhenius equation can be written with the frequency factor replaced by a solvation time as given by Zusman [2],

$$k = 1/\tau_s \exp(-Ea/RT) \qquad 1.3$$

where τ_s is the solvation time constant. Here the solvation time is a dynamical factor that involves the time scales for the solvent motions. The relationship of this solvation time to the molecular motions of the solvent can in turn be analyzed by the study of polar solvation dynamics.

II Experimental Techniques and Analysis for Polar Solvation Dynamics

A. Introduction

In the study of polar solvation dynamics the following question arises – What happens when a solute molecule in equilibrium with the solvent molecules around it undergoes a change in its electronic configuration? There are a number of ways that this can happen, for instance the creation of a charge on a previously neutral solute, a change in the direction of a dipole on the solute, or a change in the size or order of the multipole. For simplicity we will consider this change to be the creation of a charge on a previously neutral solute in a dipolar solvent. Following the creation of the charge, the polar solvent

molecules, which were randomly oriented around the neutral solvent, will try to reorient to the new charge. This reorientation results in a lowering of the free energy of the solute. The time scales for the equilibration of the new charge can be followed by the Solvent Response Function (SRF),

$$C_F(t) = [F(t) - F(\infty)] / [F(0) - F(\infty)] \qquad 1.4$$

where F(t) is the free energy of solvation at time t. The above function is normalized to the total change in free energy the solute undergoes from the creation of the charge at time zero to the solvent equilibration at time infinity. Ignoring solute motions, the first question we must ask is what type of solvent motions produce the final polarized environment around the solute, and what are their time scales? The fastest relaxations will be the solvent's electronic degrees of freedom, which will be virtually instantaneous. These will be followed by nuclear distortions including vibrations and changes in the intermolecular bonds to the first layer of solvent molecules around the solute. These distortions occur on the femtosecond timescale. The last phase will involve the orientational motions of the solvent molecules, which will be the major contributor to the solvent relaxation. This will include the fast free streaming inertial motions, the more collective hindered librational motions, diffusional rotations, and finally diffusional translations. Orientational motions are the most important motions due to the fact that they will be effective in bringing the solvent dipoles into alignment with the solute's electric field. The inertial and librational motions will occur in the first several hundred femtoseconds, while the diffusional motions can span from one to hundreds of picoseconds depending on the nature of the solvent. To

see how different solvents respond and the timescales of their responses we need a way of probing the change in free energy of the solute with time. In the following sections I will describe the experimental techniques and analysis used.

B. Experimental Methods

With the increased interest in solvation dynamics several methods have been developed to probe the SRF [3]. Many of these techniques are fairly new and their relationship to solvation dynamics is continuing to be explored [4]. One of the most direct ways of following the SRF is to follow the time dependent fluorescence of a probe molecule in solution. This allows us to see the changes in the free energy of the probe as a change in frequency of the fluorescence. Figure 1.2 illustrates how this is done. At time zero an ultrafast laser pulse excites the probe from its ground to its excited state. This results in a step function change in the electronic configuration of the probe molecule during which the solvent is stationary. The solvent then begins to relax and stabilize this new charge distribution through reorientational motions resulting in a red shift in the fluorescence. The solvent response function can then be determined from the following relationship,

$$C_\upsilon(t) = [\upsilon(t) - \upsilon(\infty)] / [\upsilon(0) - \upsilon(\infty)] \qquad 1.5$$

where $\upsilon(t)$ is the average or first moment frequency of the fluorescence at time t.

To determine $\upsilon(t)$, it is necessary to know how the probe's fluorescence spectrum evolves in time. This is not a trivial undertaking given that the time resolution

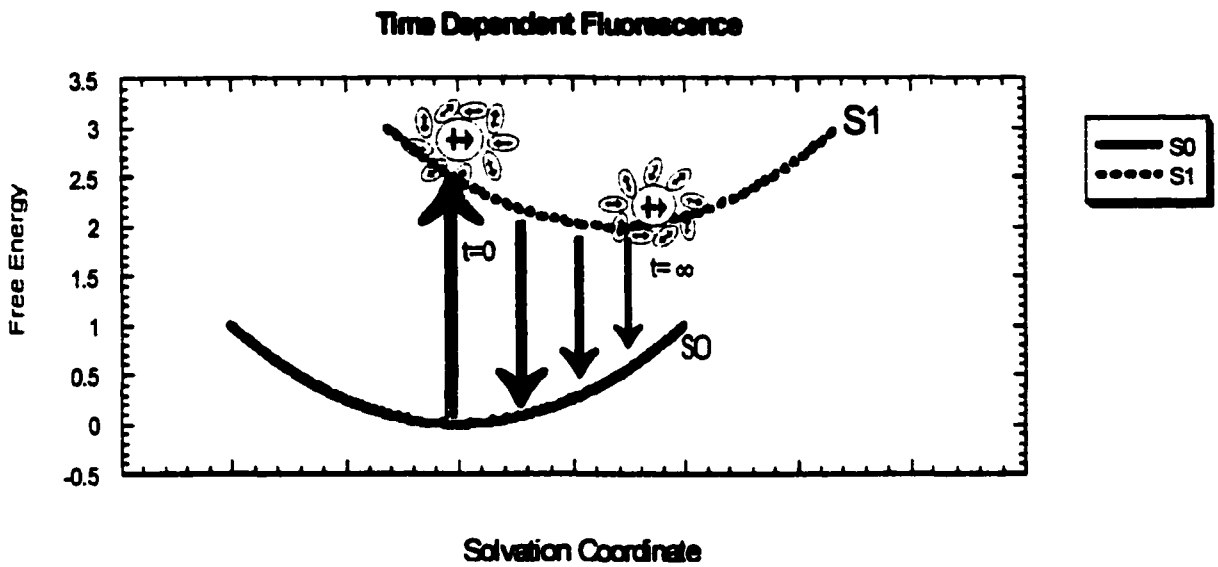

Figure 1.2
Time dependent Fluorescence begins with the excitation from S0 to S1 at time zero. The fluorescence then undergoes a time dependent red shift as the solvent relaxes to the S1 charge distribution.

desired is in the femtosecond range. The development of ultrafast lasers has therefore greatly increased our ability to follow these fast solvent relaxations. Two methods have been developed to follow the change in the fluorescence frequency in time. The first, spectral - reconstruction, involves calculating the time resolved spectrum from time resolved measurements of individual wavelengths, and will be discussed in length in the Data Analysis section II.E. The second, single wavelength technique involves determining a wavelength for the probe that is linearly related to the spectral density [5]. This method has several major disadvantages, the first being that the time resolution is limited to the instrument response function, the second being that the amount of the spectral shift which is missed is unknown, and the third being the assumption that a single polarization coordinate can describe the interactions of the solute with the solvent. We have therefore used the spectral reconstruction technique. At this point I will describe the equipment and data analysis used in the experiments presented in the following chapters before returning to polar solvation dynamics theory. These methods are typical of those used to provide experimental data for the development of current theories.

C. Fluorescence Upconversion Spectrometer

To determine the fluorescence transients we have used fluorescence upconversion spectroscopy. The basic premise behind using upconversion spectroscopy is to gate a long-time process such as fluorescence with a short gate pulse. For our experiments this involves using a femtosecond gate pulse to interrogate the time dependence of nanoseconds long fluorescence, figure 1.3. The femtosecond fluorescence upconversion spectrometer is shown in figure 1.4. This spectrometer is similar to the one

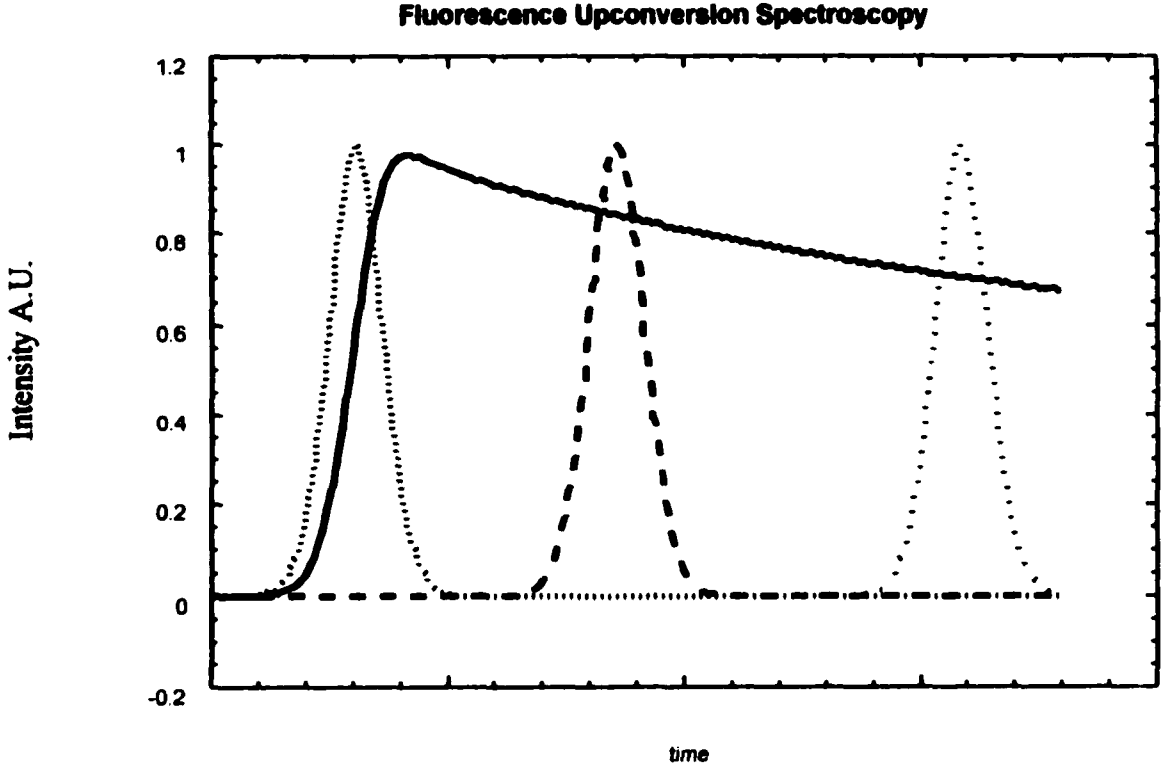

Figure 1.3
Time dependent fluorescence (solid curve) is probed by a probe pulse (dashed curves)at varying time delays

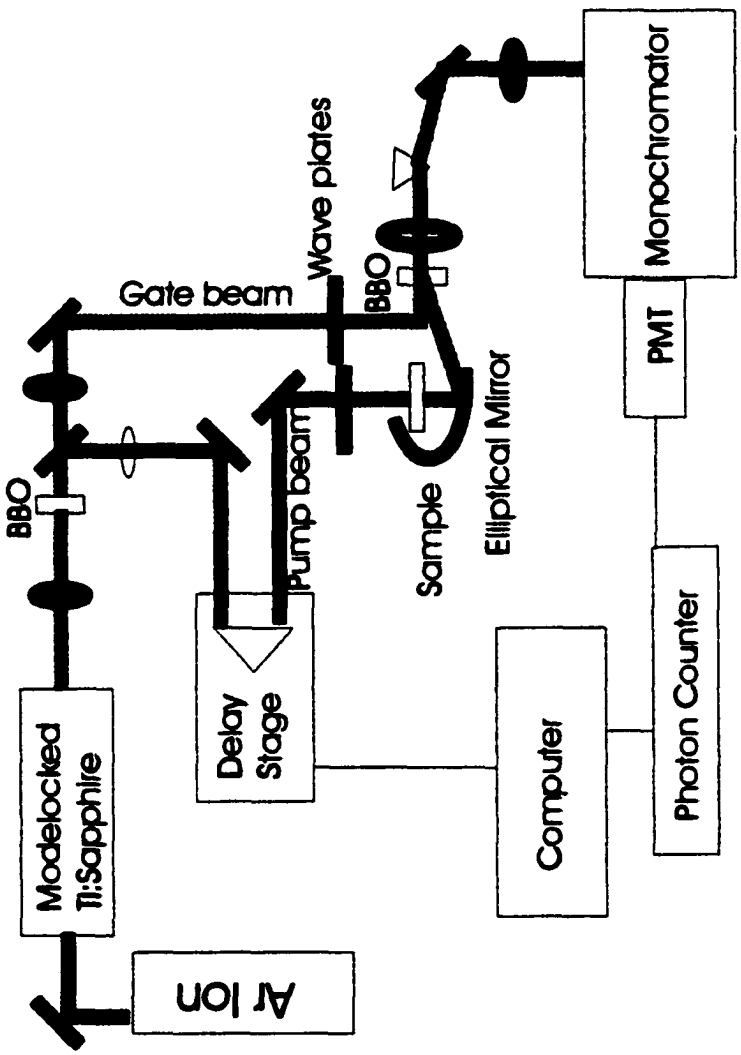

Figure 1.4
Fluorescence Upconversion Experimental Setup.

developed by Fleming and coworkers [6]. A Clark NJA-3 kit oscillator is pumped by all lines of a Coherent Innova 310 Ar^+ CW laser at 6.5W. The oscillator is passively modelocked producing 80 fs, 5 nJ pulses with a repetition rate of 100 MHz. The pulses were centered between 804 to 810 nm for the experiments reported here. The output from the oscillator is collimated and then focused onto a 1 mm barium borate crystal (BBO, type1, Inrad). The BBO crystal produces second harmonic light (~ 405 nm) with approximately ten percent conversion efficiency which is separated from the fundamental light using a dielectric beamsplitter (CVI). The blue beam is then sent through an optical delay stage and half wave plate (Meadowlark Optics) before being focused on the sample with a ten-centimeter lens. The sample is circulated using a peristaltic pump (Masterflex, Model 7553-70) through a 1-mm path length quartz flow cell. Samples were cooled in a room temperature water bath to reduce heating incurred from sample circulation. The fluorescence is collected at 180 degrees and focused onto an ellipsoidal reflector (Melles Griot) into a 0.5 mm nonlinear BBO crystal (type 1, Casix). The fundamental residual beam is then passed through a half wave plate (Meadowlark Optics) and focused onto the nonlinear crystal at small angle. The fundamental beam acts as a temporal gate allowing high time resolution of the long (ns) fluorescence. The polarization of the pump and probe beams were set to 54.7° (magic angle) to eliminate the effects of the rotational relaxation of the probe molecule on the fluorescence transients. The upconverted light was then collimated and residual fluorescence and pump beams removed through the use of spatial filtering and dispersion through a prism before being focused into the monochrometer (HR320, ISA) equipped with a 2400 line/mm holographic grating blazed at 400 nm. The bandwidth of the upconverted fluorescence is on the order of 8nm. Instrument response

functions for the experiments reported here ranged from 200 to 250 fs and fit well to gaussian profiles. The upconverted fluorescence was detected by a photomultiplier tube (R1527P, Hamamatsu). It was found that cooling of the PMT had little effect on the signal to noise so most experiments were run uncooled. The signal was amplified using a single video amplifier (CLC100, Comlinear Corporation) and then sent to a single photon counter (SR400, Stanford Research Systems). Data collection and delay stage movement were controlled by a personal computer using Labview software (National Instruments). Runs were averaged for one second at each step. Runs were averaged until acceptable signal to noise was generated. The number of runs depended on the sample concentration and wavelength of interest and varied from two to twenty runs.

D. Time Zero Analysis

Knowledge of $\upsilon(0)$ is critical for calculating the correct SRF from equation 1.5. Early experiments lacked sufficient time resolution to resolve the important inertial components of the SRF, and therefore gave results that were to some extent misleading. The discovery of inertial components by simulations and later experimental verification showed that up to 70% of the relaxation can happen during the ultrafast inertial relaxation [7,8,9]. It is therefore necessary to have an idea of how much of the solvent response has been missed. This is important in the present work due to the time resolution of our apparatus, which misses the first 250 femtoseconds or so. In acetonitrile especially this can result in missing a large part of the relaxation. It was therefore necessary to approximate the time zero spectra using the method of Fee and Maroncelli [10]. The basic principle is that different probe molecules experience different local solvation enviroments. If it is

assumed that each probe has the same absorption lineshape function g(υ), which is shifted by its particular interaction with the solvent δ, and that δ has a distribution given by p(δ), then the polar absorption spectrum is given by

$$A_p(\nu) \propto \nu \int g(\nu-\delta)p(\delta)\, d\delta \qquad 1.6$$

where the term in the integral is the convolution of g(ν-δ) with p(δ). The polar fluorescence can similarly be described by the following expression

$$F_p(t=0,\nu,\nu_{ex}) \propto (\nu^3\nu_{ex}) \int g(\nu_{ex}-\delta)\, p(\delta)\, f(\nu-\delta)\, k_{rad}(\delta)\, d\delta \qquad 1.7$$

Where ν_{ex} is the excitation frequency and the term in the integral is the convolution of the solvent distribution transferred to the excited state $g(\nu_{ex}-\delta)$ p(δ) with the fluorescence intensity function $f(\nu-\delta)$ $k_{rad}(\delta)$. Here $f(\nu-\delta)$ is the fluorescence lineshape in the same fashion as $g(\nu-\delta)$ above. Maroncelli *et al.* showed that the radiative rate constant $k_{rad}(\delta)$ has negligible effects on time zero analysis and this term has been ignored in our analysis [11].

It is necessary to determine three functions to determine the time zero fluorescence, $f(\nu-\delta)$, $g(\nu-\delta)$, and p(δ). Two of the functions can approximated from the nonpolar absorption spectra $A_{np}(\upsilon)$ and the nonpolar fluorescence spectra $F_{np}(\upsilon)$

$$g(\upsilon) \propto \upsilon^{-1} A_{np}(\upsilon) \qquad 1.8$$

$$f(\upsilon) \propto \upsilon^{-3} F_{np}(\upsilon) \qquad 1.9$$

where the υ^x terms in the above equations are necessary to make $g(\upsilon)$ and $f(\upsilon)$ directly proportional to the Einstein B coefficients. The use of the above functions assumes that the nonpolar spectra are purely homogeneously broadened and that this broadening is approximately the same in all solvents. While this may not be completely true it should be a valid approximation when calculating time zero spectra of molecules where polar interactions dominate. The last function $p(\delta)$ is approximated as a gaussian by the following,

$$p(\delta) = (2\pi\sigma^2)^{-1/2} \exp[-(\delta-\delta_0)^2/2\sigma^2] \qquad 1.10$$

where δ_0 is the average shift induced by the solvent and σ is the variance of the distribution. The full width at half maximum is related to σ by the following,

$$\text{FWHM} = (8\ln 2)^{-1/2}\sigma. \qquad 1.11$$

The next step is to determine $p(\delta)$. This is done by fitting the polar absorption spectrum to the convolution of $g(\delta)$ and $p(\delta)$ while varying the values of δ_0 and σ to give the best fit. This convolution is done in discrete time using the following,

$$A_p(\upsilon) = \upsilon \sum_{\delta=-\infty}^{+\infty} p(\delta)g(\upsilon - \delta) \qquad 1.12$$

Where the summation over δ goes from $-\infty$ to $+\infty$. The convolution summation has a simple graphical interpretation. $p(\delta)$ and the "flipped and shifted" $g(\nu-\delta)$ are plotted on the δ axis, where ν is fixed. Second, the two arrays are multiplied to obtain a plot of the summand sequence indexed by δ. Summing the values of this sequence with respect to δ yields $A_p(\nu)$, the polar absorption spectra. After determining the values of δ_0 and σ which give the best fit for the convolution of $g(\nu-\delta)p(\delta)$ to the polar absorption spectrum, the $g(\nu_{ex}-\delta)$ array is created by flipping $g(\nu)$ and shifting the ν axis by ν_{ex}. This array is then multiplied by the $p(\delta)$ array to give $g(\nu_{ex}-\delta)p(\delta)$. No convolution is implied in the notation of $g(\nu_{ex}-\delta)p(\delta)$. The discrete time convolution of $g(\nu_{ex}-\delta)p(\delta)$ with $f(\nu-\delta)$ can then be done to give the time zero fluorescence.

E. Data Analysis: Spectral reconstruction

To obtain sufficient time resolution, runs were preformed using three different step sizes. Short runs were done with 17 fs steps for 2.5 to 3 ps. These short runs were analyzed using a global analysis to deconvolve the instrument response function (IRF) from the transients. IRF's were determined by upconverting the residual ~ 405nm pump with the fundamental gate pulse and fitting it to a gaussian line shape. Short runs were fit to three or four exponentials with the last one set to the probe's fluorescence lifetime. The medium runs were done in 200 fs time steps for 25 to 30 ps, and long runs done in 2.5 ps steps for 500 ps. The medium and long runs were fitted in Kaleidagraph ignoring the initial decay. Two to three exponents were required to fit the medium and long runs and offsets were also used. Examples of short, medium, and long runs with fits are given in figure 1.5.

In order to create a single transient for a particular wavelength the last point of the longest time run is normalized to the value of the static fluorescence at that wavelength. The next shortest run is then normalized to the long run and the process repeated until all runs are normalized. When this has been completed for each wavelength it is possible to transform the transients and generate a time-resolved spectra as shown in figure 1.6. The longest time spectrum will be equivalent to the static fluorescence spectrum.

Individual fluorescence spectra are fit to lognormal functions of the type,

$$F = h\left[\exp\left\{-.6931472\left[\ln\left(1+(2\gamma\{\upsilon-\upsilon_0\}/\omega)\right)/\gamma\right]^2\right\}\right] \qquad 1.13$$

where h is the height, γ is the skew, υ_0 is the frequency maximum, and ω is the width parameter. This allows the first moment (average) frequency to be determined easily using the following,

$$\upsilon_{fm} = \upsilon - (\omega/2\gamma)\left[\exp\left\{3(\gamma^2)/[4(0.693)]\right\} - 1\right] \qquad 1.14$$

$$\Gamma = \omega[\sinh(\gamma)/\gamma] \qquad 1.15$$

where υ_{fm} is the first moment frequency, and Γ is the FWHM . The first moment frequencies give a more reliable measure of the changes in the $\upsilon(t)$ and have been used in all the results given in the following chapters.

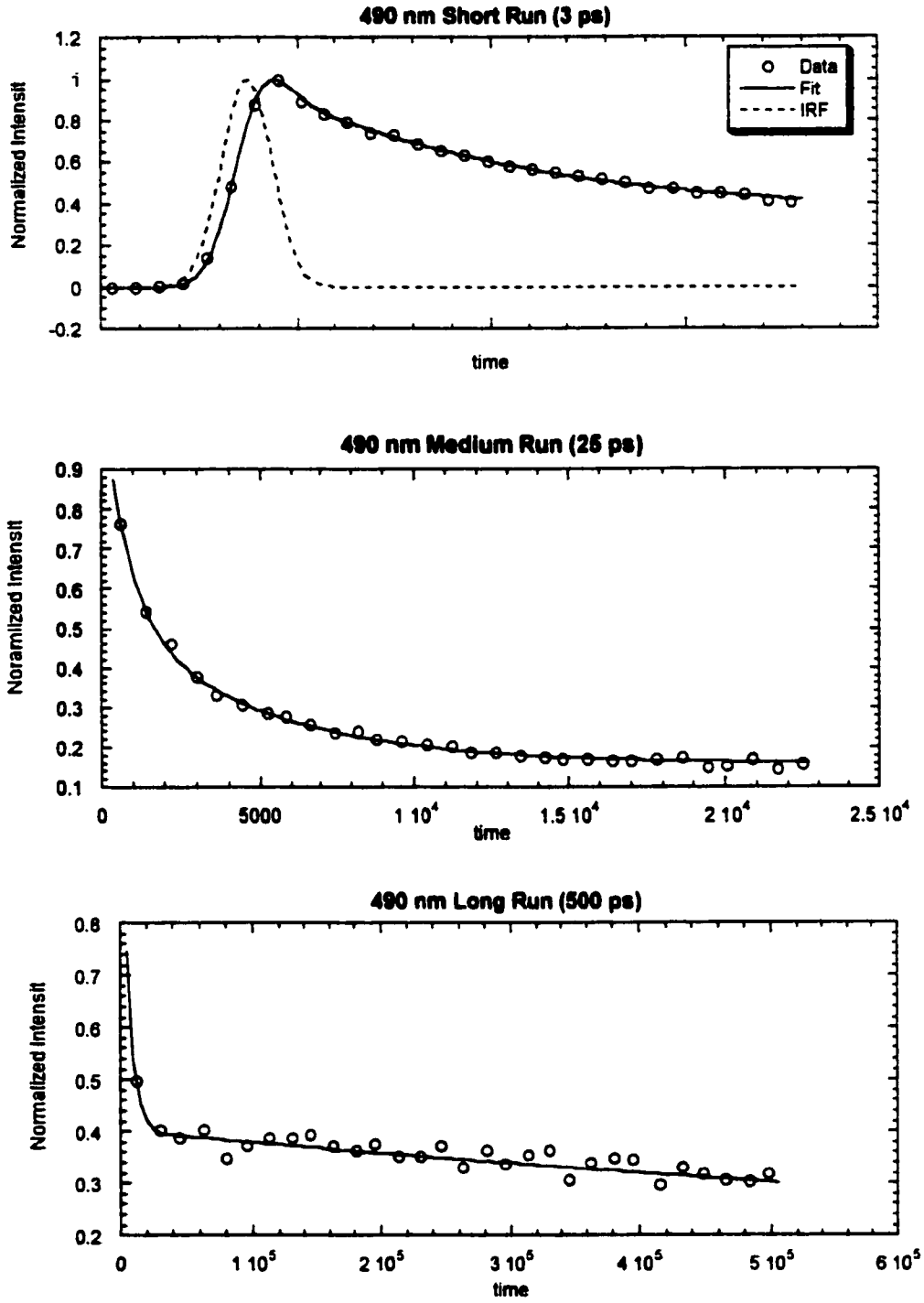

Figure 1.5
Short, medium and long runs for $X_D = 0.75$ DMSO-water mixture. Data are shown as circles, fits as solid lines, and the instrument response function is shown for the short run. Ticks for the 3 ps run are 17fs.

17

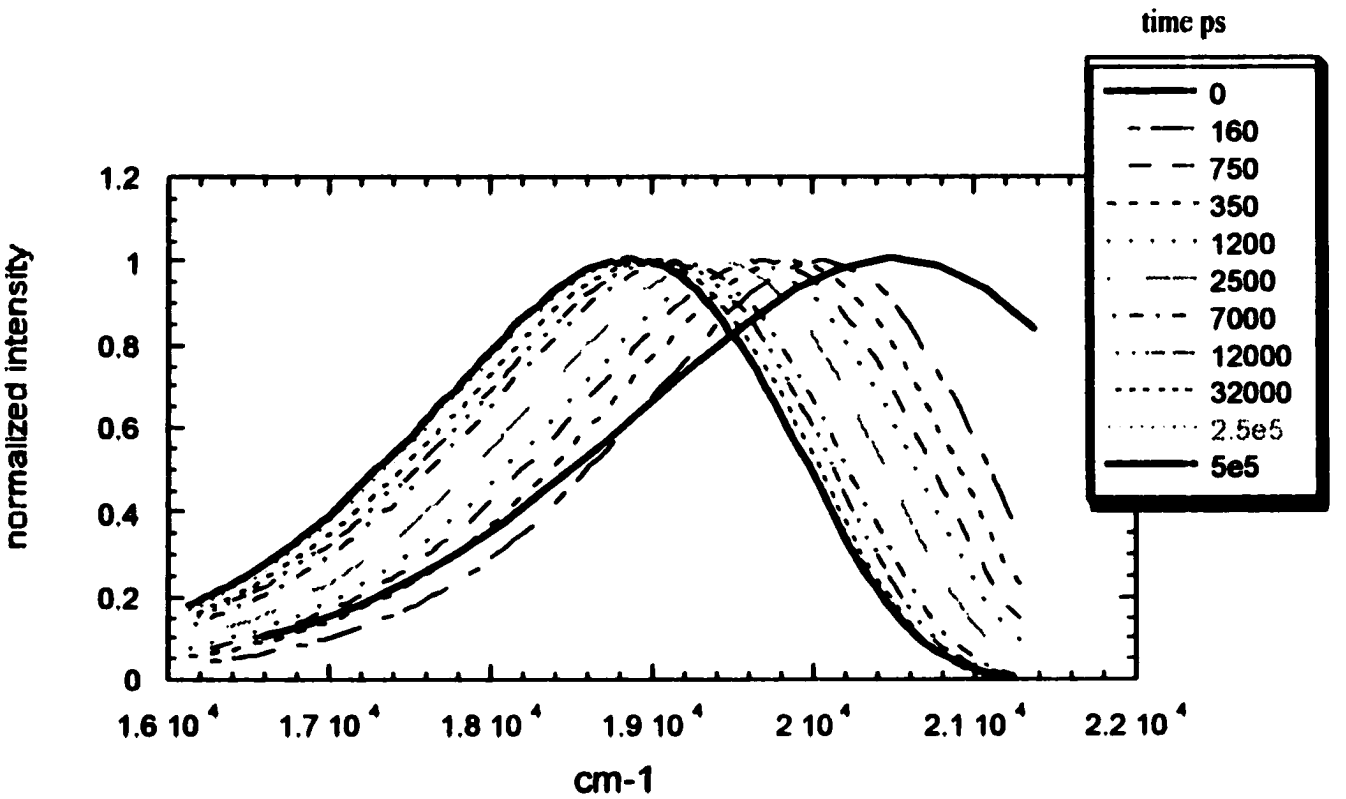

Figure 1.6
Time resolved spectra for X =0.75 DMSO-water mixture generated using fluorescence decays such as in figure 1.4 Time zero curve is approximated using the method described in text. Times are given in ps..

After the fm frequencies $\nu(t)$ have been determined for each time the SRF can be determined using equation 1.5. Time zero analysis gives $\nu(0)$ and $\nu(\infty)$ is determined by the steady-state fluorescence.

F. Choice of Fluorescence Probe

At this point it is important to note the relationship and possible problems of equating $C_F(t)$ and $C_\nu(t)$. There are two major factors that can cause $C_\nu(t)$ to differ from $C_F(t)$. The first is that $C_\nu(t)$ is sensitive to vibrational relaxation of the probe molecule. For $C_\nu(t)$ to accurately reflect $C_F(t)$ the amount of vibrational relaxation must be small compared to the polar solvent relaxation. Change in the electronic structure of the probe with relaxation can also cause $C_\nu(t)$ to differ from $C_F(t)$. The probe Coumarin 153 (C153, C540A) is a well-known and studied solvation dynamics probe [9]. It has the advantage of being a rigid dye molecule with a large change in dipole moment upon optical excitation (~6D in the ground state to ~15D in the excited state). Experiments in nonpolar solvents have shown that the degree of vibrational relaxation is small [9]. The atomic charge distributions have also been studied in both the ground and excited state and show that the charge difference between the ground and excited state is similar to a dipole change of approximately 8D [12]. C153 has also been shown to have relatively small specific interactions with most solvents. These factors make C153 an ideal probe for solvation dynamics. Although $C_\nu(t)$ and $C_F(t)$ will not be identical differences should be small allowing direct comparisons to be made.

III Theoretical Models: Methods, Results, and Predictions

A. Simple Continuum Model Predictions

Based on the description given in section II. A. above one would expect solvation dynamics to involve a very complicated response strongly dependent on the molecular nature of the solvent-solute and solvent–solvent interactions. The first level of theoretical approximation ignores this molecularity. The solvent is described as a structureless continuum, which is completely described by its frequency dependent dielectric response function, $\varepsilon(\omega)$. The dielectric response function describes how the polarization of the solvent $\mathbf{P}$ (C/m^2) responds to an electric field $\mathbf{E}$. In the case of a static electric field a simple equation relates the polarization caused by the electric field [13]

$$[\varepsilon - 1]\,\mathbf{E} = (4\pi/\varepsilon_0)\,\mathbf{P} \qquad 1.16$$

where ε is the static dielectric constant and ε_0 is the vacuum permittivity. If the electric field is varied at a frequency ω then the relationship becomes

$$[\varepsilon(\omega) - 1]\,\mathbf{E}(\omega) = (4\pi/\varepsilon_0)\,\mathbf{P}(\omega) \qquad 1.17$$

Where the static field and polarization have been replaced with their frequency dependent versions. For frequencies less than a few megahertz $\varepsilon(\omega) \sim \varepsilon$ as the molecular dipoles are capable of keeping up (reorienting) with the changing electric field. As the frequency increases into the gigahertz range, $\varepsilon(\omega)$ begins to decrease as the molecular motions to

begin to lag behind the rapidly changing field. Eventually only electronic motions are capable of following the electric field and the optical refractive index, n^2 is reached.

The frequency dependent dielectric response therefore measures the ability of the solvent to react to a changing electric field and should be very useful in determining the rate of solvent relaxation. There are several approximate functional forms for $\varepsilon(\omega)$. The Debye and Cole–Davidson are given below [13,14]:

Debye $$\varepsilon(\omega) = \varepsilon(\infty) + [(\varepsilon - \varepsilon(\infty)) / (1 + i\omega\tau_D)] \quad 1.18$$

Cole – Davidson $$\varepsilon(\omega) = \varepsilon(\infty) + [(\varepsilon - \varepsilon(\infty)) / (1 + i\omega\tau_0)^{\beta}] \quad 1.19$$

It is seen from the above equations that $\varepsilon(\omega)$ can be approximated as a function of $\varepsilon(\infty)$, ε, and the appropriate dielectric relaxation time τ_D or τ_0. The Cole-Davidson function includes an extra parameter β that has the effect of scaling the relaxation times. It is important to note that the forms given above are typically used only into the gigahertz range.

If we use the simplest Debye form for $\varepsilon(\omega)$ then the SRF can be given as

$$C_F(t) = \exp(-t / \tau_L) \quad 1.20$$

$$\tau_{L\,ION} = [\varepsilon(\infty) / \varepsilon]\tau_D \quad 1.21$$

$$\tau_{L\,DIPOLE} = [(2\varepsilon(\infty) + n^2) / (2\varepsilon + n^2)]\tau_D \quad 1.22$$

where τ_L is the longitudinal relaxation time, n is the optical refractive index, often assumed to be 1. Since $[\varepsilon(\infty) / \varepsilon]$ is less than one, τ_L is faster than the Debye dielectric relaxation time τ_D. van der Zwan and Hynes derive the above equations in detail in [15]. In short it

involves determining the time dependent reaction field acting on the excited state dipole. The reaction field is the field on the solute due to the solute induced solvent polarization. For the equilibrium continuum case the reaction field on a dipole in an Onsager cavity is

$$R = (2\mu/\varepsilon_0 a^3)[(\varepsilon - 1)/(2\varepsilon - 1)] \qquad 1.23$$

a simple function of the solute radius a, solute dipole moment μ, and solvent dielectric constant ε. In this equation ε_0 is the permittivity of free space. In the non-equilibrium case the frequency dependent reaction field is shown to be a function of $\varepsilon(\omega)$. Solving for $R(\omega)$ using the Debye formalism for $\varepsilon(\omega)$ then leads to equation 1.20 with R(t) being the transform of $R(\omega)$. Although the SCM is very basic it serves as a simple standard for comparison to experimental results. As can be seen from the form of equation 1.20 the SCM predicts a single relaxation time in the case of a single Debye solvent. It should be noted that more complex SRF's can be obtained when multiple Debye or Cole-Davidson functional forms of $\varepsilon(\omega)$ is used.

At this point it is worthwhile comparing early experimental results with the SCM. Early experiments found typical average relaxation times given by

$$\langle\tau\rangle = \int C_v(t)\, dT = \sum_i \alpha_i\tau_i \qquad 1.24$$

where the integral goes from zero to infinity, and the sum is over the amplitudes α_i and time constants τ_i from multi-exponential fits of $C_v(t)$, ranging from one to hundreds of

picoseconds. Maroncelli points out that for solvents ranging in static dielectric constants from 5 to 300, 67% of the 21 solvents studied have $\langle\tau\rangle$'s within a factor of two of the predicted continuum theory values [16]. This is certainly a good sign that use of $\varepsilon(\omega)$ is a valid step in understanding SRF's. Although these results are inspiring they are far from perfect. Experimental results for $\langle\tau\rangle$ were found to be consistently slower than $\langle\tau\rangle$'s calculated from the SCM. The experimental results were also non-exponential compared with the SCM's single exponential form.

The hunt was then on to try to explain the source of the differences between experiment and SCM. Onsager brought the first suspect forward [17]. Onsager pointed out that the continuum results for the SRF were only valid for the $\varepsilon(\omega,k=0)$ limit, where $\varepsilon(\omega,k)$ is the wave vector dependent dielectric response function. In the long range, k=0 limit, the solute probes large distances compared to the solvent intermolecular distances. This allows small motions of the individual molecules to give fast relaxations on the time scale of τ_L. In the short range, high k limit, near the solute, the solvent molecules are relaxing at a rate that is closer to the single molecule reorientation rate τ_D. Therefore the predictions of the SCM are expected to be too fast based on its neglect of the k dependence of $\varepsilon(\omega)$, as pointed out in several theoretical investigations that resulted [18,19,20]. These results lead to a wide range of attempts to try to mend the SCM. Efforts were made to account for $\varepsilon(\omega, k)$ by the use of shells surrounding the solute with different dielectric response functions [21], or functions with smoothly varying dielectric response functions [21]. Theories were also developed which allowed more sophisticated versions of $\varepsilon(\omega)$ to be used [14,65]. These models address the fact that dielectric relaxation is often not Debye-like. These changes were capable of producing non-exponential decays, which gave slower relaxations than the

SCM. Unfortunately they were fairly obscure in their predictive capabilities due to the lack of "real" or molecular parameters. Of the models above perhaps Castner's *et al.* [14] or Fried *et al.* [65] are most intriguing in its simple replacement of the Debye $\varepsilon(\omega)$ with the Davidson-Cole $\varepsilon(\omega)$, which is inherently better at reproducing multiple, scaled relaxations. At this point it was necessary to depart from continuum theory and explore models which deal with the molecularity of the solvent in a more direct way.

B. Molecular models

One of the simplest models to incorporate molecularity into the solvent was the dynamical Mean Spherical Approximation (dMSA) developed by Wolynes [22]. Its development is in the same spirit as the SCM. The Mean Spherical Approximation (MSA) approach was previously developed as a way of determining the solvation energy of an ion [23]. The molecularity of the MSA model comes from using dipolar hard spheres for the solvent molecules as well as using a charged hard sphere solute. The radii of the spheres are chosen to match the molecular radii of the real solvent and solute molecules. MSA results give the solvation energy of an ion with unit charge as

$$R(\alpha) = [1 / (2\{ r_c + \Delta(\alpha)\})]((1 - [1 / \varepsilon(\alpha)]) \qquad 1.25$$

where r_c is the solute radius, $\Delta(\alpha)$ is a correction factor, and $\varepsilon(\alpha)$ is the dielectric constant. In the above equation, α is a function of the solvent's density, dielectric constant, and radius. The effective radius, $r_c + \Delta(\alpha)$, includes the correction factor, which is a function of

the solvent radius and dielectric constant. The correction factor takes into account the incomplete screening of the ion's interaction with the nearest layer of solvent molecules. It should be noted that this is the MSA equivalent of the continuum reaction field described above. Wolynes, in a manner analogous to the development of the simple continuum model, replaced the static dielectric constant with the frequency dependent dielectric response $\varepsilon(\omega)$ to obtain the frequency dependent reaction field $R(\omega)$. The transform of $R(\omega)$ to $R(t)$ then gives the dMSA SRF. Rips *et al.* [25] extended this work to dipolar solutes. Maroncelli and Fleming [24] analyzed the predictions of dMSA using the formalism of Rips *et al.* [25], and compared the results to their experimental data. This involves calculating the dMSA SRF

$$S(t) = [E(t) - E(\infty)] / [E(0) - E(\infty)] \qquad 1.26$$

which was determined via its Laplace transform

$$S(p) = [\chi(p) - \chi(0)] / p[\chi(\infty) - \chi(0)] \qquad 1.27$$

$$\chi(p) = [\, 1 - 1/\varepsilon(p) \,] / 2R [\, 1 + \Delta(p) \,] \qquad 1.28$$

$$\Delta(p) = \{3r/R) [\, 108^{1/3} \varepsilon(p)^{1/6} - 2 \,]^{-1} \qquad 1.29$$

The complex admittance $\chi(p)$ is a function of the dielectric response $\varepsilon(p)$ and the correction term $\Delta(p)$, where R is the solute radius and r is the solvent radius. It can be seen from equation 1.29 that the correction factor is frequency dependent and now reflects dynamic screening effects associated with the polarization of the solvent.

Several interesting results were found for the dMSA SRF's. First unlike SCM, dMSA SRF's are highly non-exponential even though single Debye dielectric functions $\varepsilon(\omega)$ are used. A distribution of relaxation times prevail ranging from τ_D to τ_L giving average SRF's which are longer in general than continuum predictions. The dMSA SRF's are also found to be sensitive to the solute to solvent size ratio, with small ratios giving slower relaxation and large ratios giving relaxations closer to τ_L. It is clear that at the relatively low level in which dMSA incorporates molecularity, it reproduces some of the essential features of experimental SRF's, such as multiple relaxation times, and SRF's bounded by τ_L and τ_D. Qualitative agreement with the Onsager picture of k dependent dielectric relaxation is also found. At the same time, it is similar to continuum theory in that it is depends on dielectric data and is not based on any first principle kinetic theory.

Calef and Wolynes pioneered another approach that predates dMSA [26]. In this work Calef and Wolynes developed the Smoluchowski-Vlasov theory of charge solvation. The Smoluchowski-Vlasov equation relates the diffusive aspects of the solvent relaxation to the time dependent relaxation $(\delta\rho(r,\Omega)/\delta t)$ of a deviation of the charge distribution from its equilibrium value: $\rho(r,\Omega) - \rho_{eq}(r,\Omega)$. The non-equilibrium polarization can then be written as a function of $\delta\rho(r,\Omega)$, and the solvation energy determined. The time dependent charge distribution can be expressed as a function of the translational and rotational diffusion coefficients. This requires needs the ion-dipole, and dipole-dipole correlation functions, which were approximated by Calef and Wolynes. The dipole-dipole coorelation function was approximated using MSA. Results presented by Calef and Wolynes ignored translational diffusion, and gave SRF's that were non-exponential and relaxation times that were in-between τ_D and τ_L. Chandra and Bagchi took Calef and Wolynes development

further by including translational diffusion [27]. Inclusion of translational solvent modes increases the rate of relaxation by providing new relaxation channels, especially at high k. Raineri *et al.* showed that several similar developments along these lines could be represented by

$$R(\omega) = (Q^2/i\pi\omega) \int dk \{\varepsilon_L(k,\omega)^{-1} - \varepsilon(\infty)^{-1}\}\{\sin(ka)/(ka)\}^2 \qquad 1.30$$

Where $R(\omega)$ is the frequency dependent free energy response of a harmonically varying charge Q in a spherical solute of radius a [28]. As usual, R(t) can be obtained by transform of $R(\omega)$. The second term in the integral determines the length over which the solute senses the solvent response and is the only contribution made by the solute. The first term, $\varepsilon_L(k,\omega)^{-1}$, contains all the dynamical information about the solvent. This term is a function of the rotational and translational diffusion constants of the pure solvent (related to $\rho(r,\Omega)$), and is not experimentally accessible due to its k dependence. Several approximations were developed [29,30], and results based on MSA solvent correlation functions are reviewed by Maroncelli [16].

The results based on the above models explicitly show the effects of the solute to solvent size ratio and k dependence of the solvent response function [16]. The solute-solvent size ratio affects the amplitudes of the k dependent relaxations. When the solute is large compared to the solvent only low k relaxations have appreciable amplitude. In the limit of an infinitely large solute the continuum results are obtained. For small solute to solvent ratios, the amplitudes at intermolecular distances begin to dominate, and higher k relaxations become increasingly important. The relative magnitudes of the k dependent

relaxation times τ_L are also calculated and it is seen that as k increases to intermolecular distance τ_L decreases. This is again in agreement with Onsager's prediction. The SRF can thus be seen to depend on 1) the k dependence of τ_L and 2) the weighting of these relaxation times based on the solute to solvent size ratio. It should be mentioned that Chandra and Bagchi showed that the effect of translational motion, also known as polarization diffusion, is to speed up τ_L. They showed that in some cases translational diffusion can actually reverse the Onsager inverted snowball effect. It was proposed that the importance of translations could be gauged by the factor

$$p = D_T / (2D_R\sigma^2) \qquad 1.31$$

which is the ratio of the translational diffusion to rotational diffusion divided by two times the solvent diameter squared. The usefulness of this ratio as well as the importance of translational diffusion has since been questioned [31]. While the translational effects predicted by Chandra and Bagchi are valid, their importance was perhaps overemphasized in the early literature.

Improvements to the above models have come in the way of improving upon the solvent-solute pair correlations. Here the work of Raineri and Friedman significantly improves the molecular nature of solvent and solute through the use of their interaction site model (ISM) [32] . ISM replaces the point dipolar hard spheres used above with multi-site solvents that do a much better job of representing real molecules. Surrogate forms for the solute-solvent site-site direct correlation functions have also been developed in the ISM [33] . These improvements have led to better quantitative agreement with experiments, but

do not differ qualitatively with the results given above. To get an even better understanding of solvation dynamics we now turn to the much more powerful computer simulations.

C. Computer Simulations

Computer simulations offer the most detailed insight into the nature of solvation dynamics. Ultimately we want to be able to determine what types of motions are responsible for the relaxation of the solvent to its new charge distribution. For example, we would like to know how effective inertial, librational, and diffusive motions are. We would also like to know whether rotations or translations are more important and the effect of solute parameters such as size and charge distribution. For the solvent, information on the number of solvent molecules participating will also be of interest. Several simulation methods can be used to obtain SRF's. I will describe three of these techniques, non-equilibrium (NE) simulations, equilibrium linear response (LR) simulations, and the short time instantaneous normal mode (INM) analysis.

Of the above methods non-equilibrium simulations are the easiest to understand. Here the solute is surrounded by a number of solvent molecules, usually ~200 to ~500 solvent molecules suffice. The molecules are represented by differing levels of approximation from hard spheres with point dipoles, to site-site Lennard-Jones plus Coulomb interactions. The solute is first equilibrated with the solvent and then a step function charge jump occurs. The electrostatic interaction energy, E, between the solute and solvent is then followed as the solvent relaxes to its new equilibrium value. Several runs are averaged to give <E(t)> and the difference between <E(t)> for solutes in the

ground and excited states represents a free energy difference $<\Delta E(t)>$. The SRF can then be written as

$$C(t)_{\Delta E} = [<\Delta E(t)> - <\Delta E(\infty)>] / [<\Delta E(0)> - <\Delta E(\infty)>] \quad 1.32$$

where $<\Delta E(\infty)>$ is the final equilibrium value of $<\Delta E(t)>$. This SRF can be directly compared with experimental fluorescence SRF's. Although solvation energies and shifts differ from experimental values, the effects on the SRF should be small as long as there isn't a specific solute-solvent interaction that has a strong effect on the SRF. If the solvent model does a poor job of reproducing dynamic functions, such as the dielectric response, greater disagreement with experiment will be expected [12].

A second method, which is easier in terms of computer time, but in some cases less accurate, is the equilibrium linear response method. Linear response is the application of Kubo's method [34], and assumes that the response of the system to a non-equilibrium solvation energy is linear in the charge of the solute. This means that the response of the solvent is assumed to be twice as large, but the same in time, when the size of the solute charge is doubled. This approximation is valid in the case of small charge jumps, and becomes less reliable with the increasing size of the charge jump. The key to LR is the connection of the SRF to the time correlation function of the solvent in equilibrium with the ground state solute. The ground state solute sees a solvent environment that is constantly fluctuating about its average equilibrium energy. The relaxation of these naturally occurring fluctuations is the same as the relaxation of the optically driven fluctuation (for small optical transitions). LR describes the solute charge jump as a perturbation to the

ground state system. This perturbation can be related to the fluorescence decay experiments as follows:

$$H'(t) = (\hbar\omega^0 + \Delta E_{solvent})\theta(t) = (\Delta E)\theta(t) \quad 1.33$$

where $H'(t)$ is the perturbation to the ground state Hamiltonian, $\hbar\omega^0$ is the gas phase optical transition energy, $\Delta E_{solvent}$ is the solvent-solute interaction energy, and $\theta(t)$ is a step function [35]. The evolution of the system after the charge jump is then, to first order approximation, defined in terms of the solvent time correlation function in the absence of the perturbation. For example if the solute underwent a change in dipole moment, $\Delta\mu$, then the first order change in $< \Delta E >$ with time would be given by

$$< \Delta E(t) >^1 = \int \theta(t')\Delta\mu\Phi(t-t')\, dt' \quad 1.34$$

$$\Phi(t-t') = 1/kT < \Delta E(0)\Delta\dot{E}(t)) >^0 \quad 1.35$$

$\theta(t)$ is defined above, the over dot represents the time derivative, and the italic superscripts denote order. The first order change is now given in terms of the non-perturbed system's time correlation function. The normalized SRF given by linear response is

$$C(t)_{LR} = <\delta\Delta E(0)\, \delta\Delta E(t)> / <(\delta\Delta E)^2> \quad 1.36$$

where $\delta\Delta E$ is fluctuation in the energy gap between the ground and excited state $\Delta E - <\Delta E>$, and $<\delta\Delta E(0)\, \delta\Delta E(t)>$ is the solvation time correlation function [24]. It should be

noted that $<\delta\Delta E(0)\delta\Delta E(t)>$ is assumed to be the same in the ground and excited state for linear response. This assumption is usually false for experimental systems where the excited state solvent is generally more ordered due to the larger charge moment of the solute (i.e. it has a larger force constant). Carter and Hynes [35] show that the use of the $<\delta\Delta E(0)\delta\Delta E(t)>$ in equilibrium with the excited solute leads to more reliable SRF's at long times. At short times the ground state $<\delta\Delta E(0)\delta\Delta E(t)>$ is just as effective. To determine the SRF in LR: 1) the solvent is allowed to reach equilibrium with the solute, 2) the solute-solvent interaction energy is measured at some given time resolution in the excited or ground state, 3) the solvent time correlation function is determined from the time dependence of the fluctuations of ΔE, 4) the SRF is calculated according to eqn. 1.36.

Another important development is defining the SRF in terms of the solvent velocity autocorrelation function G(t) [36,37,43]

$$C(t) = 1 - <(\delta\Delta E)^2>^{-1} \int (t-\tau)\, G(\tau)\, d\tau \qquad 1.37$$

$$G(t) = <\Delta\dot{E}(0)\, \Delta\dot{E}(t)> \qquad 1.38$$

where $\Delta\dot{E}(t)$ denotes the time derivative of ΔE. This representation has the advantage that $\Delta\dot{E}$ can be separated into its rotational and translational components, subsequently allowing G(t) to be separated into rotational and translational components.

The last method of interest is the Instantaneous Normal Mode analysis (INM) [36,37,38,40]. INM considers the solvent as a collection of coupled harmonic oscillators for times that are short, ~100 to 500fs,. The goal is to determine the solvent modes and

their frequencies. This allows the determination of the frequencies and types of solvent motions that are most effective in relaxing the solute-solvent interaction energy.

For the short times considered by INM, the solvent configuration at time t = 0, R_0, and time t, R_t, should be close to each other, where t time and R is position. This allows the potential energy of the system to be expanded in powers of $R_t - R_0$

$$V(R_t) = V(R_0) + \Sigma V'(R_0 - R_t) + \tfrac{1}{2} \Sigma '(R_0 - R_t) V''(R_0 - R_t) + \ldots \quad 1.39$$

where V′ and V″ are the first and second derivatives of the potential. V′ is the instantaneous force felt by the molecules, while V″ is the dynamical matrix at time zero [36]. INM truncates $V(R_t)$ at second order allowing the dynamical matrix to be diagonalized and the independent modes that propagate the system to be determined (i.e. the eigenvectors). The frequencies of the normal modes can also be determined (i.e. the eigenvalues). Since the potential energy of the liquid can be expressed as a set of uncoupled harmonic oscillators the time dependent positions and velocities can be expressed as functions of the time zero positions and velocities, and the time correlation functions can be solved. The effectiveness of various modes can be determined by their ability to alter the solute-solvent interaction energy. For a particular mode α with INM coordinate q_α, an efficiency rating can be determined

$$c_\alpha = (\delta \Delta E) / (\delta q_\alpha) . \quad 1.40$$

The square of the efficiency rating can then be used to weight the modes and a solvation spectrum $\rho_{solv}(\omega)$ results. At short times the SRF can be approximated in terms of $\rho_{solv}(\omega)$ as

$$C(t) = \exp(-\tfrac{1}{2}\ \omega_{solv}^2 t^2) \qquad 1.41$$

$$\omega_{solv}^2 = [\ k_B T / \langle(\delta\Delta E)^2\rangle] \int \rho_{solv}(\omega) d\omega. \qquad 1.42$$

At longer times the SRF can be determined from the velocity autocorrelation functions G(t) (eqn. 1.37), which again can be expressed in term of $\rho_{solv}(\omega)$

$$G(t) = k_B T \int \rho_{solv}(\omega) \cos \omega t\ d\omega \qquad 1.43$$

Application of these INM techniques leads to SRF's that are good for several hundred femtoseconds. The use of velocity autocorrelation functions gives this method the ability to separate translational and rotational components. It also allows the examination of the importance of solvation shells.

D. Simulation Results

The use of simulations has resulted in some fairly drastic improvements in the understanding of solvation dynamics. These range from the discovery of the inertial portion of the SRF to a better understanding solute effects on solvation. They have also served as a test for the previously discussed theories, often pointing to where they were lacking and leading to their improvement. The more important developments are discussed below.

As mentioned above the inertial portion of the solvent response function was initially missed in experiments due to the low time resolution of the experiments. Simulations led to the discovery of this important solvent relaxation [7]. Early simulations on water and acetonitrile predicted that up to 70% of the relaxation actually occurred by this mechanism [7,40]. The large inertial response in these solvents is due to their small moments of inertia (see below). The nature of the inertial response was explored via simulation. Initial studies were done by of Maroncelli [40] and Perera and Berkowitz [41]. Maroncelli showed that freezing all but one solvent molecule could reproduce the inertial portion of the LR calculated SRF, while Perera and Berkowitz showed that turning off the solvent-solvent interactions had the same result. These studies revealed the free streaming nature of the inertial response. Essentially the molecules are moving as if they were free molecules independent of the other molecules. Simulations also revealed the gaussian nature of this inertial decay. In the INM treatment (as well as others) the SRF can be expanded in a power series of the velocity correlation function G(t)

$$C(t) = 1-(k_BT/\langle(\delta\Delta E)^2\rangle)(\tfrac{1}{2} t^2G_0 + 1/24\, t^4 G_2 + \ldots) \qquad 1.44$$

where G_0 is a pairwise sum over solute-solvent interactions. Here each solvent contributes to G_0 independent of the other solvent molecules, revealing the independent nature of the inertial response. The gaussian nature of the inertial relaxation is evident from the first term in the series and can be represented as

$$C(t)_{inertial} = \exp(- \tfrac{1}{2} \omega_s^2 t^2) \qquad 1.45$$

$$\omega_s^2 = G_0/\langle(\delta\Delta E)^2\rangle \approx (4\pi\rho\mu^2 / 3I_{eff})\, f(\varepsilon,n) \qquad 1.46$$

where ω_s is the solvation frequency, ρ is the number density, μ is the dipole moment, I_{eff} is the effective moment of inertia, and $f(\varepsilon,n)$ is a dielectric factor close to unity. The approximation is for the case of an ion solute in a dipolar solvent [42] and is included to show the importance of the dipole density and the moment of inertia.

Simulations have also elucidated the relative importance of rotations and translations. This was first accomplished in INM by separating the solvation spectrum ρ_{solv} into its rotational and translational components. This comes from the relationship between ρ_{solv} and G(t) given above in equation 1.43 [36]. For other simulations separation of G(t) into its components is done according to the method of Steele [43]. Results for separation of G(t) into rotational and translational components are well presented by Ladanyi and Stratt [37,38] and Ladanyi [44] (INM analysis and NE results). These studies showed that for acetonitrile and CO_2, ρ_{solv} is dominated by rotational modes even when the density of states favors translational modes. This is basically due to the symmetry of the interactions. For dipoles, rotation is an effective relaxation mechanism. On the other hand, translation of the positive and negative poles by a small amount cancels. Therefore for interactions of dipoles and quadrupoles, which have multipolar interaction patterns, rotations should dominate the relaxation.

The dominance of rotations has been used by Maroncelli *et al.* [42] to approximate the SRF in terms of the single molecule dipole autocorrelation function. This treatment leads to an interesting insight into the importance of the static effects of solvation. In this treatment, translational effects were ignored, and the solvent was approximated by dipolar

hard spheres. The single particle dipole autocorrelation function and SRF approximation are given by

$$C_\mu(t) = <\mu\cdot\mu(t)>/\mu^2 \qquad 1.47$$

$$C(t) \cong \{C_\mu(t)\}^\alpha \qquad 1.48$$

where α is a factor that relates the single dipole autocorrelation function to the SRF. LR defines this factor as [42,45]

$$\alpha = \{ <(\delta\Delta E)^2>_s / <(\delta\Delta E)^2> \} \cong (4\pi\rho\mu^2 / 3k_BT) f(\varepsilon,n) \qquad 1.49$$

where $<(\delta\Delta E)^2>_s$ is the single molecule value of $<(\delta\Delta E)^2>$, ρ is the solvent density, μ is the dipole moment, $f(\varepsilon,n)$ is a dielectric function usually close to unity, and the approximation is for a ion in a dipolar solvent [42]. From the above equations it can be seen that the factor α is proportional to the dipole density and that it relates the amount of angular motion needed to relax a typical solvation fluctuation. As the dipole density increases the amount of motion necessary to relax the fluctuation decreases. This reflects the nature of the static correlations of the solvent. Highly polar solvents will have large correlations between individual solvent molecules that will counteract their reorientation to the solute. In the absence of solvent-solvent interactions, the solvent molecule will go through large angular displacements to stabilize the solute. On the other hand if the solvent-solvent correlations are strong, reorientation to the solute will be less favorable due to the breaking of the solvent-solvent interactions. Therefore for solvents with high dipole densities, the net

displacements will be smaller, or in other words small angular motions will be more effective in relaxing the system. This effect is very apparent for acetonitrile where the dipole density is high (only small motions are needed). As noted by Ladanyi and Maroncelli [45] this simple model fails in its lack of intermolecular velocity correlations, that are absent in $C_\mu(t)$, and become important after short times. Nevertheless it is fairly powerful for such a simple model.

Two other important revelations given by simulations are the collectivity of the solvation and the importance of the first solvation shell. When ΔE is expressed as a pairwise-additive sum of solute-solvent interactions, the collectivity of the response can be gauged by looking at the interactions of the solute with single solvent molecules compared with the solute's interaction with a pair of solvent molecules. This leads to $C(t) = C_{ss}(t) + C_{sp}(t)$, where ss represents single solvent interactions and sp solvent pair interactions. For polar molecules the cancellation of the negative $C_{sp}(t)$ with the positive $C_{ss}(t)$ causes the relaxation of C(t) to be rapid. The degree of cancellation is a sign of the collectivity of the response and is largest for strongly polar solvents. The cancellation of $C_{ss}(t)$ and $C_{sp}(t)$ is lowest at early times. This is, to some extent, not surprising since the inertial response should be single particle in nature, with the collectivity of the solvent growing in with time (eqn 1.44). These results agree with the discussion above, where increased solvent correlations lead to large α factors quenching the relaxation, but here intermolecular velocity correlations are not ignored.

Simulations have shown that ~ 50% or more of the solvation is done, by the typically 10 to 30 molecules, in the first shell. This is not surprising since it is in agreement with continuum predictions. The importance of the first shell dynamics, on the other hand,

are more important. These effects can be projected out in the INM case in the same way as the rotations and translations. For other simulations some radial distance is chosen based on the location of the first peak in the radial distribution function of the solvent. The main finding here is that the initial librational like part of the SRF in water and acetonitrile comes primarily from the first shell [16]. Interestingly INM analysis also shows that the first solvent shell response is slower than the total response [37], in agreement with the models described previously.

Finally it should be mentioned that simulations have also investigated the importance of solute size and charge distribution (moment). Increasing the size of the solvent is generally shown to increase the rate of solvation. This is in agreement with other models described above. The order of the perturbation to the solute charge distribution has two effects. The first is a decrease in the effective range of solvation. The second is the increase in the importance of translational modes. Modeling on the probe used in these studies, C153, shows the change in the charge distribution to well approximated by a ~8D dipole change.

E. Relationship between Solvation Dynamics and Longitudinal Dielectric Relaxation

For the continuum predictions given above the SRF was related to the longitudinal dielectric relaxation. This relationship is based on the fact that when the charge distribution of the solute is changed, a displacement field is created $\mathbf{D}(r,t)$, which in turn induces a polarization field $\mathbf{P}(r,t)$. The solvation energy can be given as [65]

$$E(t) = \int dr\, \mathbf{P}(r,t) \cdot \mathbf{D}(r,t). \qquad 1.50$$

In the above continuum solvents we considered the creation of a ion, which only has a longitudinal field, and obtained the SRF for a Debye solvent as a single exponential with a time constant equal to the longitudinal relaxation time. For solutes with higher order poles there will also be contributions from the transverse field, but even here the longitudinal response will be more closely related to the SRF [16]. In general the longitudinal dielectric relaxation in the absence of a solute can be associated with a relaxation in the electric field after a jump in D [67]. What concerns us at this point is why the longitudinal relaxation is faster than the Debye relaxation.

For a polar single component solvent there are both short and long-range interactions. The long-range correlation g^L can be expressed as follows [68]:

$$g^L = [\,\varepsilon/(2\varepsilon+1)^2\,]\,[\,\rho(\mu g^s)^2/k_B T\varepsilon_0\,] \qquad 1.51$$

$$g^s = 1 + 3\langle \sum_j \cos\theta_{1j} \rangle \qquad 1.52$$

where ε is the static dielectric, constant ρ is the number density, μ is the dipole moment, g^s is the Kirkwood g factor, θ_{1j} is the dot product of the polar angles of molecules 1 and j with the external frame, and ε_0 is the permittivity of free space. The long-range correlations can be shown to have the same radial and angular form as a dipole-dipole interaction, and goes as $1/r^3$ [68]. If we consider a tagged dipole, μ_1 ,and look at other dipoles a large distance, r ,away, we will see that dipoles along the axis of μ_1 will be more likely to be found aligned with μ_1. If we look perpendicular to μ_1 we will find dipoles aligned anti-parallel to μ_1 with

a probability that is half that along the parallel axis. This long-range effect is dependent on ε and will large for large ε.

To see how long range interactions effect the longitudinal and transverse dielectric relaxations, we consider the wave vector dependent dipole density

$$M(k) = \sum_j \mu_j \exp[ik \cdot r_j] \qquad 1.53$$

First consider k to be along the z-axis, and we are interested in a tagged dipole μ_1. If we look at the pair interactions of μ_1 with a spherical shell of dipoles at a distance r away, then the sum of the interactions over the shell will be zero. As mentioned above dipoles that are along the μ_1 axis will tend to be in alignment with μ_1, while those along the axes perpendicular to the μ_1 axis will tend to be anti-parallel. When considering the dipole density, we will be interested in M(k), which will include the k dependent exponential factor. This factor will oscillate along the z-axis, causing contributions from different shells along the z-axis to cancel. Figure 1.7a shows that when μ_1 is aligned with k along the z-axis, the oscillation of the k dependent exponential factor cancels the positive contributions from the dipoles along z. This leaves the predominately negative pair contributions, making the overall pair contribution negative. Figure 1.7b show that when we place k along the x-axis the exponential k factor cancels the negative contributions along the x-axis, resulting in a overall positive pair contribution. We are interested in the longitudinal dielectric relaxation that is determined by

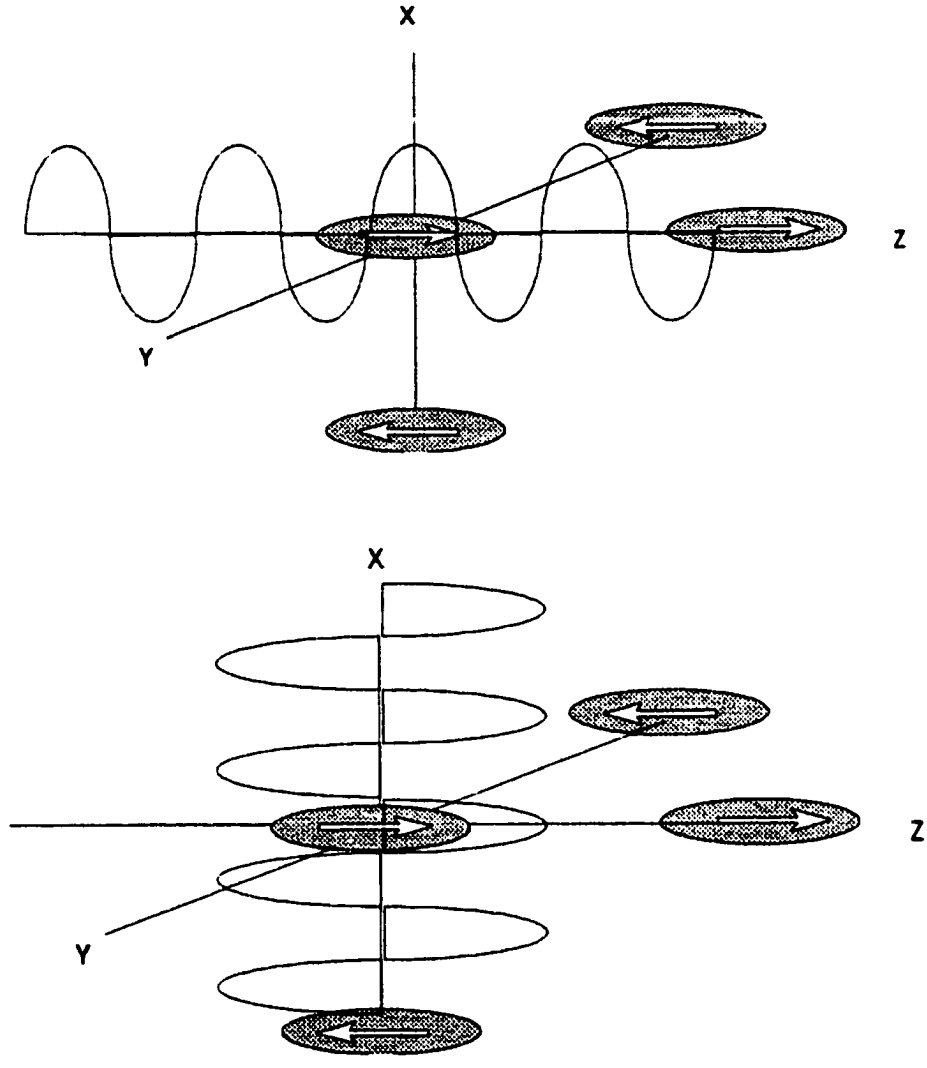

Figure 1.7
a) (top) k aligned with dipole (z-axis), results in cancellation along the z (positive) axis.
b) (bottom) k (x-axis) not aligned with dipole (z-axis), results in cancellation along the x (negative) axis.

$$\Phi_L(k,t) = (1/ <|M_z(k,0)|^2>) (< M_z(k,0) \cdot M_z(-k,t) >) \quad 1.54$$

Since $M_z(k,t)$ is small due to the effectiveness of cancellation from anti-parallel dipoles (negative pair terms), small changes in dipole orientations have a large impact. In other words, $M_z(k,t)$ is easier to change than the single molecule dipole vector. The more effective the pair cancellation the faster the response will be. For a dipolar solvent the well known relation

$$\tau_L = \tau_D [\varepsilon(\infty)/\varepsilon] \quad 1.55$$

reminds us that the long-range pair correlations are proportional to ε. It is important to remember, as pointed out by Kivelson and Friedman [67], that τ_L and τ_D originate from the same molecular dynamics, and that τ_L and τ_D do not involve fast and slow reorientations respectively. These results show that the longitudinal relaxation is sensitive to long range correlations which effectively speed up, or quench the relaxation. This is similar to the discussion above for the translation factor α, and the pair cancellation of the SRF. We will therefore find the longitudinal dielectric relaxation to be a useful aid.

F. Nonpolar Solvation

So far the above discussion has focused on polar solvation dynamics. In one of the experiments pursued benzene was used as a co-solvent. It is therefore necessary to discuss the implications of nonpolar solvation. The big difference here is the lack of a permanent dipole moment. Therefore theories that include the dipole moment of the solvent are not useful here. In these cases the higher order multipoles will become important. The ability of nonpolar solvents to relax C153 has been observed experimentally [46]. In the case of benzene a large quadrupole is responsible for such relaxations. Nonpolar solvation has been studied through simulations with the results showing that it is very similar to polar solvation in many aspects. The fact that polar-like bi-phasic responses and fairly large time dependent fluorescence shifts are produced in nonpolar solvents was shown by Gardecki *et al.* [46]. Later simulation investigations into the nature of nonpolar solvent response by Reynolds *et al.* [47] confirmed the importance of the quadrupole interactions. Theories that involve interaction site models can deal with nonpolar solvation easily [48]. Simulations have also been preformed on the solvation dynamics of the quadrupolar solvent CO_2 [44,38]. These simulations were quite complete showing the relaxation method is similar to polar relaxation, having an inertial and diffusive component. The dominance of rotations is still observed, but to a lesser degree. The collectivity of the response, as determined by cancellation of the $C_{sp}(t)$ with $C_{ss}(t)$, is smaller and the response is closer to single particle relaxation than in polar solvents. The contribution of the first solvent shell is proportionally higher than in polar solvents, which is not surprising due to the shorter-range nature of the quadrupole interaction.

IV Solvation Dynamics in Binary Solvent Mixtures

The solvation explored here is solvation in binary solvent mixtures. The use of binary solvent mixtures to customize solvent properties is common in many chemical reactions and in chromatography. Upon mixing we can expect the addition of new solvent-solvent and solute-solvent interactions to complicate matters. Often times this is exactly what is desired, that is the creation of new solvent properties that were not present in the pure solvents. These effects can include, bringing together reactants that would otherwise not be mutually soluble, stabilizing solutes in a mixture that would not be stable in either of the pure solvents, customizing the rates of solvent relaxations.

The mixing of two solvents can lead to an array of effects that may or may not be related to the mole fractions of the individual solvents. When some property Ξ of the binary system can be described as

$$\Xi = x_1 (\Xi_1) + (1- x_1)(\Xi_2), \qquad 1.56$$

where x_1 is the mole fraction of species one, and Ξ_i is the value of Ξ for the pure solvent i, it is said to be a linear property of the system. Properties that may or may not be linear include density, dielectric constant, solute dipole stabilization, solute solubility, and viscosity. The dynamic properties of the binary system will certainly be more complicated than in either of the pure solvents. For example, there will be a combination of time constants for diffusion and reorientation that will vary from the values of the individual constituents to values that are very different due to interspecies interactions. These interspecies interactions can result in strong deviations from the ideal behavior mentioned

above. When a solute is involved, as in fluorescence experiments, the interaction of the solvents with solute can also be described as linear or nonlinear.

Deviation of steady-state fluorescence from linearity is often used as a sign of preferential solvation (PS) [49,51]. A dye molecule is said to be preferentially solvated by solvent 1 if the ratio of solvent 1 to solvent 2 molecules in the first solvent shell is larger than the bulk ratio. PS is a complicated function of solute-solvent and solvent-solvent interactions. One way that PS can occur is when one of the solvent species has a specific interaction with the solute. This interaction can be a strong electrostatic interaction such as a hydrogen or dipole-ion bond. Recent theoretical treatment of ionic solvation has shown that a difference in dipole strength, or solvent size can result in PS, with large dipoles and small molecules being preferred [51]. Knowledge of PS and its effects is therefore desirable. This has lead to the investigation of the effects of preferential solvation on chemical reactions [52], and research into spectroscopic determination of PS. Spectroscopic determination of PS can be determined from the deviation of the fluorescence maximum from predictions based on the interaction energy of the dye and the solvent. This is most easily accomplished by treating the solvent as a continuum, using the Onsager function for the reaction field R [53,54]. In the continuum limit the change in the solute's dipole energy is given by

$$\Delta E = -2\mu^2 / a^3 R \qquad 1.57$$

$$R = [\,(\varepsilon-1)/(\varepsilon+1)\,] \qquad 1.58$$

where a is the solute radius. It should be noted that the bulk ε itself is not necessarily a linear function of the system, and that the reaction field is highly nonlinear with ε (figure 1.8). Neglect of ε effects has led to the incorrect determination of PS in the literature [53]. Any case in which PS is determined without knowledge of how ε varies with mole fraction is suspect. For that matter even the continuum model is somewhat lacking since its predictions for the reaction field neglects the molecularity of the solvent, but it should serve as a good first order approximation.

Compared to pure solvents, investigation into solvation dynamics in binary mixtures has been sparse to date, despite their popularity and importance. The systems studied have included nonpolar-polar mixtures [55,56], as well as polar-polar mixtures [57,58,59], and with a few exceptions have been studied with poor time resolution. The main findings of these works show that there can be a long time response of the system related to the slow translational diffusion (dielectric enrichment) of the more polar solvent towards the solute (excited state PS). Day and Patey show that for systems with fairly large differences in dipole moment the SRF's can be very similar to the pure solvent results [60]. When the difference in dipole moments become large enough, however, they do see slow relaxation due to solvent shell redistribution, with a strong dependence on mole fraction. Similar simulation results have been seen by Skaf for the slow preferential solvation of a negative ion by water in DMSO-water mixtures [62]. Interestingly this slow response was not observed for the cation in the same solvent mixtures, showing the complexity of PS. Cichos *et al.* have also reported a slow response in methanol-hexane mixtures both by experiment [56] and simulation [63]. Two other interesting systems that have been studied are acetonitrile(ACN)-propylenecarbonate(PC) and methanol-water. In the simulation

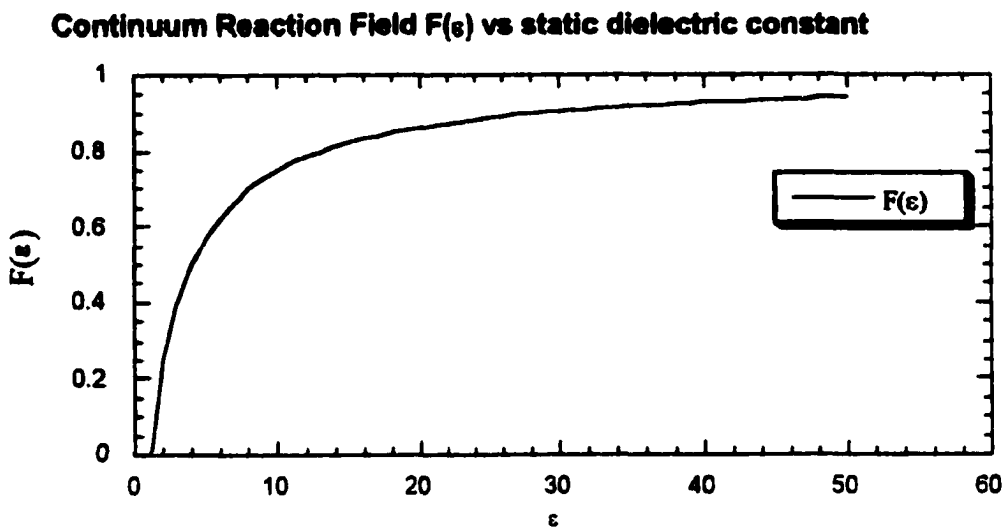

Figure 1.8
Continuum Reaction Field for dipolar solvent as a function of the static dielectric constant. See text for further details.

studies on methanol-water mixtures the effects of hydrogen bonding and solute size were examined [64]. It was shown that hydrogen bonding to the ion-pair solute was more important in the small solute, and that hydrogen bond breaking resulted in a fast relaxation for the charge reversal of the solute. A slow response was also observed as the reformation of the hydrogen bond, which is due to slower diffusion like processes. For the hydrophobic large solute solvation dynamics were seen to be consistent with the longitudinal dielectric relaxation of MeOH-water mixtures determined in a separate simulation [66]. The large solute was also seen to prefer solvation by the methyl group resulting in drastic changes in the SRF at high water concentrations, where this was no longer possible. The ACN-PC solvent system was chosen as a system for which the polarities of the solvents were very similar but the relaxation times differ by an order of magnitude [58]. This system was proposed as a system that could be used to differentiate between static and dynamic effects of solvation on electron transfer reaction.

V. Goals

In the following chapters, we will be interested in how mixing solvents affects solvation dynamics. Based on the above discussions, the effects can be divided into the inertial and diffusive regimes. For the inertial regime, differences in the moments of inertia will, of course, be important. The diffusive regime should be strongly correlated with solvent rotational and translational time scales determined by dielectric relaxation. Preferential solvation should be expected in cases where there is a strong difference in solvent polarities, resulting in long time translational diffusion.

We have chosen two systems to explore. The first is dimethylsulfoxide (DMSO)-water mixtures. This system is highly associated and non-ideal, displaying large deviations from ideality for many properties such as dielectric response, viscosity, free energy of mixing, rotational diffusion, and translational diffusion. It is an interesting system in that DMSO is a hydrogen bond acceptor, but not a donor, where as water is both a donor and acceptor. The formations of stoichiometric complexes, which may affect solvent relaxation, are also of interest. Many of the mixture's properties peak at the 33% DMSO concentration and are bi-valued. This will allow us to examine the effects of properties with the same value but differing mole fractions. Finally it is a well-studied system both experimentally and by simulation allowing analysis of the results in light of previous investigations.

The second system is benzene-acetonitrile. This is a non-associating system that should behave much more ideally. It is interesting in that acetonitrile has a large dipole moment and small moment of inertia, whereas benzene is a nonpolar slower solvent. This is the first report of a quadrupolar-polar mixture and the combination of these two very different solvents should result in some interesting results. While experimental data on these mixtures is less available the individual solvents are both well studied as representatives of their respective classes of solvents.

References for Chapter One

1. R. A. Marcus, J. Chem. Phys. 43, 679 (1965).
2. L. D. Zusman, Chem. Phys. 49, 295 (1980).
3. E. W. Castner, and M. Maroncelli, J. Mol. Liqs. 77, 1 (1988).
4. G. Fleming, and M. Cho, Annu. Rev. Phys. Chem. 47, 109 (1996).
5. J. A. Gardecki, and M. Maroncelli, J. Phys. Chem. A. 103, 1187 (1999).
6. S. Rosenthal, R. Jimenez, G. Fleming, J. Mol. Liqs. 60, 25 (1994).
7. M. Maroncelli, and G. Fleming, J. Chem. Phys. 89, 5044 (1988).
8. M. J. Lang, X. J. Jordanides, X. Song, and G. R. Fleming, J. Chem. Phys. 110, 5884 (1999).
9. M. L. Horng, J. A. Gardecki, A. Papazyan, and M. Maroncelli, J. Phys. Chem. 99, 17311 (1995).
10. R. S. Fee, and M. Maroncelli, Chem. Phys. 183, 235 (1994).
11. M. Maroncelli, R. S. Fee, C. F. Chapman, and G. R. Fleming, J. Phys. Chem. 95, 1012 (1991).
12. P. Kumar, and M. Maroncelli, J. Chem. Phys. 103, 3038 (1995).
13. N. Hill, W. Vaughan, A. Price, and M. Davies, *Dielectric Properties and Molecular Behavior*, edited by T. M. Sugden (Van Nostrand Reinhold Company, London, 1969).
14. E. W. Castner Jr., G. R. Fleming, and B. Bagchi, Chem. Phys. Lett. 143, 270 (1987).
15. G. van der Zwan, and J. T. Hynes, J. Phys. Chem, 89, 4181 (1985).
16. M. Maroncelli, J. Mol. Liqs. 57, 1 (1993).
17. L. Onsager, Can. J. Chem, 55, 1819 (1977).

18. D. Calef, and P. G. Wolynes, J. Chem. Phys. 78, 4145 (1983).

19. V. Friedrich, and D. Kivelson, J. Chem. Phys. 86, 6425 (1987).

20. R. F. Loring, and S. Mukamel, J. Chem. Phys. 88, 3246 (1988).

21. E. W. Castner Jr., G. R. Fleming, and B. Bagchi, J. Chem. Phys. 89, 3519 (1988).

22. P. G. Wolynes, J. Chem. Phys. 86, 5133 (1987).

23. L. R. Pratt, Mol. Phys. 40, 347 (1980).

24. M. Maroncelli, and G. Fleming, J. Chem. Phys. 89, 875 (1988).

25. I. Rips, J. Clafter, and J. Jortner, J. Chem. Phys. 88, 3246 (1988).

26. D. Calef, and P. G. Wolynes, J. Chem. Phys. 78, 4145 (1983).

27. A. Chandra, and B. Bagchi, Chem. Phys. Let. 151, 47 (1988).

28. F. O. Raineri, Y. Zhou, H. L. Friedman, and G. Stell, Chem. Phys. 152, 210 (1991).

29. A. A. Kornyshev, A. M. Kuznetsov, D. K. Phelps, and M. J. Weaver, J. Phys. Chem. 91, 7159 (1989).

30. R. F. Loring, Y. J. Yan, and S. Mukamel, J. Phys. Chem. 87, 5840 (1987).

31. E. W. Castner Jr., M. Maroncelli, and G. R. Fleming, J. Chem. Phys. 86, 1090 (1987).

32. F. Raineri, H. Resat, B. C. Perng, F. Hirata, and H. Friedman, J. Chem. Phys. 100, 1477 (1994).

33. H. Friedman, F. Raineri, F. Hirata, and B. C. Perng, J. Stat. Phys. 78, 239 (1995).

34. R. Kubo, Rep. Proc. Phys. 29, 255 (1966).

35. E. Carter, and J. T. Hynes, J. Chem. Phys. 94, 5961 (1991).

36. R. Stratt, M.Cho, J.Chem. Phys. 100,6700 (1994)

37. B.M.Ladanyi, R. Stratt, J. Phys. Chem. 99, 2502, (1995)

38. B.M. Ladanyi, R. Stratt, J. Phys. Chem. 100, 1266, (1996)

39. R. Stratt, and M. Maroncelli, J. Phys. Chem. 100, 12981 (1996).

40. M. Maroncelli, J. Chem. Phys. 94, 2084 (1991).

41. L. Perera and M.L. Berkowitz, J. Chem. Phys. 97, 5253 (1992); 96,3092 (1992)

42. M. Maroncelli, P. Kumar, and A. Papazyan, J. Phys. Chem. 97, 13 (1993).

43. W. A. Steele, Mol. Phys. 61, 1031 (1987).

44. B. M. Ladanyi, *Electron Transfer in Condensed Media*, edited by A. A. Kornyshev, M. Tosi, and J. Ulstrup (World Scientific, Singapore, 1997).

45. B. M. Ladanyi, and M. Maroncelli, J. Chem. Phys. 109, 3204 (1998).

46. J. Gardecki, M. L. Horng, A. Papazyan, and M. Maroncelli. J. Mol. Liqs. 65-6, 48 (1995).

47. L. Reynolds, J. A. Gardecki, S. T. U. Frankland, M. L. Horng, and M. Maroncelli, J. Phys. Chem. 100, 10337 (1996)

48. B. C. Perng, and B. M. Ladanyi, J. Chem. Phys. 110, 6389 (1999).

49. W. Acree, S. Tucker, and D. Wilkins, J. Phys. Chem. 97, 11199 (1993).

50. P. Chatterjee, K. Medda, S. Bagchi, J. Solution Chem. 20, 249 (1991)

51. A. Chandra, and B. Bagchi, J. Chem. Phys. 94, 8367 (1991).

52. L. Zusman, J. Chem. Phys. 102, 2580 (1995).

53. W. Zurawsky, and S. Scardata, Photochemistry and Photobiology, 60, 343 (1994).

54. P. Suppan, J. Chem. Soc., Faraday Trans. 1. 83, 495 (1987).

55. N. Petrov, A. Weissner, and H. Staerk. J. Chem. Phys. 108, 2326 (1998).

56. F. Cichos, A. Willert, U. Rempel, and C. vonBorczyskowski, J. Chem. Phys. 108, 2326 (1998).

57. W. Jarzeba, G. Walker, A. Johnson, P. Barbara, Chem. Phys. 152, 57 (1991).

58. J. A. Gardecki, M. Maroncelli, Chem. Phys. Lett. 301, 571 (1999).

59. H. Shirota, and E. W. Castner Jr. submitted to J. Chem. Phys.

60. T. J. F. Day, and G. N. Patey, J. Chem. Phys. 106, 2782 (1977).

61. A. Yoshimori, T. J. F. Day, G. N. Patey, J. Chem. Phys. 109, 3222 (1988).

62. D. Laria, and M. S. Skaf, J. Chem. Phys. 111, 300 (1999).

63. F. Cichos, R. Brown, U. Rempel, and C. von Borcvyskowski, J. Phys. Chem. 103, 2506 (1999).

64. M. Skaf, and B. M. Ladanyi, J. Phys. Chem. 100, 18258 (1996).

65. L. E. Fried and S. Mukamel, J. Chem. Phys. 93, 932 (1990)

66. B. M. Ladanyi and M. Skaf, J. Phys Chem. 100,1368 (1996)

67. D. Kivelson and H. Friedman, J. Phys. Chem. 93,7026 (1989)

68. P. Madden and D. Kievelson, Adv. Chem. Phys. LVI (1984)

Chapter Two

Dimethylsulfoxide (DMSO) – Water

Part One

The DMSO-Water System

I Introduction

DMSO and water are both ubiquitous solvents in chemistry. Water is, of course, the universal solvent, known for its ability to host the numerous biological reactions necessary for life, as well as a wide variety of other important reactions. It is a highly polar molecule with its electronegative oxygen atom holding the extra electron density. Its tetrahedral structure, with two hydrogens and two lone pairs, is ideal for hydrogen bonding, with each molecule making four hydrogen bonds in the solid state. Water's polarity and high degree of association are key factors when considering its solvation abilities. We therefore should predict it to be effective in dissolving other polar species, while also being effective in rejecting species that cannot provide strong solute-solvent interactions. DMSO on the other hand could be considered as one of the organic universal solvents. DMSO is, like water, a highly polar molecule, however, unlike water, DMSO is an unassociated solvent. Due to its two lone pairs on its oxygen atom, it is a hydrogen bond acceptor, but not a donor. The two

methyl groups on the other hand present a much more nonpolar attribute to the molecule. This combination of polar and nonpolar characteristics makes DMSO an incredible solvent. It has also been used for the delivery of drugs as well as a drug itself. When these two solvents are mixed several interesting properties emerge.

II Equilibrium Structure of DMSO-Water Mixtures

When DMSO and water are mixed the strongest interactions involve the redistribution of H-bonds. As mentioned above, DMSO is a H-bond acceptor. Based on simple Lewis dot structures, it can be seen that DMSO is capable of accepting two to three H-bonds, while water can both accept and donate two hydrogen bonds. The resulting equilibrium structures of these mixtures have been investigated both experimentally and by simulation.

From Figure 2.1 it can be seen that the free energy, enthalpy, and entropy of mixing are highly non-ideal, with the maxima and minima at 33% DMSO (mole fraction X_D = 0.33) [1,2,3]. At this mole fraction, the mixing is highly exothermic. The viscosity is also shown and displays similar trends, while the static dielectric constant behaves more ideally. The above non-idealities have led to the investigation of the DMSO-water structure via X-ray and neutron scattering [4]. These studies show that the addition of a small amount of DMSO leads to sharpening of the radial distribution function of water. This increased order was speculated to be due to either the hydrophobic effect or strong hydrogen bonding to the DMSO oxygen. These studies also showed evidence of the formation of 1DMSO-2H_2O complexes in which two water molecules are H-boned to the DMSO oxygen.

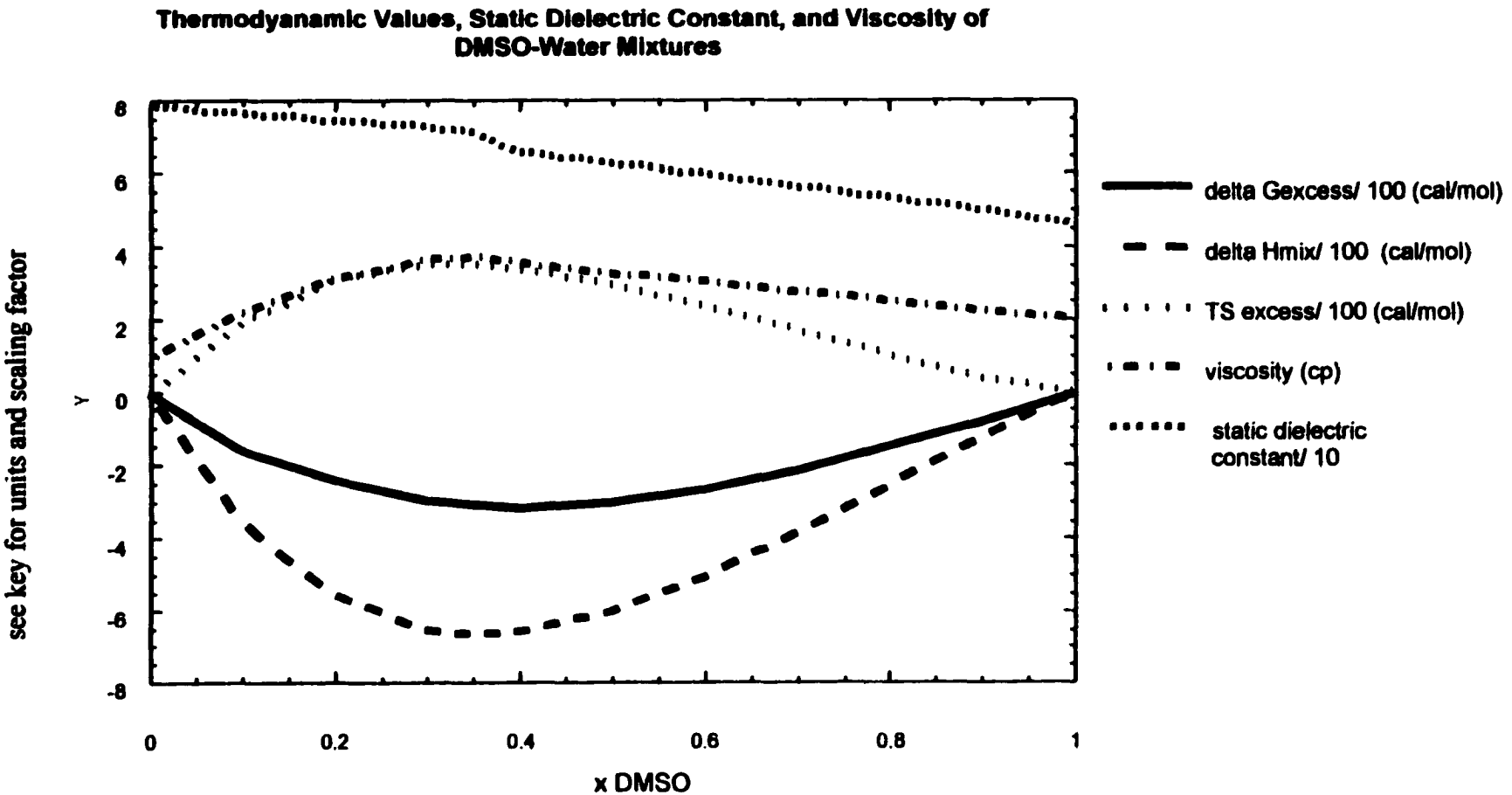

Figure 2.1

Various functions versus mole fraction DMSO, values have been divided by factor shown in the key to put all curves in the same plotting range. See text for references.

The experimental results were reproduced by several simulation studies. From the simulations, it was determined that the 1DMSO-2H_2O complexes existed over the entire range of compositions studied [5,6,7]. The hydrophobic effect was investigated at X_D = 0.33 and found not to be important [8]. This, however, may be due the highly structured nature of the 1DMSO-2H_2O complex, which has a stoichiometeric ratio of DMSO to water H-bonds. Hydrophobic effects at lower concentrations were not studied. A separate study revealed that with increasing DMSO concentration, the amplitudes, but not the positions of the g_{HH} radial distribution function change [5]. These results showed waters first solvation shell becomes more structured with increasing DMSO, while at the same time the number of water-water H-bonds decrease. This was explained due to the fact that the DMSO H-bond is stronger than the water-water H-bond, and the increase in the water-water attractive potential due to the presence of the methyl groups.

The static dielectric constant is seen to decrease with DMSO concentration. The importance of H-bonding on ε was shown by the mean field results of Luzar [9], who showed that the static dielectric constant could be well reproduced using only short-range specific interactions. Extensive modeling has also been done by Skaf, who notes that the Kirkwood g factor decreases ~ 40% with increasing DMSO concentration despite an increase in dipole strength [10]. This suggests that dipole-dipole correlations are larger in the high water mole fractions, and decrease with the addition of DMSO. The $h^{110}(r)$ dipolar symmetry projections are also given by Skaf. For pure DMSO it is seen that an anti-parallel alignment is favored as shown by a negative dip in $h^{110}(r)$. Water on the other hand has a large positive going peak due to its strongly directional H-bonds. These results are in line with the highly structured H-bonding in water and the non-associating structure

of DMSO. Interestingly, the mixtures show a positive going peak not present in either pure solvent. This peak is attributed to the DMSO-water complex seen in the above studies and is maximum at X_D= 0.35. Recent simulations by Skaf have also shown the existence of 2DMSO-1H_2O complexes [12]. These complexes are proposed to exist throughout the entire composition range, and their importance is expected to be seen for DMSO mole fractions over 50%.

From the above studies we can see that the DMSO-H_2O system is strongly interacting, with strong H-bonds being formed between DMSO and water resulting in 2DMSO-1H_2O and 1DMSO-2H_2O complexes. The next section looks at the effects of these complexes on the dynamics of the mixtures.

III Dynamic DMSO-Water Experiments and Simulations

Several dynamic experiments have also been performed on DMSO-H_2O mixtures. These include dielectric relaxation [11], NMR [13,14,15], and quasi-elastic neutron scattering [4]. As with the steady-state experiments above simulations give further insight into the experimental results obtained. The experiment most directly related to solvation dynamics is dielectric relaxation. Kaatze *et al.* give results for the complex dielectric spectrum from 1MHz to 40GHz throughout the entire composition range [11]. From these results the frequency dependent dielectric constant, $\varepsilon(\omega)$, is fit to a Cole-Davidson plot, and the resulting principal dielectric relaxation times τ_s are shown in figure 2.2. From figure 2.2 it can be seen that the τ_s goes through a maximum which is consistent with the 1DMSO-2H_2O complex. The relaxation times in the frequency range explored are related to diffusional processes and

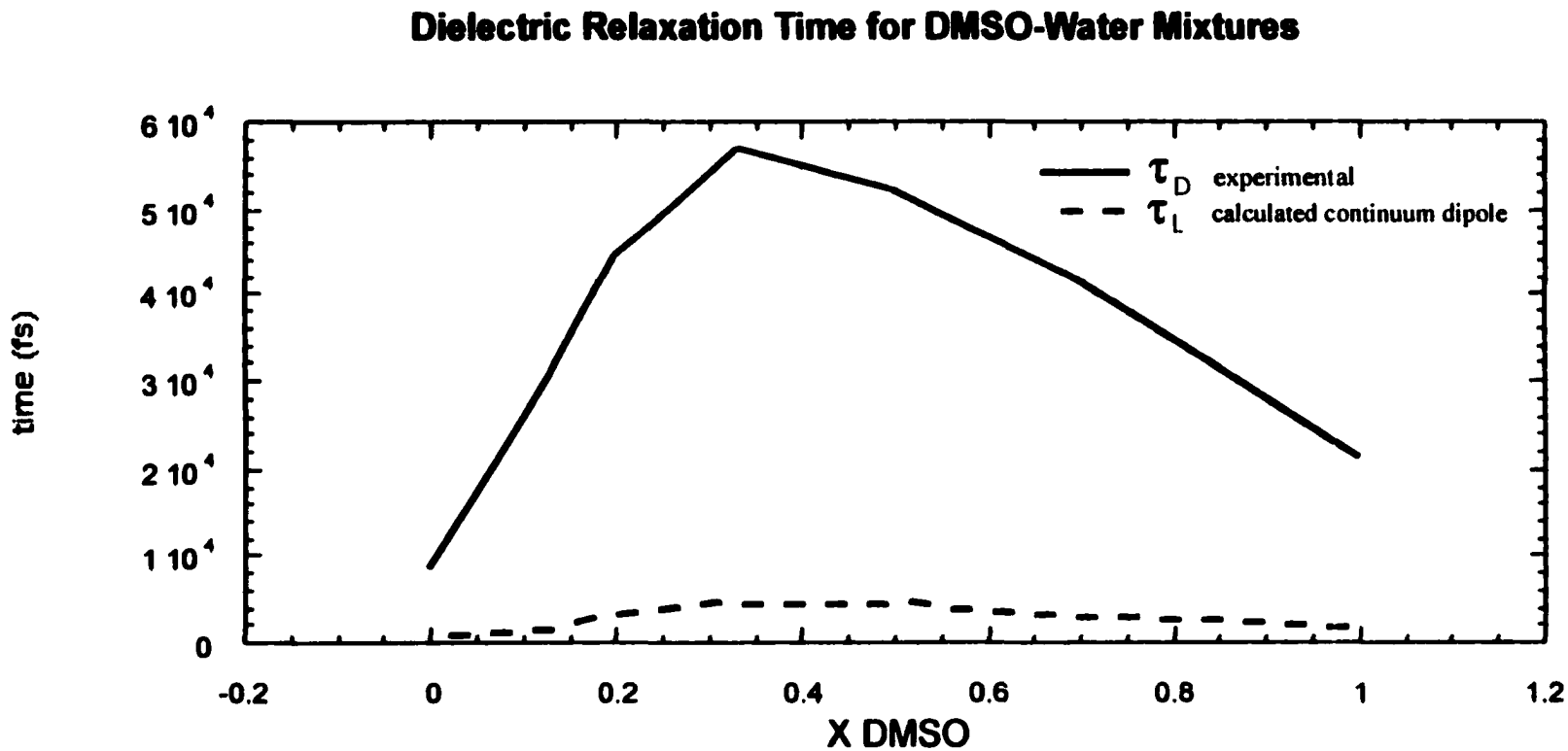

Figure2.2

Dielectric relaxation time constants τ_D and τ_L versus mole fraction DMSO. τ_D is taken from Kaatze (see text for reference) and τ_L is calculated for a nonpolarizabe dipole in a continuum solvent $\tau_L = [(2\varepsilon(\infty)+1)/(2\varepsilon(0)+1)]\ \tau_D$

omit inertial and librational effects. These relaxation times therefore show a very pronounced slowing of the diffusional relaxation, with the addition of DMSO to water having a larger effect than the addition of water to DMSO. At $X_D = 0.10$ the relaxation time is about 3.5 times slower than pure water. It should be noted that Kaatze *et al.* attempted to fit the data to a sum of two Debye terms, but the results were not realistic.

The values of the Cole-Davidson β values from equation 1.19, are plotted in figure 2.3. It can be seen that the values are relatively small. The β values scale the principal relaxation times, and β increases as the distribution of relaxation times increase. If we follow the plot, we see that the addition of DMSO to water results in an increase in the β value. This increase results from the perturbation of water by DMSO, and from the additional contribution of DMSO to the dielectric spectrum. The β value reaches a maximum at $X_D = 0.10$ and then decreases to a local minimum at $X_D = 0.33$. The small value of β at $X_D = 0.33$ implies that the mixture is highly homogeneous at this mole fraction. The β value then rises to a local maximum at $X_D = 0.80$ and then falls to the pure DMSO value. It is interesting to evaluate these results in relation to the DMSO-H_2O complexes [16]. Upon addition of either component to the other pure species, the appropriate complex forms. This accounts for the rise in β, as the pure component and complex now exist together. On the water rich side the continued addition of DMSO past $X_D = 0.10$ results in the lowering of β as the mixture becomes closer and closer to the very homogeneous 1DMSO-2H_2O. On the DMSO rich side, the transformation of the 2DMSO-1H_2O complex to the 1DMSO-2H_2O complex is seen to set in at $X_D = 0.80$. The continued addition of water then results once again in the gradual approach to the low $X_D = 0.33$ β value.

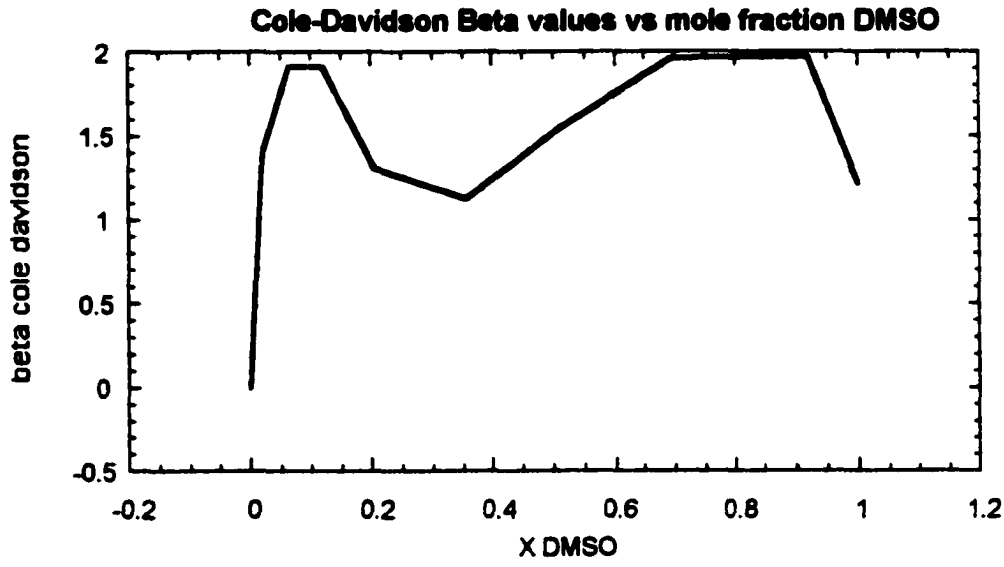

Figure 2.3
Beta values from the Cole-Davidson fits given by Kaatze (see text for reference, and Cole-Davidson equation).

Kaatze *et al.* also note that addition of water to DMSO results in one of the highest molal shifts ($d\tau/dm$) of the principal dielectric relaxation time ever found, and that its value is similar to those seen for large organic ions. Finally they make an interesting statement about the idea of a rigid 2DMSO-1H_2O complex. Although the low value of β implies a very homogeneous mixture it does not necessarily imply a rotating entity. This can be rationalized in view of the principal dielectric relaxation time of acetone-water mixtures, which would imply a 1 acetone- 4 H_2O complex or an even worse 1 to 9 complexes for acetonitrile-water mixtures based on the above argument.

Several studies have been done on DMSO-water mixtures using NMR. Similar trends for H-H relaxation, O-H rotational correlation time, and translational diffusion constants have been observed, which all show a slowing of the mixture. All of the above times are slowest for the 1DMSO-2water mixture. The effect of DMSO on the diffusion of water seems to be more severe than the effect of water on the diffusion of DMSO.

The DMSO-water system has been investigated by quasi-elastic neutron scattering (QENS) at only one mole fraction, $X_D = 0.07$ [4]. The main findings being that the translational diffusion coefficient for water decreases from 2.7 cm^2/s for pure water to 1.1 cm^2/s for $X_D = 0.07$. The rotational time was also seen to increase form the pure value of 1.7 ps to 1.9 ps.

Skaf has presented intensive investigation of the DMSO-H_2O mixtures via simulation [10]. These simulations have presented values for the dielectric relaxation time, longitudinal dielectric relaxation time, O-H reoreintation time, S-O dipole reorientation time, translational diffusion constants for water and DMSO, and librational relaxation

times. The simulation results are for the most part in good agreement with the experimental values given above. It is seen that the simulations slightly overestimate the water-DMSO interaction and the DMSO self-diffusion coefficient.

Added insight can be obtained from the simulation results. The comparison of the single particle dipole time correlation function with the collective self-species dipole time correlation function shows the degree of cross correlation within a given species. For water the degree of self-association is large at all mole fractions, while DMSO self-association is small at all mole fractions. This suggests that water molecules tend to interact strongly upon mixing, a result that is not surprising. The DMSO relaxation on the other hand is closer to the single particle relaxation. The dielectric relaxation time constant, τ, is given by the integration of dipole density time correlation function, $\Phi(t)$. Simulations allow $\Phi(t)$ to be broken down into self and inter-species contributions. At high DMSO mole fractions, the DMSO contribution dominates, and at high water concentrations, the water contribution dominates. The important difference is that the water contribution at high water concentrations is much slower than pure water, while the DMSO contribution is much less affected at high DMSO concentrations. Near equimolar concentrations the inter-species term dominates, and reaches its maximum at X_D=0.33. In all cases, the inter-species contribution is always slowest.

The longitudinal dielectric relaxation, which is more sensitive to fast dynamics, is considered to be more relevant to solvation dynamics. For high water mole fractions, the fast librational relaxation, characteristic of pure water, is seen. The magnitude of this librational component rapidly decreases with the addition of DMSO. For all mixtures the diffusional relaxation is longer than in either of the pure solvents. When the longitudinal

dielectric relaxation is analyzed in terms of its contributions from water, DMSO, and cross terms it is seen that the cross terms are large and negative. This is common and has also been reported for methanol-water mixtures [22]. The negative cross terms accelerate the relaxation by canceling with the positive long-time contributions from water and DMSO. Simulation results show that this cancellation is most effective for high DMSO concentrations, resulting in relaxation very similar to the pure solvent.

Calculation of the far infrared spectra for the mixtures is also of interest [10]. The calculated far infrared spectrum of DMSO is featureless and centered at 50 cm^{-1}. The addition of water has very small effects on this band, indicating that the DMSO librations are relatively unaffected by water. The calculated librational band for water is also featureless and peaks at about 680 cm^{-1}. The addition of DMSO to water has two effects. The first is the band peak shifts to its maximum value of 800 cm^{-1} for $X_D = 0.33$ mixture. This shows that the fast reorientation of water is most hindered at $X_D = 0.33$. The second effect is the splitting of the band, which becomes more prevalent as the DMSO concentration increases. This feature is attributed to the creation of the 2DMSO-1H2O complex, which results in a trapped water molecule having reduced interactions between its oxygen atom and the surroundings. This results in more facile spinning of the oxygen atom in the direction perpendicular to the molecular plane, giving rise to the lower energy 630 cm^{-1} band.

Part Two

Quasi-elastic Neutron Scattering (QENS) Experiments

I Introduction

Neutron scattering is a powerful tool for the examination of static and dynamic properties of solutions [37,38]. Neutron scattering techniques take advantage of the neutron's wave-particle nature and its electric neutrality. These two qualities allow the neutron to probe materials in the same manner as X-ray diffraction, but with greater penetration due to the lower interaction of neutrons with electrons. When a neutron beam is incident on a sample two types of scattering can occur, figure 2.4. The first type is elastic scattering, in which there is no transfer of energy between the neutron and the sample. This type of scattering is useful in determining structural features of solids and liquids. The second type of scattering involves the gain or loss of energy through interaction with the sample. This is referred to as inelastic scattering. Transfer of energy is followed by the scattering vector Q shown in figure 2.4. In this figure k is the wave vector given by the relationship

$$\hbar k/2\pi = mv \qquad 2.1$$

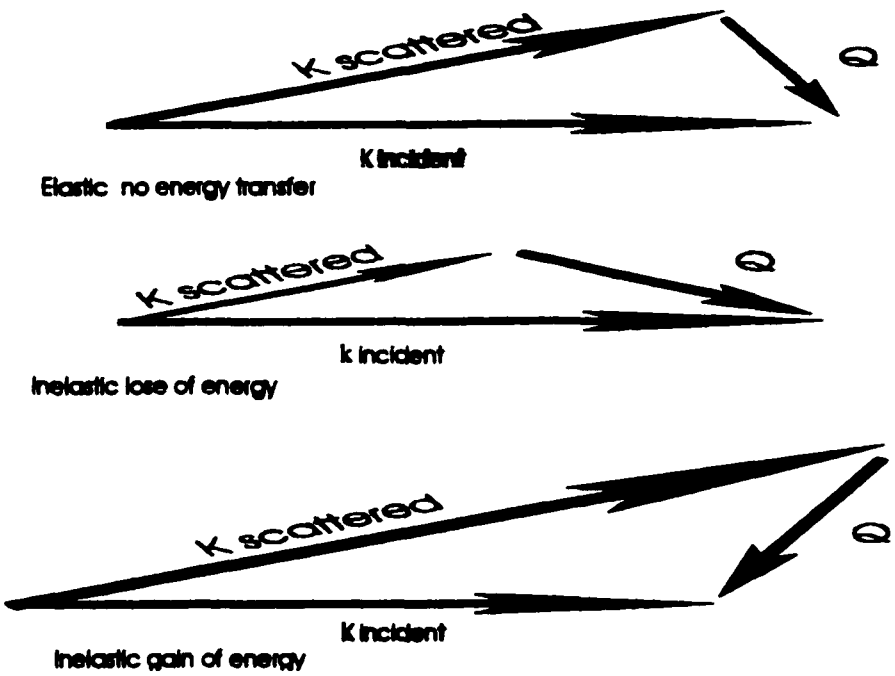

Figure 2.4 Elastic (top) and inelastic (bottom two) scattering of a incident neutron with wave vector k incident. Scattering direction and energy transfer are determined by the Q vector.

where h is Planck's constant, m is the neutron mass, and v is velocity. From figure 2.4 it can be seen that Q depends on the incident and final wave vectors. Energy transfer from the sample to the incident neutron can be analyzed in terms of the motions of the sample, as discussed below.

II. Results and Analysis

A. Materials

Deuterated samples were purchased from Cambridge Isotope. Water was purified using a Milli-Q filtration system. DMSO (ACS) grade was dried over molecular sieves and filtered through 2 μm nylon filters. Samples were prepared by weight. Samples were run in Aluminum cells holding ~ 1 ml of sample. Vanadium was used to determine the instrument response.

B. QENS Spectrometer

The data were collected using the QENS spectrometer at Argonne National Laboratory's Intense Pulsed Neutron Source [36]. High energy neutrons from a pulsed spallation source are slowed using a solid methane moderator. This beam is chopped resulting in a "white" beam of neutrons with a pulse length of approximately 75 microseconds. This beam is incident on the sample with useful energies ranging from approximately 1.5 to 200 meV. For quasielastic experiments incident energies from about 1.5 to 8 meV corresponding to energy transfers of –1.5 to 5 meV were analyzed. Data were

collected at 21 Q's ranging from 0.38 to 2.63 $Å^{-1}$, as defined by the scattering angle and neutron velocity (see figure 2.4, and following paragraph).

QENS works by analyzing the final neutron energies. This is done by Bragg diffraction of the scattered beam. A variety of Bragg angles select final energies ranging from 2.95 to 3.49 meV depending on the exact Bragg angle that each detector makes relative to its respective analyzer crystal bank. The energy transfer is determined from the total time-of-flight (moderator-sample-analyzer-detector). This is the quantity recorded when the neutron hits the detector. The Bragg angles are fixed and only the incident beam energies are swept, corresponding to different times-of-flight. The energy transfer is the difference between incident and final energies.

C. Scattering Model

Following Teixeira *et al.*, the inelastic contribution to the scattering function is written as a convolution of rotational and translational motions [34]. These motions are assumed to be decoupled in order to make the model tractable. This assumption is questionable for water samples, but has been used extensively for the analysis of a variety of water environments [34,35]. The scattering function is therefore given as

$$S(Q,\omega) = [\exp(-Q^2\langle u^2\rangle/3)]\, T(Q,\omega) \otimes R(Q,\omega) \qquad 2.2$$

$$T(Q,\omega) = \Gamma_t(Q) / [\, \pi(\Gamma_t^2(Q) + \omega^2)\,] \qquad 2.3$$

$$\Gamma_t(Q) = L^2Q^2 / \{6\tau_0[1+(L^2Q^2/6)]\} \qquad 2.4$$

$$R(Q,\omega) = j_0^2(Qa)\delta(\omega) + (1/\pi)\Sigma\,(2l+1)j_l^2(Qa)\,\{\, l(l+1)D_r \,/\, \{[l(l+1)D_r]^2 + \omega^2\}\,\} \qquad 2.5$$

$$D_t = L^2 / (6\tau_0) \qquad 2.6$$

$$\tau_r = 1/(6D_r) \qquad 2.7$$

Where the exponential gives the probability that the neutron is scattered, $\langle u^2 \rangle$ is the Debye–Waller factor, T is the Lorentzian translational diffusion term, R is the rotational diffusion term, Γ is the FWHM for jump diffusion over mean jump distance L, τ_0 is the average residence time between jumps, D_t is the translational diffusion constant, a is the radius of gyration (taken as 0.98 angstroms), j_l are spherical Bessel functions, D_r is the rotational diffusion constant, and τ_r is the rotational time constant.

D. Mixture Results

Results for H-bond lifetimes (residence time), translational diffusion constants, and rotational time constants are given in table 2.1.

Table 2.1 Translational diffusion constants, H-bond lifetimes, and rotational time constants for water in DMSO-water mixtures as determined by QENS.

XDMSO	D_t (10^{-5} cm^2/sec)	$\tau_{H\text{-}bond}$ (ps)	τ_r (ps)
0.0	2.5 ± 0.07	1.57 ± 0.12	1.07 ± 0.08
0.11	1.2 ± 0.04	3.1 ± 0.3	1.17 ± 0.06
0.25	0.93 ± 0.06	7.1 ± 0.8	1.46 ± 0.1
0.33	0.65 ± 0.05	7.2 ± 1.1	1.50± 0.1
0.50	0.64 ± 0.06	9.2 ± 1.3	1.22 ± 0.05

III Discussion

Analysis of S(Q,ω) results in the determination of the hydrogen bond lifetime, the translational diffusion constant, and the rotational diffusion constant all shown in table 2.1.

The hydrogen bond lifetime has been determined via simulation for pure water and for the $X_D = 0.33$ mixture [5]. The simulation results give water-water H-bond lifetimes of 1.2, and 3.3 ps respectively. The water-DMSO lifetime is given as 4.8 ps at $X_D = 0.33$. The pure water lifetime is in good agreement with QENS result of 1.57 ps. For mixtures the QENS results are averaged over water-water and water-DMSO H-bonds. The QENS results are about a factor of two larger than the simulation lifetimes at $X_D = 0.33$, and show a steady increase in H-bond lifetime with DMSO concentration. This result is consistent with the water-DMSO hydrogen bond being stronger than the water-water H-bond.

NMR and simulation have determined the translational diffusion constants for DMSO-water mixtures. The NMR results [13] along with our QENS results are shown in figure 2.5. It can be seen that our results are in good agreement with NMR and simulation results, showing that the strong interactions are effective in slowing down the mixtures considerably.

The results for the rotational time constant for water are shown in figure 2.6. These results are consistent with strong H-bonding. τ_r has a maximum at $X_D = 0.33$ which is consistent with the 1DMSO-2water complex. These results are also consistent with trends determined by simulation [10] and NMR [15] for the O-H vector single particle relaxation times, and with NMR proton relaxation times [13]. The values determined by NMR are highly sensitive to the model parameters, which has lead to values that range from 0.1 ps for proton relaxation [13] to values from 1.9 ps for the O-H vector of pure water[15]. The value for the O-H vector single particle relaxation constant for mixtures have been reported with values ranging from 8 ps [15] to ~17 ps [33] at $X_D = 0.33$, depending on the choice of constants in the models. All the above measurements (including ours) suffer from the

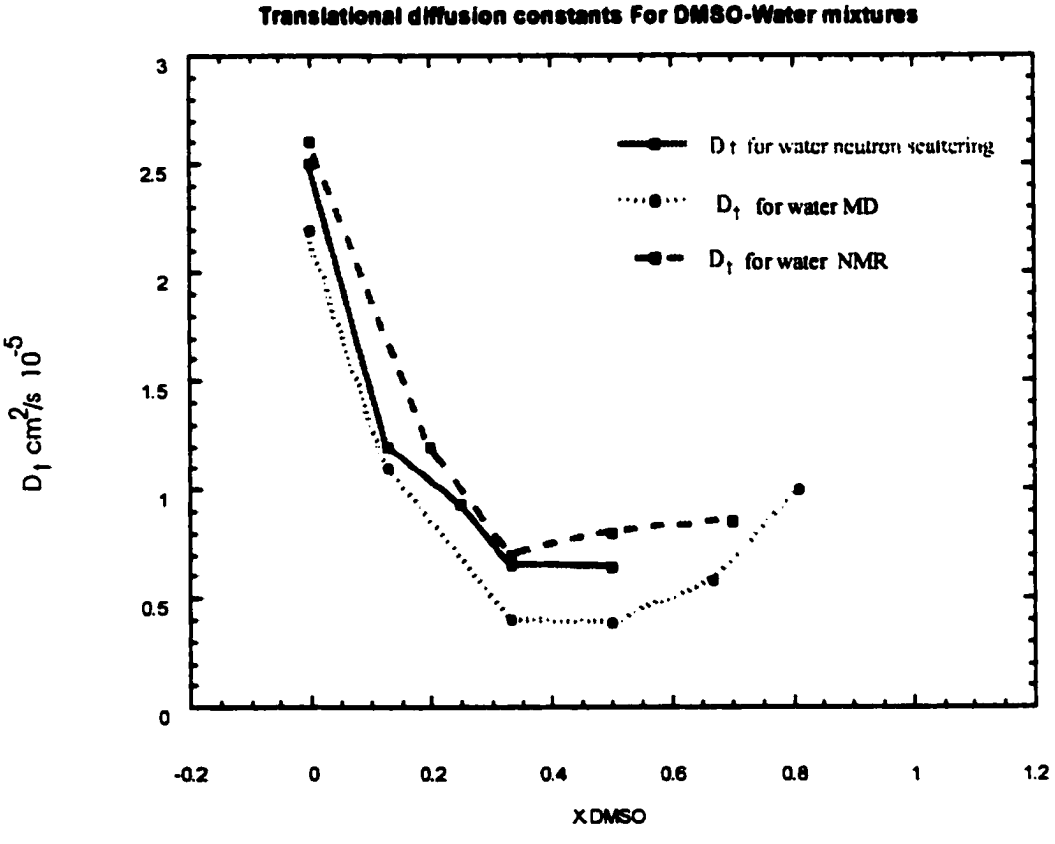

Figure 2.5
Translational Diffusion constants for DMSO-water mixtures. Results from simulation, QENS, and NMR are given. See text for references.

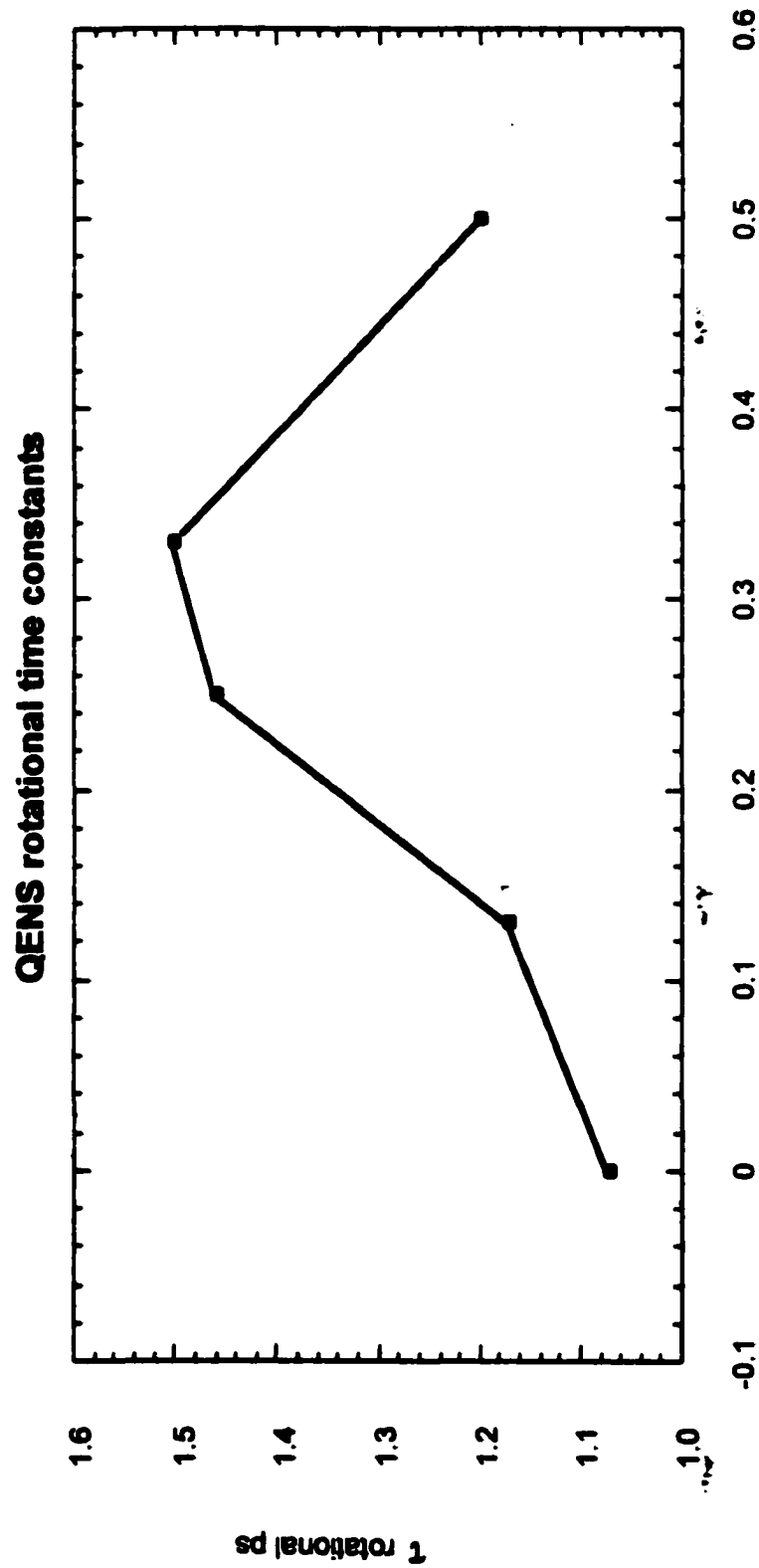

Figure 2.6
Rotational time constants for DMSO-water mixtures determined by QENS

assumption that the water rotation is isotropic. The formation of complexes with long lifetimes may make this assumption invalid. The main difficulty with the NMR analysis is the determination of the intra and intermolecular contributions. As mentioned above the assumption of uncoupled rotation and translation are also inherent in the models, which will cause further problems [34,41,42]. We have chosen our analysis to be comparable with other neutron scattering experiments on water. These experiments have been directed at such things as the behavior of water at different temperatures [34] and in restricted environments [35]. Our results are interesting in the strong effects on both translation and rotation of water at room temperature. Limitations of the model make quantitative analysis difficult, but the effects of H-bonding of the mixtures on water can be clearly seen.

Part Three

Fluorescence Upconversion

I Solvation Dynamics in the Pure Solvents

The solvation dynamics of water have been well studied by both experiment and simulation. Water, as mentioned in the introduction, was one of the earliest solvents modeled and was important for the discovery of inertial relaxation [17]. Due to its small size and mass, water has very small moments of inertia, which results in large inertial relaxation of the SRF. Due to its hydrogen bonding, water also displays a large librational relaxation due to the frustrated rotations of the hydroxy group under the influence of the H-bond restoring force. These librations show up in the far-infrared spectrum as a broad peak centered at 680 cm^{-1}. Simulations and experiments show that these two relaxation mechanisms result in water having an ultrafast relaxation [17,18,19,21]. SRF's determined by experiment place 50% or more of water's relaxation occurring within the first 55 fs [19]. Unfortunately these experiments, even with very good time resolution, do not resolve the ultrafast water response. Simulations predict even more, 70% to 90%, of the relaxation to occur in an even shorter time scale (as low as 25 fs!)[17,20]. Recent experiments using photon echo spectroscopy also agree with these even faster numbers and show that they are primarily due to solvation [21]. These predictions depend on the nature of the solute, as can be seen in several simulations [17,20]. This is primarily due to the extent of solute-solvent

hydrogen bonding that occurs. These hydrogen bonds can be rapidly destroyed, slowly replaced, or damped by solute-solvent interaction leading to a increase or decrease in the relaxation. Solute size is also seen to affect the extent of hydrogen bonding to the solute, with hydrogen bonds decreasing with increasing solute size [22,23]. After this fast relaxation, a diffusional relaxation occurs which has a time constant of about 500fs. In summary, water has one of the fastest SRF's possible due to small moments of inertia, high degree of librational relaxation, and high polarity. Since our probe, C153, is not soluble in water, a related Coumarin ,C343, is used in the above experiments. However, the results should be comparable.

Both experiment and simulation have also studied the solvation dynamics of DMSO. Compared with water two things stand out: 1) DMSO's inertial response is slower, and 2) DMSO lacks librational relaxation. Both experiments and calculations put DMSO's inertial time constant at about 200 fs [24]. This slow time compared to water is expected due to the rather large increase in mass (18g/mol compared to 78g/mol). The abscence of a librational response is also expected due to the non-associative nature of DMSO. The SRF for DMSO is slower on all time scales with Horng *et al.* reporting two additional diffusional components with time constants of 2 ps and 11 ps [24]. The 11 ps component has a rather small amplitude and the average relaxation time is given as 2 ps. The SRF of DMSO is typical of a non-associating polar liquid.

II Simulations of Ionic Solvation Dynamics in DMSO-Water Mixtures

Simulations on ionic solvation of DMSO-water mixtures have been published by Day and Patey [25] and by Laria and Skaf [26]. Day and Patey look only at the equimolar

mixture where as Laria and Skaf have run X_D = 0.0, 0.25, 0.50, 0.75, and 1.0. I will therefore refer to the more complete simulations by Laria and Skaf. In this study the initial state was equilibrated to a neutral Cl atom, and at time zero a step function charge was created. Solvation dynamics were investigated for both cationic and anionic solutes. For pure water it is seen that the cation has a larger librational response accounting for 80% of the relaxation and lasting 300 fs. The anion librational response accounts for 55% of the relaxation and lasts for 100 fs. The smaller librational response for the anion is due to the stronger H-bonding to the solute, which results in a stronger damping. For pure DMSO the anion relaxation is slightly faster than the cation and both SRF's lack any significant librations. The DMSO response is also slower as mentioned above.

For the solvent mixtures the results are very different. The anion response displays the usual fast response followed by a slower response that increases with the DMSO concentration. Separation of the SRF into DMSO and water contributions shows that the water response becomes increasingly slower with the addition of DMSO. The DMSO response shows a fast over relaxation resulting in a negative SRF. These results arise from the DMSO being initially attracted to the new charge, having its methyl groups actually drawn closer to the negative ion. This is followed by the slow replacement of the DMSO by the translational diffusion of water to the anion. Therefore, the high DMSO concentrations have the slowest response due to the long time necessary for water translation. These results agree with other simulation results mentioned in the introduction [27]. The long diffusional relaxation makes estimating the average SRF almost impossible based on dielectric data or other dynamic experiments, and shows the importance of preferential solvation in these simulations.

For the cation, the SRF's are very different. All cationic SRF's are similar to the pure DMSO response. The water response is follows dielectric relaxation trends for the cation, as can be seen from the separation of the SRF's into their water and DMSO contributions. The water contribution has a librational response that is slowest for the X_D = 0.25 and X_D = 0.50, and a diffusional relaxation that follows the trends for dielectric relaxation given above. It is interesting that the X_D = 0.75 water response is slowest for the anion, but fastest for the cation. The amount of fast response is also smallest for the anion and largest for the cation. The DMSO response stays very close to that of pure DMSO, with the exception of X_D = 0.25. For X_D = 0.25, an over relaxation is once again observed that is really due to the final equilibrium state favoring a higher proportion of water, rather than an over relaxation per se.

The dynamics for both the cation and anion are highly influenced by the equilibrium configurations of the initial and final states. From table 2.2, it can be seen that the average relaxations do not follow any trend established above in the experimental review. It should be noted at this point that the solute used in the following experiment (C153) is much larger, and multipolar in both the ground and excited state compared with the Cl atom used in the simulations.

Table 2.2 Simulation results (Laria and Skaf [26]) for <τ> DMSO-water

X DMSO	<τ> Cl^+ (ps)	<τ> Cl^- (ps)
1.0	0.50	0.33
0.75	0.56	3.3
0.50	0.35	3.1
0.25	0.75	1.2
0	0.11	0.17

III Results and Analysis

A. Materials

DMSO (ACS grade) was purchased from Aldrich and dried overnight on molecular sieves. DMSO was then filtered through 2 μm nylon filter, before mixing. Water was purified with a Mili-Q filtration system (18 MΩ/cm). Solutions were mixed using volumetric pipets, or the appropriate quantities determined by weight. Coumarin C540A (C153) was purchased from Exciton and used without further purification. C153 was added to the solution to give an optical density of approximately one or less in a 2mm cell. This yielded an O.D. of less than 0.5 in the 1 mm flow cell. The dye solutions were then filtered through a 2 μm nylon filter. The low DMSO mole fraction samples were allowed to sit overnight to ensure that the dye was equilibrated.

B Steady-State Spectra

Absorption spectra were taken on HP 8452A diode array spectrophotometer and Cary 2400 spectrophotometer. The spectrophotometers gave results that were indistinguishable and the Cary results were used for the time zero analysis. Fluorescence spectra were collected on AVIV ATF105 spectrofluorometer. The steady-state spectra shown in figure 2.7 were fit to lognormal fits described in the Introduction. First moment (fm, average) values (see chapter I) for the peaks were determined and are given in table 2.3.

C Time Zero Analysis

The parameters for time zero analysis are given in table 2.4. Time zero analysis is described in the Introduction. The parameters δ and σ indicate the shift and variance of the gaussian function, $\rho(\delta,\sigma)$, which, when convoluted with the nonpolar absorption spectrum

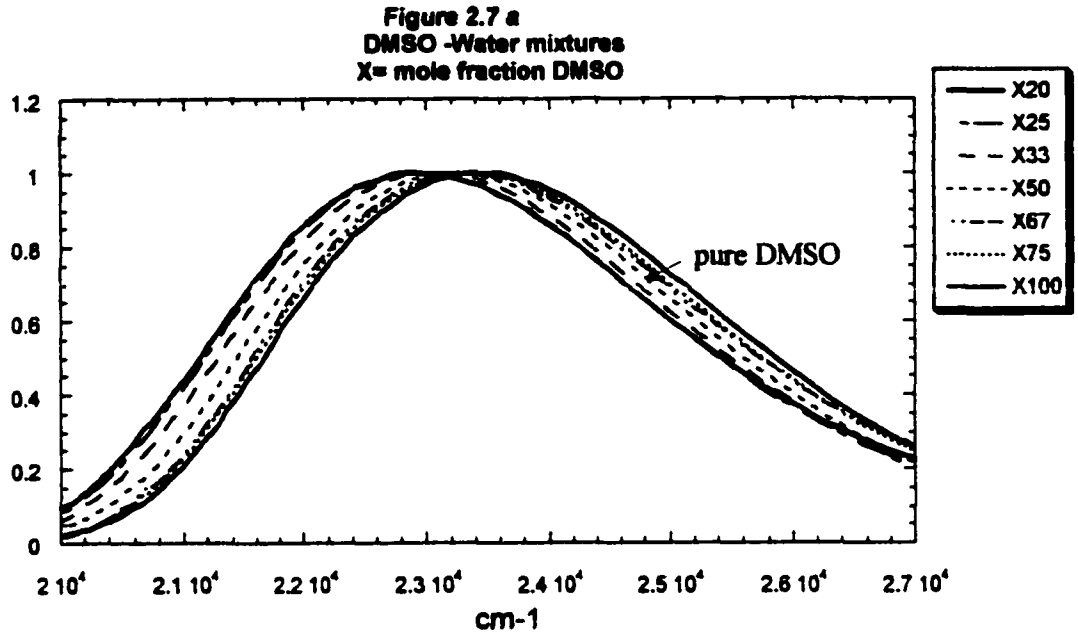

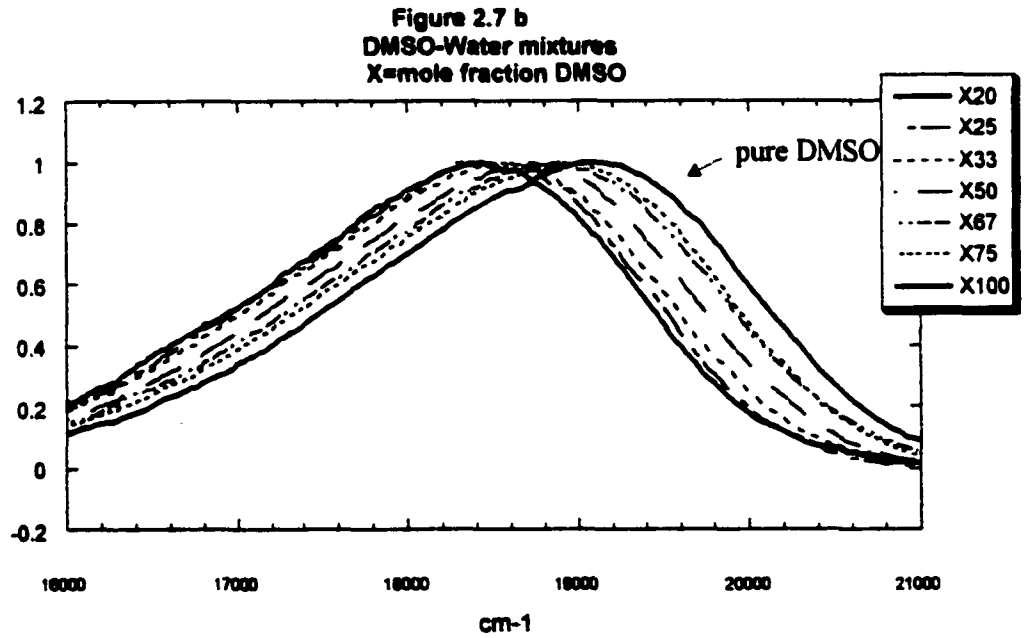

Figure 2.7
a) Steady-state absorption spectra for DMSO-water mixtures.
b) Steady-state fluorescence spectra for DMSO-water mixtures.

Table 2.3 Steady-state spectra results DMSO-water, see Chp. 1 Introduction for lognormal fitting definitions.

X DMSO	Fluorescence fm (cm^{-1})	Fluorescence FWHM (cm^{-1})	Absorption fm (cm^{-1})	Absorption FWHM (cm^{-1})
1.0	18983	2685	23498	4142
0.75	18824	2659	23426	4145
0.67	18768	2708	23415	4237
0.50	18628	2641	23267	4124
0.33	18477	2626	23121	4201
0.25	18417	2567	23031	4251
0.20	18360	2597	23024	4360

Table 2.4 Time-zero results DMSO-water. See Chp. 1 Introduction for time-zero analysis technique.

X DMSO	Time-zero fm (cm^{-1})	δ_0 (dm^{-1})	σ (dm^{-1})	Time Zero FWHM (cm^{-1})
1.0	20548	205	77	3510
0.75	20502	211	78	3520
0.67	20446	210	78	3524
0.50	20337	232	78	3532
0.33	20203	245	79	3540
0.25	20176	254	85	3605
0.20	20157	258	88	3636

give the polar absorption spectrum. The values of the fm time-zero frequencies, δ and σ are given in table 2.4.

D. Fluorescence Upconversion

Time dependent Stokes shifts were determined using the fluorescence upconversion technique and time zero analysis described in the Introduction. Instrument response functions for this set of experiments ranged from 200 to 250 fs. Fluorescence decays were measured in 17fs steps for 3 ps, 200 fs steps for 25 ps, and 2.5ps steps for 500 ps. The reconstructed time resolved spectra were fitted to lognormals and the first moment frequencies used for determining C(t) as described in the Introduction. C(t)'s were easily fitted to both three exponential and to stretched exponential fits, no difference in goodness of fit was discernable

IV Discussion

As can be seen from figure 2.8, the DMSO-water mixtures present SRF's that are quite complicated. The SRF's give average relaxation times that are non-monotonic, and well fitted by three exponentials. The result for pure DMSO is in good agreement with that reported by Maroncelli [24]. Water is conspicuous in its absence due to C153's insolubility in this solvent. The following discussion will be presented in four parts: A) Ultra-fast relaxation, B) Diffusional relaxation, C) Static spectra, preferential solvation, and C153's charge distributions, D) Summary and Conclusions

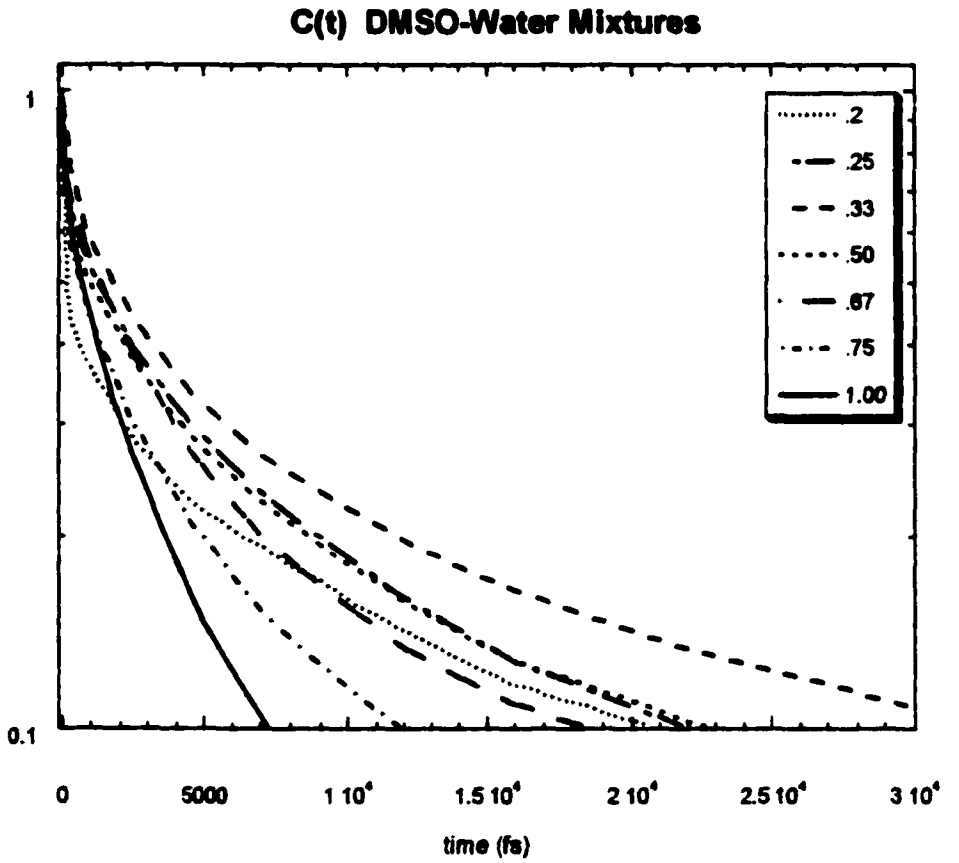

Figure 2.8
C(t) for DMSO-water mixture plotted on semi-log scale. DMSO mole fraction is given in the legend.

A Ultra-fast Relaxation

Based on the solvation dynamics of the pure solvents we expect a very large inertial relaxation for mixtures containing water and DMSO. As mentioned in the introduction to this chapter, pure water has very small moments of inertia resulting in an incredibly fast inertial $\tau_{1/e}$ that is just 15 fs. The much more massive DMSO on the other hand has a inertial $\tau_{1/e}$ that is calculated to be more than ten times greater, ~ 170ps. Both these responses are faster than the time resolution of our experiment (IRF ~ 250 fs), therefore the inertial and librational time periods are not resolved. I will refer to both of these responses as the (missed) fast response.

This fast response is the harder to decipher, but an idea of the magnitude missed response is can be determined from the use of time zero analysis. Time zero analysis is described in the Introduction. The relevant values from the time zero analysis are shown in table 2.4. The amount of the response missed varies largely with mole fraction, being largest for $X_D = 0.2$ and smallest for $X_D = 0.33$. The response that occurs in the first 250 fs has varying contributions from both inertial single particle motions and collective librational motions. For high water concentrations the inertial response will decay rather quickly and large percentage of the missed response will be collective. For DMSO the majority of the missed response is inertial. With this in mind I will try to make some educated guesses as to what is happening in the missed portion of the SRF based on the inertial solvation frequencies and the amplitude of the missed response. This will involve the use of a combination of results from linear response and continuum theory, to determine what the inertial solvation frequency would be in a binary, linearly responding, continuum fluid. Although this will give us some idea of the inertial frequency, it will not tell us at

what point the relaxation becomes collective. The collective behavior demonstrates drastically different mole fraction dependencies that are very slow due to the strong intermolecular interactions.

From figure 2.8 it can be seen that the fast response is non-monotonic in mole fraction, reaching its slowest value at $X_D = 0.33$. Here the fast response is slower than in either of the pure solvents. The initial response is fastest for the $X_D = 0.20$, which is substantially faster than any of the other mixtures. Other mixtures show initial responses that are slightly faster than DMSO for the first several hundred femtoseconds. All the mixtures show curve crossings with DMSO with the exception of $X_D = 0.33$. These curve crossings occur between 300 – 400 fs in most mixtures, while $X_D = 0.75$ crosses at ~ 1ps, and $X_D = 0.20$ crosses at ~ 2ps due to its comparatively large fast response. The values for the tri-exponential fits are given in table 2.5. The value of the first exponential τ_1 for DMSO is consistent with previously reported values, and with the inertial time period of ~ 200 fs predicted by simple inertial and dipole density considerations [24]. For the mixtures, τ_1 peaks at $X_D = 0.33$ with a rather large value of ~ 500 fs, and is between 77 fs and 200 fs for the remaining mixtures. These values for τ_1 should not be over emphasized for two reasons: 1) they are not resolved experimentally, and 2) they are closely associated with the intermediate τ_2 values therefore, small changes to τ_1 can be offset by changes to τ_2 without diminishing the quality of the fit. Nonetheless, large differences, such as those between $X_D = 0.20$ and $X_D = 0.33$ are easily identified. The values of τ_0 are given in table 2.6. The τ_0 values go through a maximum at $X_D = 0.33$. It is obvious from figure 2.8 that these mixtures do not follow a simple mole fraction dependence for the fast response, and that the fast water relaxation is unexpectedly low for the water rich side.

Table 2.5 C(t) fit parameters for DMSO-water mixtures. Amplitudes (a) and times (τ) for three exponential fits of the SRF's are given.

X DMSO	a1	τ1 (fs)	a2	τ2 (fs)	a3	τ3 (fs)
0.20	0.55	77	0.24	2666	0.21	31026
0.25	0.32	113	0.44	2887	0.24	27949
0.33	0.38	462	0.44	5215	0.18	67599
0.50	0.39	139	0.43	3708	0.18	44393
0.67	0.26	92	0.55	2629	0.19	32816
0.75	0.42	162	0.46	3062	0.12	46904
1.0	0.37	204	0.51	2200	0.12	15459

Table 2.6 Relaxation times for DMSO-water mixtures. Characteristic solvation times and dynamic Stokes shifts are given.

X DMSO	τ_0 (fs)	$\tau_{1/e}$ (fs)	$\langle\tau\rangle$ (fs)	stretched tau (fs)	stretched alpha (fs)	$\Delta\nu$ (cm^{-1})
0.20	139	950	7170	923	0.27	1814
0.25	333	3050	7976	2878	0.41	1777
0.33	1093	3825	14191	4317	0.46	1747
0.50	345	2625	9538	2521	0.37	1730
0.67	330	2730	7688	2821	0.46	1700
0.75	360	1700	6760	1613	0.41	1697
1.00	493	1500	3130	1498	0.53	1588

One of the first things we want to know is the period over which inertial relaxation is important. This allows us to predict the amount of collective behavior included in the missed response. Within the inertial period we expect that the molecules behave individually and that the velocity time correlation function G(t) is well approximated by the single particle $G_s(t)$. Following INM analysis, G(t) can be expanded in a power series of time, giving the following for the SRF

$$C(t) = 1 - (1/\langle \delta\Delta E^2 \rangle) \int (t-\tau)\, G(\tau) \delta\tau \qquad 2.8$$

$$C(t) = 1 - (1/\langle \delta\Delta E^2 \rangle)\, (\tfrac{1}{2} t^2 G_0 + {}^1/_{24}\, t^4 G_2 + \cdots) \qquad 2.9$$

$$C(t)_{inertial} \approx \exp\{ -(t^2/2)\, \omega_s^2 \} \text{ with } \omega_s^2 = \{G_0/\langle \delta\Delta E^2 \rangle\} \qquad 2.10$$

where G_0 is a pairwise sum over solute-single solvent contributions to $\langle \Delta \dot{E}^2 \rangle$, and $C(t)_{inertial}$ ignores contributions beyond t^2. In the equation 2.10 we can see that, in linear response, ω_s^2 (as well as C(t)) contains a static, $\langle \delta\Delta E^2 \rangle$, contribution, and a dynamic, G(t), contribution. The static contribution is the square of the average fluctuation in the solvation energy. This term is proportional to the solute-solvent interaction energy, and is also affected by solvent-solvent correlations. The solvent-solvent correlations serve to damp the fluctuations. The static contribution reveals that smaller motions are needed to relax strongly interacting solvents due to smaller net changes to the system upon perturbation. The dynamic term is related how fast the individual solvent motions are, and below we will relate it to the moment of inertia of the solvent for the free streaming portion of the SRF.

Binary mixtures contain two solvents. This will make G(t) a function containing cross terms, but the fact that G_0 is a sum only over single solvent molecules will be helpful. This lets us express the solvation frequency in terms of the individual components. Using continuum approximations and ignoring translations as described in ref [28]

$$G_0 = G_{0\,DMSO} + G_0\ water \tag{2.11}$$

$$C(t) = \exp\{(\tfrac{1}{2} t^2)\,(1/\langle \delta\Delta E^2 \rangle)\,\{\, G_{0\,DMSO} + G_0\ water\,)\,\} \tag{2.12}$$

$$= \exp\{(\tfrac{1}{2} t^2)\,(1/\langle \delta\Delta E^2 \rangle)\,(\langle \Delta \dot{E}_D^2 \rangle + \langle \Delta \dot{E}_w^2 \rangle)\} \tag{2.13}$$

$$= \exp\{(\tfrac{1}{2} t^2)\,[1/(k_B T)(1-1/\varepsilon)]\,[(\mu_D^2 \langle w1_D^2 \rangle / 3\Sigma r_{iD}^4) + (\mu_W^2 \langle w1_w^2 \rangle / 3\Sigma r_{iw}^4)]\} \tag{2.14}$$

$$= \exp\{(\tfrac{1}{2} t^2)\,[1/(k_B T)(1-1/\varepsilon)]\,[(4\pi\rho/3)\{(X_D \mu_D^2 \langle w1_D^2 \rangle) + (X_w \mu_w^2 \langle w1_w^2 \rangle)\}\} \tag{2.15}$$

$$\langle w_l^2 \rangle = 2k_B T / I_{avg} \tag{2.16}$$

where ε is the static dielectric constant, ρ is the number density, X_α is the mole fraction, μ_α is the dipole moment, I_{avg} is the average moment of inertia perpendicular to the dipole, and $\langle w1_\alpha^2 \rangle$ is the average squared rotational frequency in a direction perpendicular to the dipole. These equations show that the dynamic response is now dependent on the quite different inertial responses of water and DMSO. The static response on the other hand is just a continuum function of the static dielectric constant. Calculation results for DMSO-water mixtures using equation 2.15 are shown in figure 2.9. Here it can be seen that water's small moment of inertia dominates, resulting in a rapid monotonic decrease in the $\tau_{1/e}$ with the addition of water to DMSO. These results indicate that for most of these systems, the missed response includes collective behavior for up to 200fs. For real systems the non-linearity and

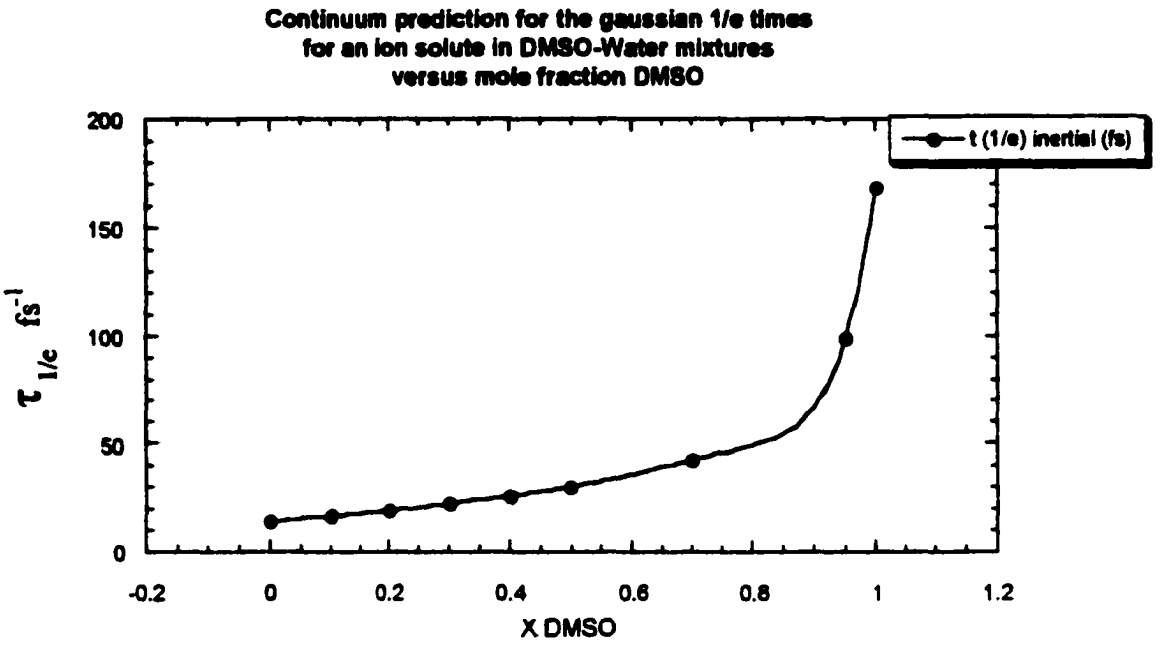

Figure 2.9
Continuum predictions for the $\tau_{1/e}$ times for inertial relaxation, given by $\tau_{1/e} = 1.4(\omega_s)^{-1}$. The high non-ideality is due to waters fast response and high number density. Line is to guide the eye. See text for method.

molecular nature of the solvent will cause deviations in the solvation frequency and its effectiveness in relaxing the system.

Based on the predicted inertial frequencies given above and the experimental inertial amplitudes, it appears that the efficiency of the inertial motion in relaxing the SRF depends on mole fraction. This may be a solute specific effect, an effect of the solvent mixture itself, or a combination of the two. If we think of this in terms of the solute dependent initial and final equilibrium states, when there is a large change in the solvent configuration, inertial motions will relax a smaller portion of the response. If we think of the solvent mixture itself then inter-species interactions will be involved that will be evident in the longitudinal dipole density relaxation of the mixtures. We will look at the longitudinal dielectric relaxation next.

Insight into the SRF's can be gained from the longitudinal dielectric relaxation given by simulation. In simulations of methanol-water mixtures Skaf and Ladanyi [22] note that for their large solute, the SRF parallels results found for the longitudinal dipole density time correlation function $\Phi_L(t)$. They suggest that this result indicates that the large solute does not disturb the solvent structure significantly. Consequently the SRF reflects collective dipolar fluctuations, that are strongly dependent on the solvent H-bonding interactions. Comparison of the simulation results for the SRF's and $\Phi_L(t)$'s for the large solute water-methanol mixtures shows that the inertial responses of the SRF are well predicted by the inertial responses of $\Phi_L(t)$. The amplitude of the librational response is also strongly correlated, but seems to be consistently larger for $\Phi_L(t)$. For the four hundred femtoseconds shown, the crossing of the pure methanol $\Phi_L(t)$ response with mixture $\Phi_L(t)$ responses are at the same as the pure methanol SRF crossings with the mixture SRF's.

Based on the good agreement above, and given the large size of C153 we might expect similar results for the DMSO-water SRF's.

Recently Skaf has reported $\Phi_L(t)$'s for a variety of mole fractions ranging from $X_D = 0.13$ to $X_D = 1.0$ [10]. Skaf's results show that there are significant changes in the inertial response when as increases X_D from $X_D = 0.13$ to $X_D = 1.0$. In less than 200 fs the decays are easily distinguished based on degree of relaxation: $X_D = 0.35 < 0.50 < 0.13 < 0.81 < 1.00$, with DMSO relaxed ~ 80% and $X_D = 0.35$ relaxed ~ 55%. As expected the DMSO response is purely inertial in this time period, whereas the $X_D = 0.13$ response includes a high degree of collectivity. Skaf did not simulate pure water, but it is given by Impey *et al* [39]. Their results show that the inertial response is responsible for ~ 80% of the relaxation of Φ_L for pure water. The rest of the relaxation is complete in ~ 800 fs. Relaxation components past ~ 200 ps reflect diffusive motion for all mixtures. The inertial responses of both components are seen to increase monotonically with their respective concentrations.

These results can be clarified by inspecting the intra-species $\Phi_{dd}(t)$, $\Phi_{ww}(t)$ and inter-species $\Phi_{dw}(t)$ contributions to $\Phi_L(t)$ given by Skaf. It is well known that the $\Phi_L(t)$ decays faster than $\Phi(t)$ due to the decreased importance of rotational diffusion [32]. This is due to the fact that the single molecule contributions are positive while the pair contributions are negative. This results in the pair contributions canceling the diffusive portion of $\Phi_L(t)$, which leads to faster relaxation dominated by inertial and librational motions. For example, it has been shown that for methanol-water mixtures, the formation of water pockets at high methanol concentrations reduces the size of the negative methanol water cross term, and therefore reduces the inertial effectiveness. Examination of Skaf's DMSO-water results shows that cross term cancellation is important. The fastest relaxation occurs at $X_D = 0.81$

where the cancellation of $\Phi_{ww}(t)$ and $\Phi_{dd}(t)$ by $\Phi_{dw}(t)$ is very close to complete, resulting in inertial dominance of the relaxation. It should be noted that the addition of 19% water to DMSO results in a relaxation that is only slightly slower than pure DMSO, with the $\Phi_{ww}(t)$ relaxation being negligible. On the other hand addition of 13% DMSO to water results in much less effective cancellation, and the contribution to the relaxation from DMSO is not trivial. At $X_D = 0.35$ the cancellation of $\Phi_{ww}(t)$ and $\Phi_{dd}(t)$ with $\Phi_{dw}(t)$ is least effective, resulting in the least effective simulated inertial relaxation.

The $\Phi_{dw}(t)$ terms result from the averaging over all DMSO-water pairs. When there is a high degree of long-range, anti-parallel alignment, $\Phi_{dw}(t)$ will be large and negative [29,30]. Skaf's results show that $\Phi_{dw}(t)$ is negative for all mixtures and is large for all mixtures except $X_D = 0.81$. This can be explained in terms of the complexes being formed. For the mole fractions that are rich in water, the 1DMSO-2water complex results in large negative values of $\Phi_{dw}(t)$. This is consistent with simulation and neutron scattering results that show DMSO is incorporated into the tetrahedral structure of water. For the DMSO rich side, $\Phi_{dw}(t)$ is a factor of three smaller than for the water rich side. This can be accounted for by the formation of the 2DMSO-1water complex that brings two DMSO's into anti-parallel alignment about a single water. This structure places the water dipole out of alignment with DMSO dipoles, which may result in the lower value of Φ_{dw}.

For mole fractions $X_D \leq 0.50$ $\Phi_{dw}(t)$ is large, negative, and grows a small amount as the water concentration increases. It is also apparent that the amount that $\Phi_{dw}(t)$ in these mixtures is almost identical. As mentioned above the degree of cancellation follows the following trend: $X_D = 0.33 < 0.50 < 0.13$. This trend is consistent with the decrease in the single particle relaxation rates due to complex formation which are slowest at $X_D = 0.33$.

Therefore the increased diffusional tail appears due to the incomplete cancellation of pure and cross contributions due to the slowing of the pure component responses compared to the cross contribution. For high DMSO concentrations, $\Phi_{dw}(t)$ is small, as mentioned above, and to because the DMSO structure is little affected by the addition of water, $\Phi_{dd}(t)$ and the total SRF are very similar to pure DMSO.

These results are in good agreement with the experimental SRF's except that the effectiveness of the inertial response is greater for the simulated $\Phi_L(t)$'s than it appears for the experimental SRF's. For example, the inertial relaxation accounts for over 80% for $\Phi_L(t)$ for DMSO, whereas the inertial relaxation for the experimentally determined DMSO SRF is closer to 40%. Maroncelli reports a slightly higher experimental value of 50% with a slightly longer time constant for DMSO. These results imply that, as with methanol-water mixtures, $\Phi_L(t)$ is effective in predicting the nature of the solvent relaxation for large solutes, but overestimates the degree of inertial response for C153. The decreased inertial response compared to simulations may be a general trend due to the specific nature of C153, and the accuracy of the model [31]. Maroncelli and Kumar have shown that simulation results for C153 in methanol overestimate the fast relaxation due to the inadequacies of the solvent potential, which is too fast for both the SRF and dielectric relaxation. They also show that ignoring solvent polarizability can result in simulation results that are too fast. This would explain the smaller fast responses seen here for the experimental SRF's, but there may be other factors contributing. For instance, the experimental response for $X_D = 0.33$ appears extremely slow even with considerations above taken into account.

To get a better understanding of the efficiency of the inertial response we now turn to non-equilibrium simulation results. As mentioned above the efficiency of the inertial response depends on both static and dynamic factors. There is only a certain amount of rotation that can occur during the inertial period. The time in which this rotation occurs will be accounted for by the dynamic factor. The percent of the total relaxation this accounts for, on the other hand, is determined by the static considerations. This was well illustrated by Maroncelli *et al.* [28], who showed the effect of increasing the charge on dipolar dumbbell solvents. These solvents were identical except for the magnitude of the charges on the atomic sites, which varied from 0.1e to 0.5e. Since all the solvents had identical mass they all underwent ~10 degree inertial rotations, but the amount of relaxation that resulted increased dramatically with increasing charge. This reflects the fact that the solvents with large dipoles require smaller total rotations to relax the solvent. These results are described well by linear response, but there may be additional effects that lie outside of linear response. Laria and Skaf's simulation results for ionic solvation dynamics in DMSO-water mixtures show that the degree of inertial relaxation depends strongly on the charge of the ion solute [26]. In these simulations a neutral Cl, in equilibrium with the solvent, is given a step function charge jump. The SRF is then followed using the non-equilibrium simulation technique. For pure DMSO ~ 90% of the anion response is inertial versus ~ 60% for the cation. These simulations also allow separation of the water and DMSO contributions. When looking at the water response for $X_D = 0.75$ it is seen that the water's inertial response accounts for ~ 50% of water's SRF for the cation versus ~ 12% for the anion. The reason for these discrepancies are the differences in the final equilibrium configurations for the cation and anion (they both start from the same configuration). If we

consider the pure DMSO case, the ~ 90% inertial relaxation has to be viewed in the light that both the neutral and anion Cl prefer to be solvated by the methyl group. This will result in small motions being very effective in relaxing the system. The cationic case will require larger rotational motions since it prefers the DMSO oxygen. In the case of the X_D = 0.75 mixture the relaxation of water is also very different for the two ions. For the anion large translations are needed by water to reach equilibrium making the inertial response less effective. In view of these results the discrepancies in the inertial amplitudes between the SRF's and the simulated $\Phi_L(t)$'s are probably not only mixture specific, but also due to "non-linear" changes in the solvent distribution. This can be due to large differences in the equilibrium initial and final states, that are not well represented by the natural, solute independent, fluctuations of linear response. Separation of these two effects is not possible, but in the case of X_D = 0.33 the rather large deviation may indicate that the reordering the solvent structure is greatest here. This may be due to the higher order of the 1DMSO-2H_2O mixture surrounding the ground state of the dye, and suggest that the excited state of C153 is capable of competing with the solvent-solvent interactions. Discrepancies for mixtures that are less ordered would therefore be smaller. The solvent reorganization will also be affected by the large changes in the charges on C153. This will be especially important for DMSO-water mixtures since DMSO is more effective in solvating cations while water is more effective in solvating anions. Skaf's results show that the difference in solvation energies can be as large as a factor of two for the two pure solvents.

In summary, the experimentally measured SRF's are not resolved for the first ~ 250 fs. Time zero analysis allows the determination of how much of the response was missed, which gives us an indication of how effective the early response is in relaxing the system.

We see that the amount of the missed relaxation is maximum for the $X_D = 0.20$, is smallest for $X_D = 0.33$, and intermediate for the remaining mixtures. The result for $X_D = 0.20$ is not surprising due to the fast relaxation of pure water. In contrast, the result for $X_D = 0.33$ is surprising since the solution is 67% water. The simple continuum prediction for the solvation frequency at $X_D = 0.33$ shows that it should still be close to that of pure water. This points to a reduction in the effectiveness of the inertial response or equivalently an increase in the importance of diffusion. This can be explained in terms of solvent specific and solute specific contributions. For the solvent effects we turn to the longitudinal dielectric relaxation data of Skaf. Separation of $\Phi_L(t)$ into pure and cross terms reveals that cancellation is affected by the type of complex formed, and the changes in the pure component relaxations. This is important for water rich mixtures, where cancellation effects are minimum for the 1DMSO-2water mixture. The result is decreased inertial amplitude and increased diffusional relaxation. For high DMSO concentrations, the SRF is similar to pure DMSO because water is ineffective in changing DMSO's structure. The inertial amplitudes are consistently larger for $\Phi_L(t)$'s compared to the SRF's. This behavior has been seen for other solvents and is probably due to the model. Nonetheless the simulations show that pure solvent effects are responsible for the decreased inertial amplitude in the mixtures and the trends agree with trends in the SRF's. However the decreased inertial effectiveness appears to be more pronounced for the $X_D = 0.33$, which may be due to specific interactions of the solvent with C153. This may be due to the greater organization of the ground state dye solvation shell, which would undergo the highest degree of change upon excitation. This effect is increased in importance due to the binary nature of the solvent, which results in one solvent being more capable of solvating a

particular solute site. Upon excitation this may require large changes in the solvent distribution and orientations, which down plays inertial motion.

B. Diffusional Relaxation

The diffusional relaxation for the mixtures also shows non-monotonic behavior with mole fraction. Rotational and translational diffusion is responsible for the response that follows the inertial and librational relaxation. Experimental dielectric relaxation experiments are well suited for studying this part of the solvent response. We will therefore compare our results with the dielectric relaxation data of Kaatze *et al.* [11]. As discussed above relaxation of the SRF is collective. This will result in $\langle \delta\Delta E\delta(0)\delta\Delta E(t)\rangle$ containing both pure and cross terms. For the inertial period these cross terms could be ignored, but here they will be important. As seen above, slowing of the pure solvent diffusion can result in increased diffusional contributions.

The principal dielectric relaxation time constants given by Kaatze are shown in figure 2.2 along with continuum predictions for the longitudinal relaxation time for a dipole. Here the role of complex formation is seen, with τ_s reaching a maximum around $X_D = 0.33$. The results shown are for the mixtures, but, as seen in part two of this chapter, the diffusional relaxations for the individual components follow the same trend. The role of strong H-bonding between DMSO and water are seen. From figure 2.2, we can see that the diffusional time constant is expected to be greatest for $X_D = 0.33$ and should decrease as follows: $X_D = 0.33 > 0.50 > 0.25 > 0.67 \approx 0.20 > 0.75$. Examination of table 2.6 shows that the stretched exponential time constants and the $\tau_{1/e}$ values are in poor agreement with these values, while the $\langle\tau\rangle$ values follow the above trend exactly. The lack of agreement

for $\tau_{1/e}$ is not surprising due to the large non-diffusional contribution at early times. Figure 2.10 shows that the τ_2 and τ_3 time constants from the three exponential SRF fits follow trends in τ_L and τ_D respectively. The average relaxation times are dominated by the long diffusional relaxation resulting in times that are much larger than in either of the pure solvents. In figure 2.11, $<\tau>$ is plotted versus $\tau_D/5$, and the dependence of $<\tau>$ on τ_D can be seen explicitly. As with the fast responses discussed above, the behavior at $X_D = 0.33$ stands out. The plot of $<\tau>$ versus mole fraction DMSO shows a strong spike at $X_D = 0.33$, suggesting it is strongly affected by diffusional processes. This is consistent with a large degree of reorganization of the solvent, indicating that the rotations and translations required to relax the $X_D = 0.33$ mixture are larger than the other mixtures.

C. Steady-State Spectra, Preferential Solvation, and C153 Charge Distribution

From the steady-state spectra shown in figures 2.7, it can be seen that the addition of water to DMSO results in a monotonic red shift in the fluorescence and absorption spectra. This can be attributed to the increased polarity of the solvent since water has a static dielectric constant that is ~1.7 times greater than DMSO's.

Figure 2.12 shows the positive deviation from ideality for the graph of the fluorescence fm frequency versus $F(\varepsilon)$. This deviation appears to be more sharply curved at high water concentrations and deviates towards higher energy. The fluorescence frequencies increase with DMSO concentration indicating that the non-ideality arises from preferential solvation of the C153 excited state by DMSO. This is to some extent not surprising given that C153 is not soluble in water. Skaf and Ladanyi have observed similar results for methanol water mixtures, where their large solute was preferentially solvated by

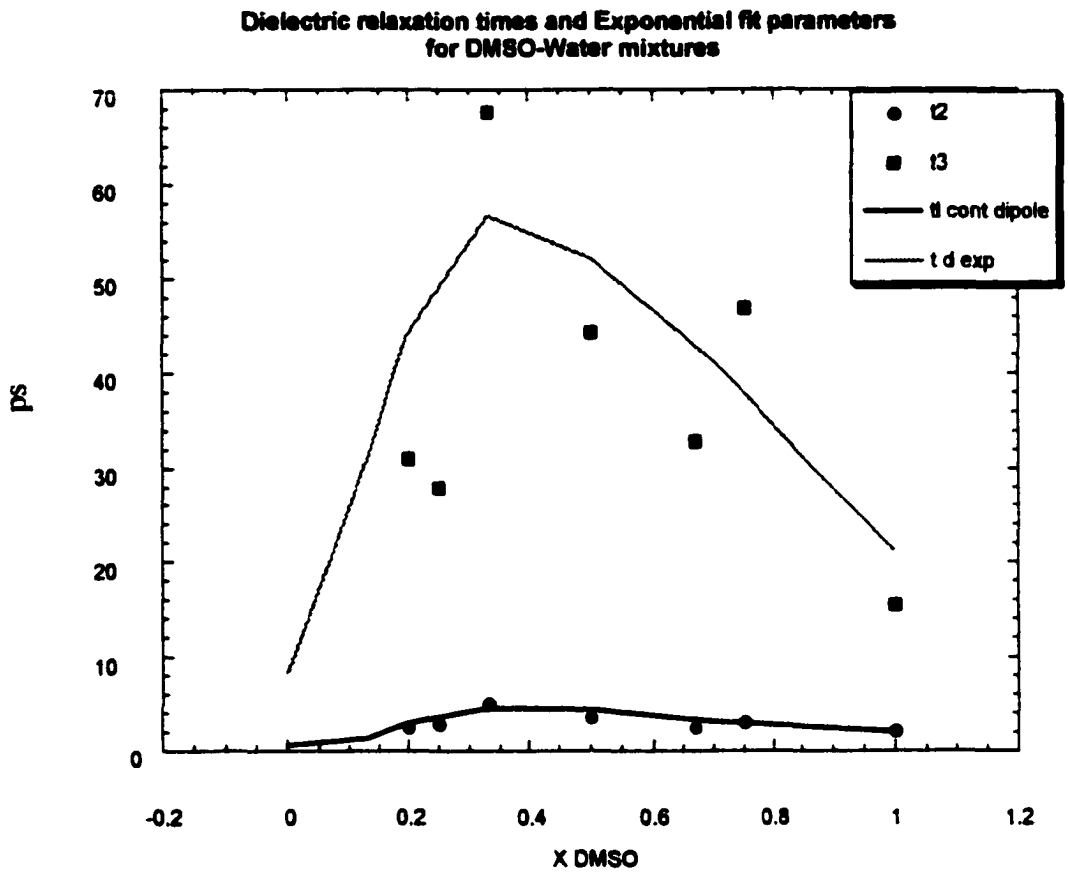

Figure 2.10
Time constants from exponential fits of C(t) versus mole fraction DMSO. Dielectric values are the same as figure 2.2.

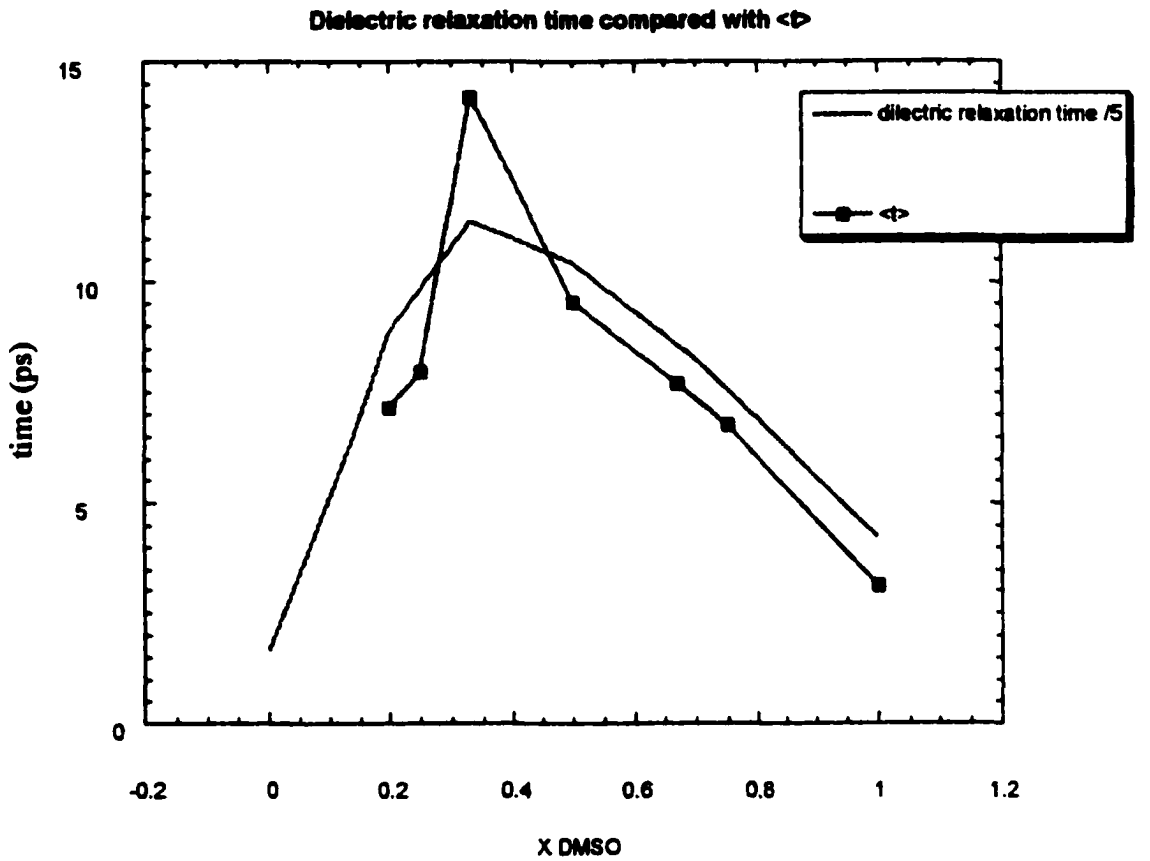

Figure 2.11
Dielectric relaxation time and average SRF time versus mole fraction DMSO. Dielectric data are same as figure 2.2 divided by five.

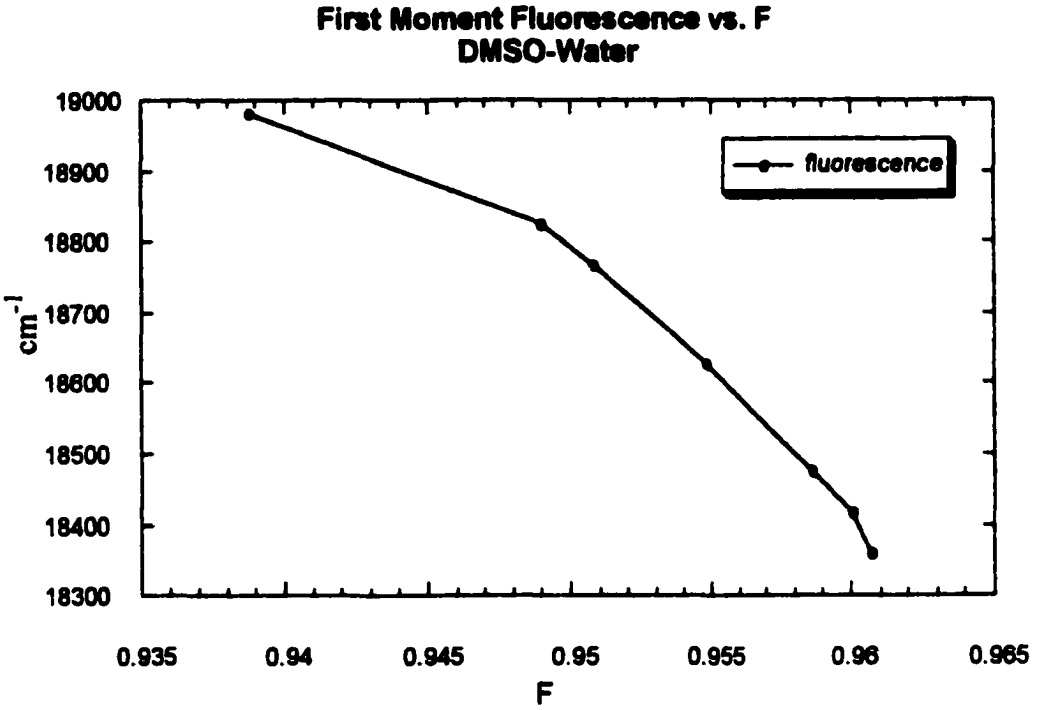

Figure 2.12
First moment fluorescence frequencies versus the continuum reaction field. See text for fm and reaction field equations. High water concentrations are at low fm frequencies. First moments are in cm^{-1}. Pure water is not included due to insolubility of C153. Deviations are to higher frequency (towards DMSO).

the methyl group. The hydrophobic nature of their solute above was due to its large size, which prohibited the hydrogen bonding to the solute. Solvation of C153 by the DMSO methyl groups would allow the DMSO oxygens to form hydrogen bonds with water in a way similar to that suggested for methanol. Therefore preferential solvation in these mixtures is likely due to the maximization of H-bonds. In the case of pure water, this results in the insolubility of C153. Since C153 is likely solvated preferentially in both the ground and excited state it is hard to say how large an effect this will have on the SRF's. It is likely that the excited state will result in an environment that is more friendly to water than the ground state, but the same may hold for DMSO.

Laria and Skaf's results show that full positive and negative charges should be solvated by DMSO and water, respectively. As shown in figure 2.13, atomic sites in C153 undergo substantial changes upon excitation [40]. The nitrogen atom 1 in particular undergoes a large charge reversal, while atoms 12, 14 and 17 receive a greatly enlarged electron density. These types of changes may result in large reorganization of the solvent shells. The carbonyl oxygen 18 has the largest negative charge, making it the most suitable for H-bonding to water, but undergoes very little change.

D Summary and Conclusions

From the discussion above it is seen that the SRF's are affected by a combination of both solvent and solute specific factors that apply to both the inertial and diffusional responses. Separation of these two factors is not possible. The DMSO-water interactions have several effects that depend on the solvent alone, and complexation of the solvent

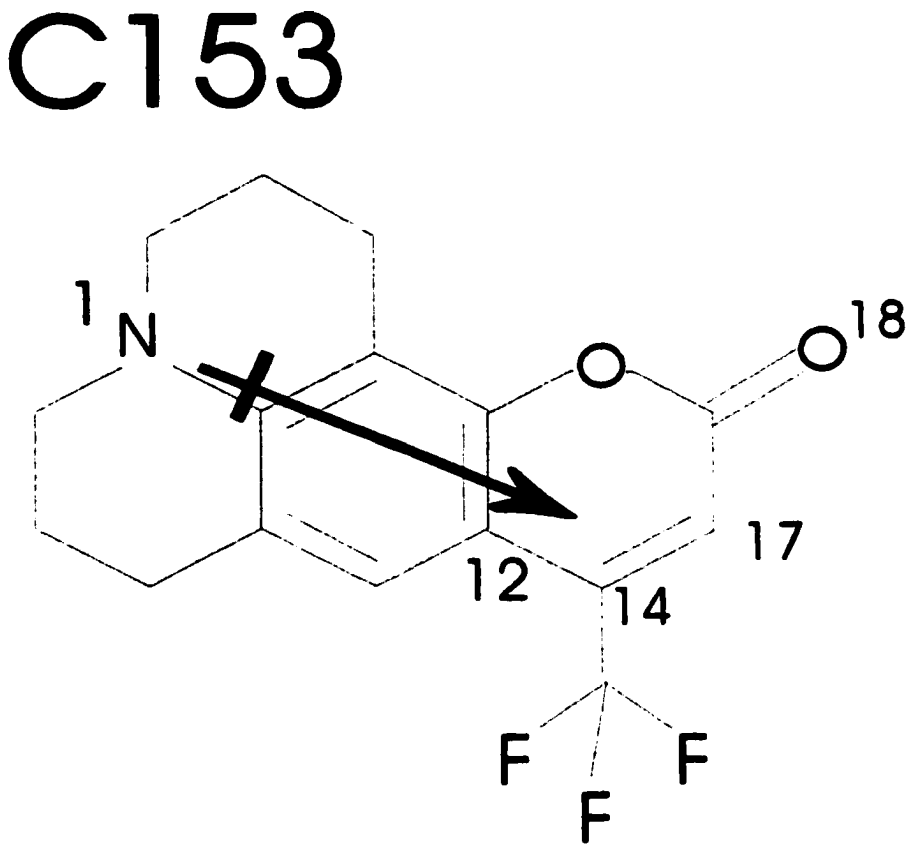

Figure 2.13
C153, the dipole shows the direction of charge transfer which results in the appearance of the charge difference between S0 and S1 as a dipole. Atoms 1, 12, 14, and 17 undergo the largest changes. Atom 18 has the largest negative charge and is most likely to hydrogen bond, but only undergoes a small change in charge. Atom numbering follows that of Chicos *et al.*[40]

mixture is seen to have large effects on the SRF's. One of these effects is to slow down the diffusional motions of DMSO and water due to strong H-bonding. Binary solvents result in cross terms for $\Phi_L(t)$, which will cancel to differing degrees with the pure solvent responses. For water rich mixtures, where the 1DMSO-2water complex predominates, slowing of the pure solvent relaxation results in poor cancellation with the cross term, which does not change much at these compositions. This increases the amount of diffusion necessary to relax the system and therefore decreases the effectiveness of the inertial relaxation. For DMSO rich mixtures, where the 2DMSO-1water complexes are favored, the cross terms are smaller and the water response is negligible. Therefore these mixtures have SRF's that are close to the pure DMSO response. These results confirm that $\Phi_L(t)$ is effective at predicting SRF's for large solutes with small charge densities.

These results may be further complicated by the initial and final equilibrium states of the solvent in the presence of C153. These states may be beyond fluctuations attainable by the solvent itself. C153 is likely preferentially solvated by DMSO in both the ground and excited state, but to what extent is unknown. Solvent reorganization will be increased by the large changes in site charges mentioned above, and the preference of DMSO and water for cations and anions respectively. Further investigation of the equilibrium configurations via simulation is warranted.

The experimental results found here are not directly comparable with the simulation results done on these mixtures. This is primarily due to the large effects that the small ions have on the equilibrium states of the mixtures. It is reassuring to see that for our results the dielectric data and $\langle\tau\rangle$'s are in agreement. The lack of agreement for simulations is due to

the large preferential solvation of the anion by water, and is not reproduced here for our hydrophobic solute.

These results show that binary mixtures are capable of producing environments and dynamics that are well outside those of the individual components alone. Here these results are a function of strong interspecies interactions and are not necessarily intuitive. The availability of simulation data is incredibly helpful in analysis of these systems, and I would like to thank Prof. Skaf for preprints of his work on these systems.

References for Chapter Two

1. H. L. Clever, and S. Pigott, J. Chem. Thermodynamics, 3, 221 (1971).
2. J. M. G. Cowie, and P. M. Toporowski, Can. J. Chem. 39, 2240 (1961).
3. E. Tommila, and A. Pajunen, Suomen Kemistilehti B. 41, 172 (1968).
4. G. Safford, P.C. Schaffer, and P. S. Leung, J. Chem. Phys. 50, 2140 (1969).
5. A. Luzar, and D. Chandler, J. Chem. Phys. 98, 8160 (1993).
6. I. Vaisman, and M. Berkowitz, J. Am. Chem. Soc. 114, 7889 (1992).
7. E. Hawlicka, Polish J. Chem. 70, 821 (1996).
8. A. K. Soper, and A. Luzar, J. Phys. Chem. 100, 1357 (1996).
9. A. Luzar, J. Mol. Liqs. 46, 221 (1990).
10. M. Skaf, J. Chem. Phys. A. 103, 10719 (1999).
11. U. Kaatze, R. Pottel, and M. Schafer, J. Phys. Chem. 93, 5623 (1989).
12. I. Borin, and M. Skaf, J. Chem. Phys. 110, 6412 (1999).
13. K. J. Packer, and D. J. Tomlinson, Trans. Faraday Soc. 67, 1302 (1971).
14. T Tokuhiro, L. Menafra, and H. Szmant. J. Chem. Phys. 61, 2275 (1974).
15. B. C. Gordalla, and M. D. Zeidler, Mol. Phys. 59, 817 (1986).
16. I. Borin, and M. Skaf, Chem. Phys. Lett. 296, 125 (1988).
17. M. Maroncelli, and G. R. Fleming, J. Chem. Phys. 89, 5044 (1988).
18. P. F. Barbara, and W. Jarzeba, Adv. Photochem. 15, 1 (1990).
19. R. Jimenez, G. R. Fleming, P. V. Kumar, and M. Maroncelli, Nature, 369, 471 (1994).

20. J. S. Bader, and D. Chandler, Chem. Phys. Lett. 157, 501 (1989).

21. M. J. Lang, X. J. Jordanides, X. Song, and G. R. Fleming, J. Chem. Phys. 110, 5884 (1999).

22. M. Skaf, and B. M. Ladanyi, J. Phys. Chem 100, 18258 (1996).

23. C. F. Chapman, R. S. Fee, and M. Maroncelli, J. Phys. Chem. 99, 4811 (1995).

24. M. L. Horng, J. A. Gardecki, A. Papazyan, and M. Maroncelli, J. Phys. Chem. 99, 17311 (1995).

25. T. J. F. Day, and G. N. Patey, J. Chem. Phys. 110, 10937 (1999).

26. D. Laria, and M. Skaf, J. Chem. Phys. 111, 300 (1999).

27. T. J. F. Day, and G. N. Patey, J. Chem. Phys. 106, 2782 (1997).

28. M. Maroncelli, V. Kumar, and A. Papazyan, J. Phys. Chem. 97, 13 (1993).

29. P. Madden, and D. Kivelson, Adv. Chem. Phys. LVI (1984).

30. D. Kivelson, and H. Friedman, J. Phys. Chem. 93, 7026 (1989).

31. P. Kumar, and M. Maroncelli, J. Chem. Phys. 103, 3038 (1995).

32. see introduction

33. B. C. Gordalla, and M. D. Zeidler, Mol. Phys. 74, 975 (1991).

34. J. Teixeira, M. C. Bellissent-Funel, S.H. Chen, and A. J. Dianoux, Phys. Rev. A. 31, 1913 (1985)

35. K. W. Herwig, W. D. Dozier, J. S. Huang, Mater. Res. Using Cold Neutron Sources, [Proc.], 95-104, edited by P.Thiyagarajan, World Scientific, Singapore, (1999)

36. K.F. Bradley, Nuclear Instruments and Methods in Physics Research A270, 78 (1988)

37. R. Pynn, Los Alamos Science 19, 1 (1990)

38. M. Bee, *Quasielastic Neutron Scattering*, edited by D. J. Millen, Adam Higler, Bristol, (1988)

39. R. W. Impey, P. A. Madden, and I.R. McDonald, Mol. Phys. 46, 513 (1982)

40. F. Cichos, R. Brown, U. Rempel, and C. von Borcvyskowski, J. Phys. Chem. B. 103, 2506 (1999).

41. C.Liao, F. Sciortino, S. Chen, Phys. Rev. E. 56, 4231 (1997)

42. S.Chen, P.Gallo, F. Sciortino, P. Tartaglia, Phys. Rev. E. 59, 6708 (1999)

Chapter Three

Benzene-Acetonitrile

I The Benzene-Acetonitrile system

A Introduction

Benzene and Acetonitrile are two common yet very different solvents. The major difference between these solvents is their polarities. Acetonitrile is considered to be the prototypical non-associating highly polar solvent. Its small size and large dipole moment (~4D) give acetonitrile a rather large dipole density. Benzene, on the other hand, is much larger and lacks a permanent dipole. Benzene is a highly conjugated molecule and therefore has its own place as the prototypical aromatic solvent. The mixing of these solvents should therefore be intriguing, allowing us to move from the nonpolar to polar extremes of solvation dynamics.

B. Equilibrium Structure of Benzene-Acetonitrile Mixtures

The equilibrium structure of benzene-acetonitrile mixtures will be strongly influenced by the large dipole moment of acetonitrile. In the pure solvent acetonitrile adopts an anti-parallel dipole alignment. For the solid, this has been proposed to result in chains of aligned dipoles surrounded by anti-parallel chains [1]. For the liquid there is less

effective alignment but the trend for anti-parallel dipoles still dominates [2,11]. In contrast, benzene has its strongest interactions through its permanent quadrupole moment. This has led to a variety of proposed benzene dimers, including T-shaped, stacked, displaced stacked, and V shaped [3]. When the two solvents are mixed we expect that acetonitrile will tend to interact with itself more strongly than with benzene.

A number of studies have investigated the benzene-acetonitrile interactions [4-13]. Thermodynamic studies have revealed some interesting behavior. The excess enthalpy of mixing is positive for all mole fractions [4]. This indicates that the strong dipole interactions between acetonitriles are replaced by the weaker interactions with benzene. The small size of the excess enthalpies suggests that the interspecies interactions are not negligible, and offer a negative contribution. Examination of the excess volume [5], and the effective Debye temperature [6] offer further insight into the benzene-acetonitrile interactions. The excess volume is positive for acetonitrile rich mixtures and negative for benzene rich mixtures. For low X_b (acetonitrile rich mixtures), acetonitrile self-association is high, resulting in positive excess molar volumes upon the addition of benzene. In these cases, benzene cannot dissociate the acetonitrile clusters. For high X_b, acetonitrile clusters are broken and the acetonitrile monomers form an attractive rearrangement with benzene resulting in a negative excess molar volume. The excess effective Debye temperatures, which are functions of the ultrasonic velocity, density, and heat capacity of the mixtures, show similar results. Positive excess Debye temperatures are indicative of increased short-range order and lower compressibility. For acetonitrile rich mixtures the excess Debye temperatures are negative, while for benzene rich mixtures they are positive. This once

again suggests that compact rearrangements are formed between benzene and acetonitrile monomers at high benzene concentrations.

The nature of the benzene-acetonitrile interaction has been explored by NMR and infrared spectroscopies [7-10]. The NMR results are based on the shifts induced by the acetonitrile-benzene complexes. Benzene molecules are capable of producing ring currents that result in large high field shifts above, and below the benzene plane [7]. The large high field shift for the methyl protons of acetonitrile suggest that they reside over the benzene ring. This interaction may be thought of as a weak H-bond between the benzene pi electrons and the acetonitrile methyl groups. Schnieder [7] suggest that the cyanide group sits off the ring due to electron repulsion, and that it induces a dipole in benzene as shown in figure 3.1. Yadava *et al.* find the induced dipole moment to be 0.22 D for benzene-acetonitrile mixtures, in agreement with this prediction [8]. Mosier-Boss *et al.* find similar results form carbon 13 NMR, but suggest that the cyanide group sits over the benzene plane [9], these experiments were directed toward determining the equilibrium constants for the formation of acetonitrile dimers, and the arrangement in figure 3.1 seems more likely. Nonetheless Mosier-Boss *et al.* were able to show that the equilibrium constant for the formation of acetonitrile dimer is more than an order-of-magnitude smaller in benzene than in CCl_4 based on the carbon 13 shifts versus mole fraction. Jackowski has done further studies on the benzene-acetonitrile interactions via NMR and *ab initio* calculations [10]. The *ab initio* calculation results show several benzene-acetonitrile dimers. Most of the dimers agree with the structure proposed by Schnieder, that is weak H-bonds between benzene and acetonitrile. There is one exception in which the nitrogen acts as an electron

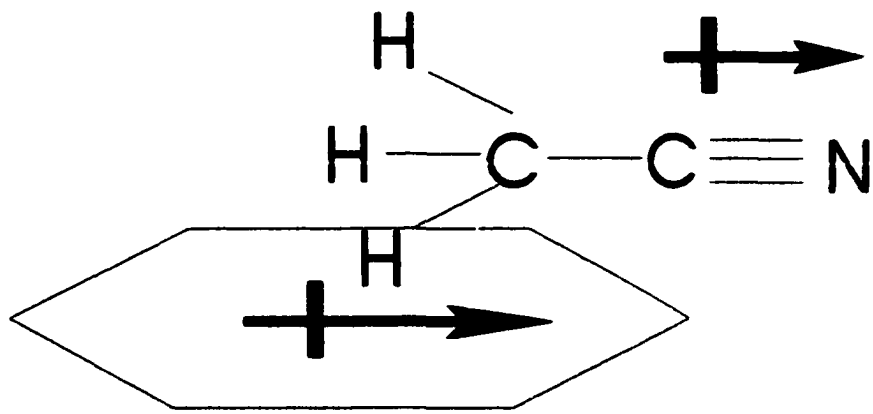

Figure 3.1
Benzene- Acetonitrile dimer suggested by Schnieder [7].

donor to benzene. Jackowski proposes that structures consisting of three benzenes surrounding the methyl group and one benzene interacting with the acetonitrile nitrogen will exist for benzene rich solutions.

Further evidence for benzene-acetonitrile H-bond interactions is found via infrared spectroscopy [13]. H-bonding leads to an increase in the C-H band intensities. Stolov *et al.* show that the intensity of the C-H band is large for pure acetonitrile suggesting that acetonitrile is capable of forming H-bonds with itself [13]. The intensity is seen be about half as large for acetonitrile-benzene mixtures, while benzene intensities are about twice that of CCl_4. Far infrared studies of acetonitrile in CCl_4 reveal the strong clustering of acetonitrile [12]. Peaks at 65, 75, and 90 cm^{-1} are assigned to the acetonitrile monomer, dimer, and clusters. From examination of the band shape upon dilution with CCl_4 it is seen that the clusters persist to mole fraction = 0.20 acetonitrile. Below mole fraction = 0.20, the clusters begin to break up. Similar behavior would be expected for benzene, with benzene being slightly more effective in breaking clusters.

The above studies suggest that acetonitrile-acetonitrile interactions will dominate in the mixtures. The benzene-acetonitrile interactions will be important for dilute mixtures of acetonitrile where the acetonitrile monomer will be prevalent. Acetonitrile is effective in inducing dipoles in benzene, and in increasing the order in benzene rich solutions.

C. Dynamic Benzene-Acetonitrile Experiments

Dynamic information on benzene-acetonitrile mixtures is less available. The most interesting experiment, dielectric relaxation, will also be less informative due to the nonpolar nature of benzene. However the available studies on the mixtures and related

systems are sufficient to predict the effects of mixing on acetonitrile and benzene. For benzene, are most interested in the rotation of the ring perpendicular to the C6 axis. This motion is effective for solvation, whereas the spinning around the axis is relatively ineffective. For pure benzene, rotation is anisotropic with the perpendicular rotation being much slower than ring spinning. This is not surprising since the spinning does not require displacement of the neighboring molecules. The perpendicular rotation on the other hand involves more steric hindrance. We will therefore be interested in how the addition of acetonitrile affects the perpendicular rotation of benzene. This has not been studied directly for benzene-acetonitrile mixtures, but has been studied for other benzene mixtures. From the simulation and NMR results of Laaksonen *et al.* it is seen that the perpendicular rotation of benzene in water is greatly hindered [14]. This is explained in terms of water's high degree of association and the ability of water's hydrogens to come into close proximity with benzene's pi cloud. Based on the excess functions described above the addition of acetonitrile to benzene results in structures that are less compressible and have a higher degree of organization than pure benzene. The formation of benzene-acetonitrile complexes should therefore result in slower perpendicular rotations for benzene.

For acetonitrile dielectric relaxation and NMR studies are insightful. Dielectric relaxation times τ_s for acetonitrile in benzene and CCl_4 solutions are reported by Subramanian *et al.* [15]. For both benzene and CCl_4 solutions τ_s increases from the neat acetonitrile value of ~ 4 ps to a maximum around $X_b = 0.20$, followed by a rapid decrease of τ_s with further dilution. The relaxation times are slightly slower in CCl_4 solutions than in benzene solutions. For benzene solutions τ_s reaches a maximum of ~ 6 ps at $X_b = 0.20$,

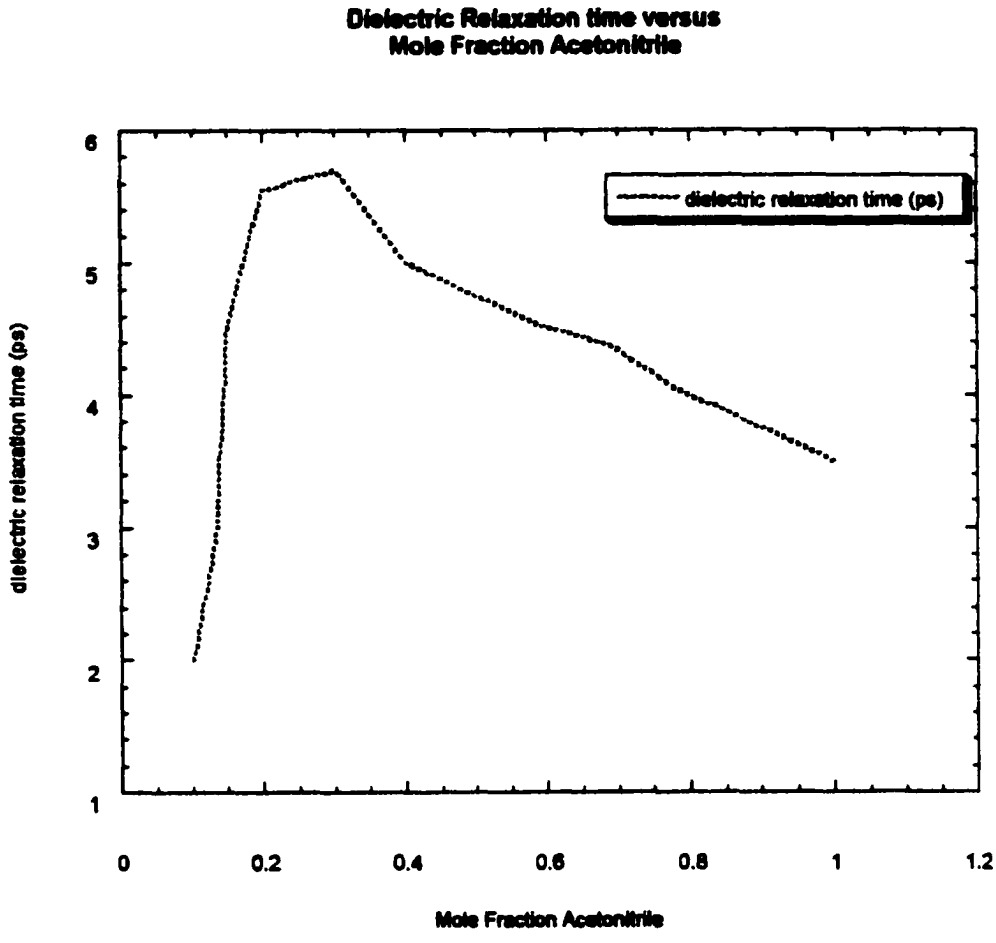

Figure 3.2
Dielectric relaxation times for acetonitrile in benzene, extrapolated from ref 15.

before rapidly decreasing to ~ 2 ps by $X_b = 0.10$,see figure 3.2. Subramanian *et al.* suggest that the maximum at $X_b = 0.20$ may be attributed to the formation of a stable complex mixture, but at the same time points out that the rapid increase in τ_s is consistent with the breaking of acetonitrile clusters. The above trend for τ_s is also seen in NMR single particle relaxation times in CCl_4 solutions. Tiffon *et al.* show that, at specific mole fractions, a plot of τ_s versus η/T is linear as the temperature is changed, where η is the viscosity [16]. However the same plot at constant temperature and varying mole fraction is non-linear, deviating at low acetonitrile concentrations to faster relaxations. Both the dielectric relaxation and NMR relaxation times agree with the far-infrared studies mentioned above, which reveal ACN clusters persisting to $X_b = 0.20$.

From the above studies the following conclusions can be drawn. Benzene rotations perpendicular to the ring plane should slow with the addition of acetonitrile due to a more compact and ordered arrangement. For acetonitrile, clusters will persist, except at high benzene concentrations. Breaking of clusters will result in a substantial increase for acetonitrile dielectric relaxation.

D. Solvation Dynamics in the Pure Solvents

Solvation dynamics of pure acetonitrile and pure benzene have been studied both experimentally and by simulations. Acetonitrile has been given special attention and is one of the most studied solvents to date. Benzene has received less attention, but has served as a prototype for the more recent investigations of nonpolar solvation.

Horng *et al.* have reported experimental results for the solvation dynamics of C153 in acetonitrile [17]. The relaxation has a large inertial component which accounts for ~ 70%

of the SRF in ~ 90 fs. The fast 90 fs time constant is due to acetonitrile's small moment of inertia. The inertial response is followed by a 630 fs component that accounts for the remaining ~ 30% of the relaxation. Several simulations have investigated acetonitrile's solvation dynamics. These simulations have been effective in determining the importance of inertial versus diffusional relaxation, rotational versus translational motions, single molecule versus pair contributions, and inner shell versus outer shell contributions [18-20].

The efficiency of acetonitrile's inertial response has been explained in terms of its high α factor [18]. The α factor is described in section III.D. This factor is proportional to the dipole density, and is related to the solvent's ability to quench fluctuations in the solvation energy, therefore decreasing the amount of motion necessary to relax the solvent. Alternatively, the inertial effectiveness can be viewed in terms of large negative pair contributions to the SRF. The negative pair contributions cancel the long time diffusional portion of the single molecule contributions to the SRF. These cancellations result from the long-range correlations of dipole pairs and show up for both the SRF and the longitudinal relaxation of the solvent. Acetonitrile's inertial effectiveness can therefore be thought of in terms of its high dipole density, or in terms of its long-range order, which are of course related.

Another interesting result from INM [20] and equilibrium [19] studies is the importance of rotations for solvation dynamics. Rotations are seen to dominate the solvation spectrum and account for 76.2% of the ultrafast relaxation even though 60% of the degrees of freedom are translational. Similarly the first shell and outer + cross contributions can be evaluated. Here it is seen that the first solvent shell is responsible for

the fast inertial relaxation, while the outer + cross contributions are negative and cancel the long time contribution from the first shell.

The experimental SRF for benzene has also been reported by Gardecki *et al.* [21]. The SRF was fit to three exponentials. The first is a 234 fs response that accounts for ~ 36% of the relaxation. This is followed by a ~ 2 ps response that accounts for an additional 60%. The small remainder relaxes with a ~ 25 ps time constant. From the above fit information it can be seen that benzene behaves very much like polar solvents, exhibiting inertial and diffusional behavior.

Reynolds *et al.* have investigated the nature of solvation dynamics for nonpolar solvents, such as benzene [22]. Of interest is the ability of nonpolar solvents to effectively solvate C153 despite the lack of permanent dipoles. To this end Reynolds *et al.* examined the interactions of the C153 charge distribution with the charge distribution of several nonpolar solvents. Their findings indicate that the ability of nonpolar solvents to solvate C153 comes from the polar bonds and non-zero charge distributions of the solvents. Benzene for example has a calculated dipole moment of 0.72D along the C-H bond, and a charge of + 0.14e on the hydrogen. Reynolds *et al.* show that the excited state solvation shifts are well accounted for by the interaction of the permanent charge distribution of the solvent molecules with C153's charge difference. Furthermore, the shifts can be well approximated by placing a multipole at the center of mass of the solvent while maintaining the full atomic representation. It is therefore not surprising that benzene displays the normal bimodal relaxation typical of solvation dynamics.

Also of interest are the longitudinal dielectric relaxation studies of Perng and Ladanyi [23]. The authors report the k dependent dielectric relaxation of several solvents

including both acetonitrile and benzene. For the low k values, the effects of pair cancellation are seen to be strong for the polar acetonitrile solvent, in agreement with the above discussion. Benzene shows much less pair cancellation resulting in a smaller inertial component and increased diffusional relaxation. The pair cancellation for benzene is non-zero, however, and is seen to be more effective than for the other nonpolar solvent examined, CO_2. These results agree with the discussions in Chapter One. Here the alpha factor that relates the single particle relaxation to the SRF should be small, or in other words the quenching of the solvent fluctuations will be small.

Finally, as mentioned above, we should expect rotations perpendicular to the benzene plane to be effective for solvation dynamics. This is due to the symmetry of the solute-solvent interaction. Spinning of the ring will have little effect on the solute-solvent interaction compared to rotating benzene in a manner that would change the solute-H distance.

II Results and Analysis

A. Materials

Benzene and acetonitrile (ACS grade) were purchased from Aldrich and dried overnight on molecular sieves. The solvents were then filtered through 2 μm nylon filters. Solutions were mixed using volumetric pipets or the appropriate quantities determined by weight. Coumarin C540A (C153) was purchased from Exciton and used without further purification. C153 was added to solution to give an optical density of approximately one in a 2mm cell. This results in optical densities of 0.5 or less in the 1 mm flow cell. The dye

solutions were then filtered through a 2 μm nylon filter. It was found that a freeze-pump--thaw cycle increased run to run stability for high benzene concentrations.

B. Steady-State Spectra

Absorption spectra were taken using HP 8452A diode array spectrophotometer and Cary 2400 spectrophotometer. The spectrophotometers gave results that were indistinguishable and the Cary results were used for the time zero analysis. Absorption and fluorescence spectra are shown in figure 3.3, and tabulated in table 3.2. Fluorescence spectra were collected on a home built fluorescence spectrofluorometer [31] and an AVIV ATF105 spectrofluorometer. Results varied with the spectrofluorometer used and the results that were closest to those given by Maroncelli [24] were used. The spectra were fit to lognormals and the first moment frequencies determined.

C. Time Zero Analysis

The parameters for time zero analysis are given in table 3.1. The parameters δ and σ indicate the shift and variance of the gaussian function $\rho(\delta,\sigma)$ which when convoluted with the nonpolar absorption spectrum give the polar absorption spectrum. The time zero first moment fluorescence frequencies also listed in table 3.1. The time zero spectra were determined using the method described in detail in the Introduction.

D. Fluorescence Upconversion

Time dependent Stokes shifts were determined using the fluorescence upconversion technique. Instrument response functions for this set of experiments ranged from 200 to

250 fs. Runs were done in 17fs steps for 2.5 ps and 200 fs steps for 35 ps. The reconstructed time resolved spectra were fitted to lognormal functions and the first moment frequencies used for determining SRF's. SRF's were easily fitted to both three exponential and to stretched exponential fits, no preference was discernable.

Table 3.1 Time-zero results for benzene-acetonitrile mixtures.

X Benzene	Time zero fm (cm^{-1})	δ (dm^{-1})	σ (dm^{-1})	FWHM (cm^{-1})
1.0	21400	93	46	3074
0.95	21260	109	51	3265
0.80	21056	132	58	3327
0.50	20931	147	69	3284

Table 3.2 Steady-state spectra results benzene-acetonitrile mixtures

X benzene	Fluorescence fm (cm^{-1})	Fluorescence FWHM (cm^{-1})	Absorption fm (cm^{-1})	Absorption FWHM (cm^{-1})
1.0	20582	3433	24374	4278
0.95	20245	3434	24223	4397
0.80	19786	3395	24002	4498
0.50	19426	3346	23887	4682

figure 3.3a

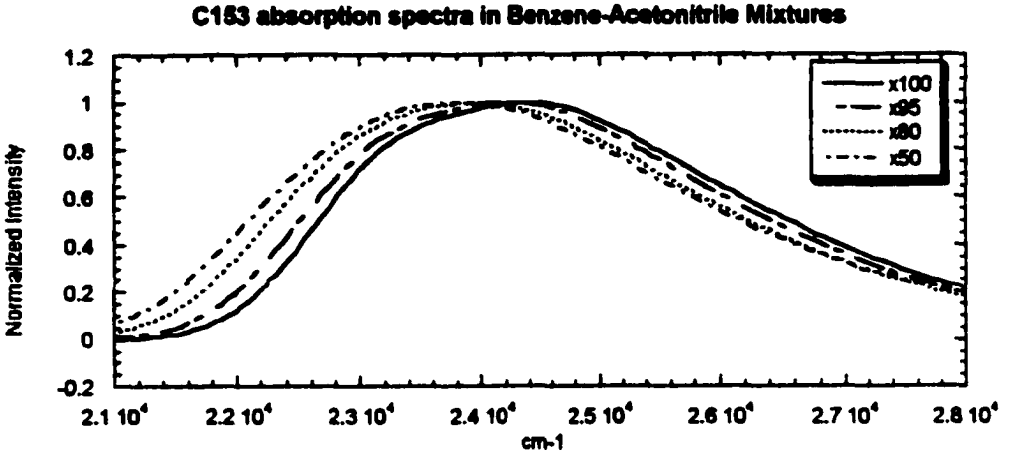

figure 3.3b

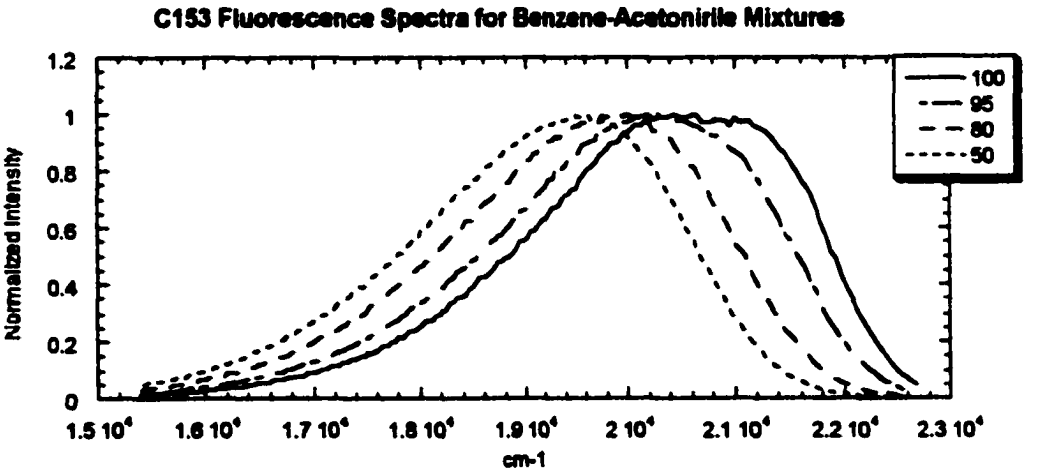

Figure 3.3 Steady-state spectra for benzene-acetonitrile mixtures
a) Absorption frequencies for benzene-acetonitrile mixtures.
b) Fluorescence frequencies benzene-acetonitrile mixtures.

III Discussion

The SRF's for benzene-acetonitrile mixtures are shown in figure 3.4. For comparison, the relaxation for pure acetonitrile is reproduced using the values given by Gardecki *et al.* [24]. The relaxation of pure benzene is in good agreement with literature values [21]. The exponential fit parameters for the SRF's are given in table 3.3. Two features are noteworthy. First, the ultrafast response increases with the addition of acetonitrile to benzene. Second the SRF's for $X_b = 0.95$ and 0.80 cross with the SRF for pure benzene. The values for τ_0, $\tau_{1/e}$, $\tau_{stretch}$, and $\langle\tau\rangle$ are also given. The 1/e times are all within 5% of the stretched exponential times, and all SRF's are well represented by stretched exponentials. A perusal of table 3.4 shows that τ_0 and $\tau_{1/e}$ both decrease monotonically with acetonitrile, with a rather large decrease upon the addition of just 5% acetonitrile. The average relaxation time, $\langle\tau\rangle$, shows non-monotonic behavior, increasing with the addition of 5% acetonitrile and then decreasing with further addition of acetonitrile.

A. Steady-State Spectra and Preferential Solvation

Based on the behavior shown above, one of the first logical questions to ask is whether or not preferential solvation of C153 occurs. C153 is equally soluble in both benzene and acetonitrile, therefore there should be no bias based on solubility. However, C153 has a large dipole in both the ground and excited state and it would therefore not be

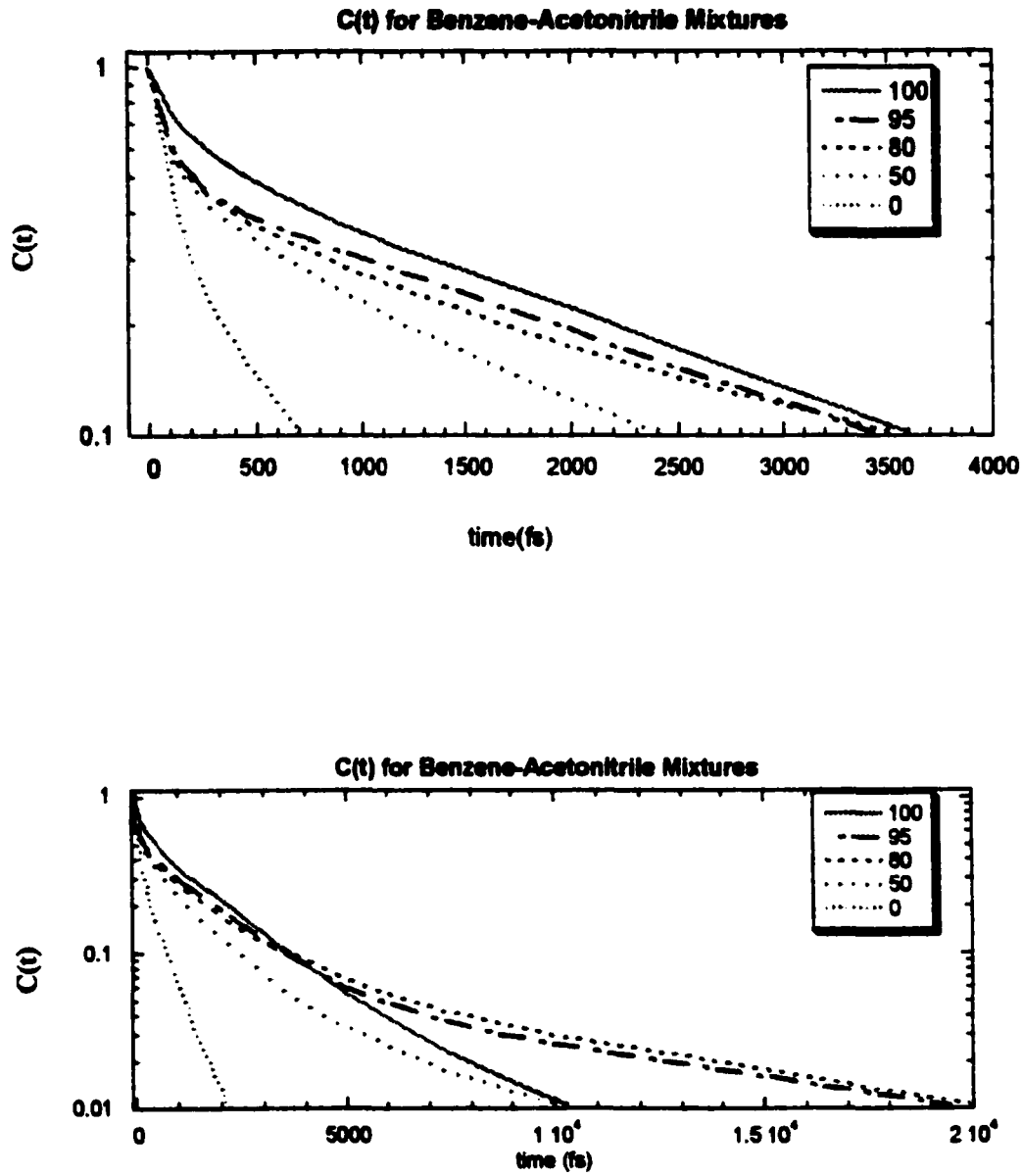

Figure 3.4
C(t)'s for benzene-acetonitrile mixtures. Note semi-log scale, top panel reflects 90 percent of C(t), bottom panel includes additional long time relaxation. Legend gives mole percent benzene.

Table 3.3 C(t) fit parameters benzene-acetonitrile mixtures. Amplitudes (a) and time constants (τ) for three exponential fits of the SRF's are given. Pure acetonitrile two exponential fit is from Gardecki *et al* [24].

X benzene	a1	τ1 (fs)	a2	τ2 (fs)	a3	τ3 (fs)
1.0	0.42	180	0.52	1748	0.06	5168
0.95	0.52	100	0.44	1969	0.04	15018
0.80	0.52	90	0.41	1614	0.07	11035
0.50	0.53	90	0.42	1443	0.05	9584
0.0	0.69	89	0.31	630		

Table 3.4 Relaxation times for benzene-acetonitrile mixtures. Characteristic solvation times and dynamic Stokes shifts are given.

X benzene	τ_0 (fs)	$\tau_{1/e}$ (fs)	$\langle\tau\rangle$ (fs)	stretched τ (fs)	stretched α	$\Delta\nu$ (cm^{-1})
1.0000	381	1253	900	900	0.57	785
0.95000	185	1485	540	549	0.42	987
0.80000	165	1437	475	492	0.41	1236
0.50000	162	923	400	386	0.44	1467
0.0000	120	260	150	164	0.61	2010

surprising if C153 favored acetonitrile. Preferential solvation of the C153 excited state has been seen both experimentally for polar-nonpolar mixtures, and also by simulation for binary mixtures with differing dipole strengths [25,26,27]. Preferential solvation of the excited state of C153 would result in a slow diffusional relaxation as seen in other binary mixtures. With the tendency for acetonitrile to cluster, and the nonpolar nature of benzene, it may be possible for C153 to be integrated into a cluster of acetonitrile molecules resulting in the dramatic decrease in solvation times.

Preferential solvation has been investigated in the literature through non-ideality of the fluorescence spectra [28,29]. The steady-state absorption and fluorescence spectra of C153 in benzene-acetonitrile mixtures are shown in figure 3.3. It is apparent that a rapid red shift occurs in both the absorption and fluorescence of C153 with the addition of a small amount of acetonitrile to benzene. The fluorescence frequencies are plotted versus mole fraction in figure 3.5. It can be seen that strong deviation from ideality occurs in these mixtures, suggesting that acetonitrile may solvate C153 preferentially. This is somewhat misleading though, as the fluorescence fm frequency is more correctly related to the stabilization of the excited state dipole. This has been pointed out by Zarawsky and Scarlata [30] who shows that preferential solvation has been incorrectly predicted based on non-ideality of the fluorescence spectra, and suggest the use of the continuum reaction field based on the static dielectric constant. Swinney *et al.* [31] have evaluated the fluorescence of two proton transfer dyes in acetonitrile-benzene mixtures and determined that there is no preferential solvation based on the linear behavior of the fluorescence maximum versus the

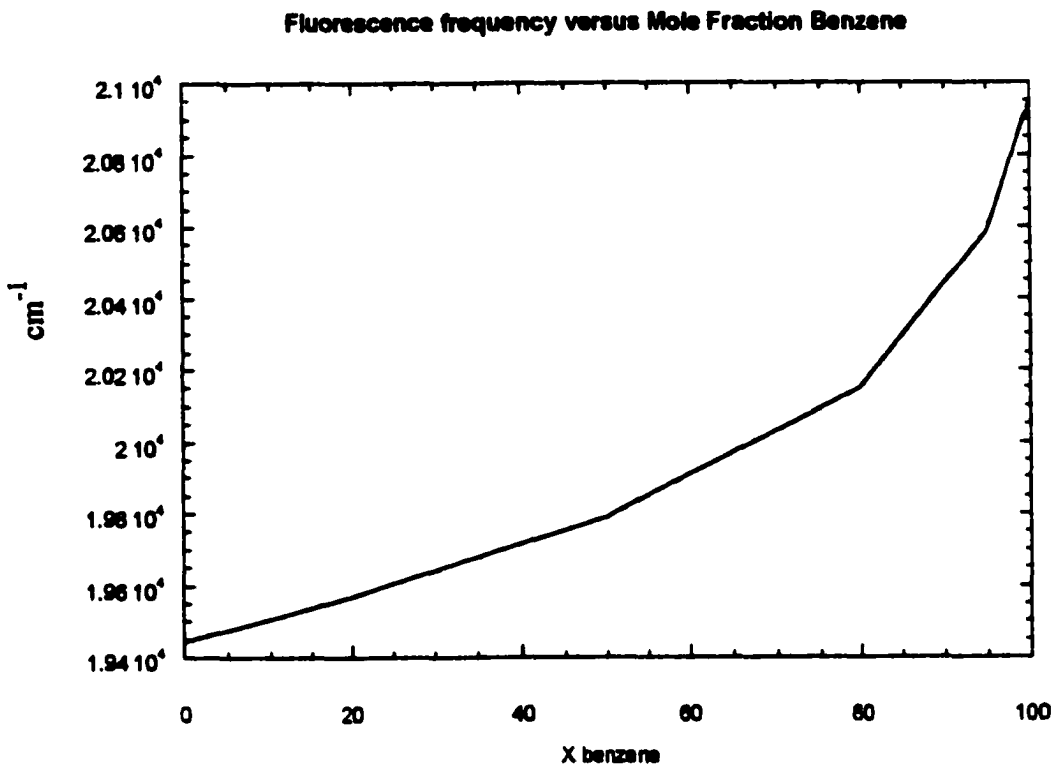

Figure 3.5
Fluorescence frequency (cm^{-1}) versus mole fraction benzene. Note the non-ideal behavior.

reaction field factor,

$$F(\varepsilon) = (\varepsilon - 1)/(2\varepsilon + 1). \qquad 3.1$$

Horng *et al.* [17] find that the fluorescence shifts for C153 are linear with the reaction field

$$F(\varepsilon, n) = [(\varepsilon - 1)/(2\varepsilon + 1)] + [(n^2 - 1)/(n^2 + 2)] \qquad 3.2$$

of Ooshika and Mc Rae [32,33] for a large number of solvents. In equation 3.2 n is the refractive index of the solvent. Figure 3.6 shows the plot the fluorescence maximum versus $F(\varepsilon)$. This plot has only small deviations from a straight line similar to the results of Swinney *et al.* Figure 3.7 shows the plot of the fluorescence maximum versus $F(\varepsilon, n)$. This plot deviates more dramatically than the plot versus $F(\varepsilon)$. The deviations in this plot from ideality follow the same trends as the excess molar volume and may be related to increased and decreased solvent density. Figure 3.8 shows how $F(\varepsilon,\eta)$ varies as a function of ε. This plot shows the non-ideality of $F(\varepsilon,\eta)$ with ε.

Due to the nonpolar nature of benzene the use of continuum reaction fields may be suspect. In fact simulation results show that preferential solvation by acetonitrile indeed occurs at high benzene concentrations [35]. First moment frequencies and FWHM's for absorption and emission are tabulated in table 3.2. It is worth noting that the FWHM's show large increases with the addition of acetonitrile at low mole fractions of acetonitrile.

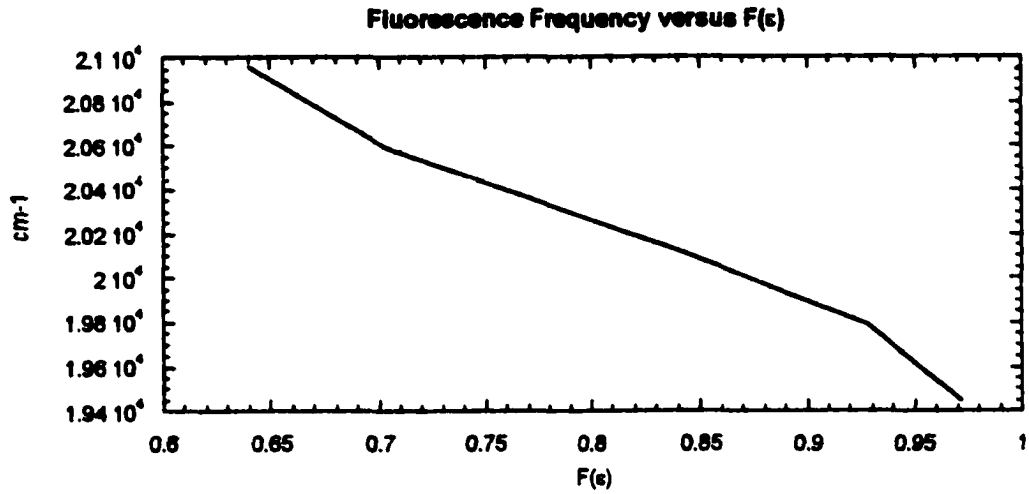

Figure 3.6
Fluorescence frequency versus the continuum reaction field F(ε).

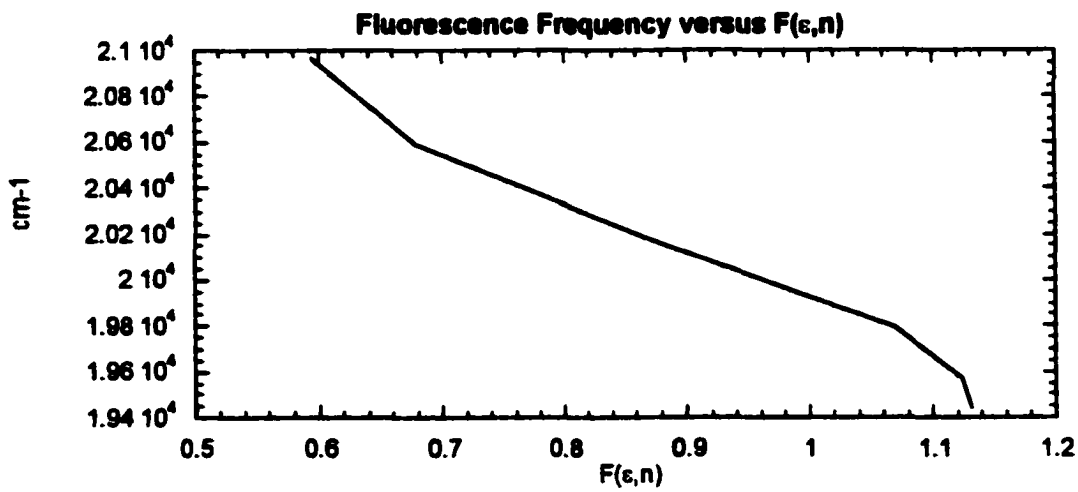

Figure 3.7
Fluorescence frequency versus the continuum reaction field F(ε,n).

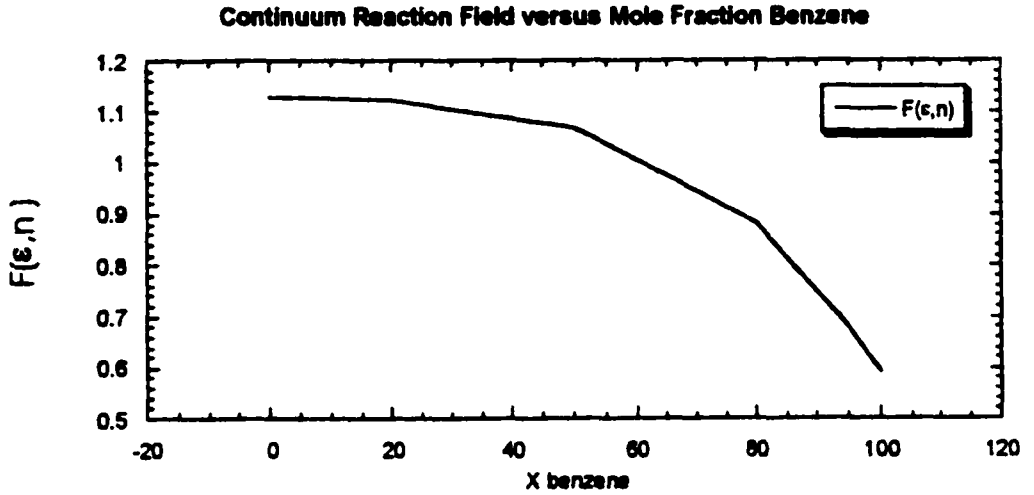

Figure 3.8
Continuum reaction field as a function of mole fraction benzene. See text for definition of F(ε,n).

The FWHM's are smaller in the fluorescence spectra due to the influence of the considerably larger dipole moment of the excited state C153.

B. Ultrafast Relaxation

As discussed in the chapter 2 the instrument response function is ~ 250 fs. Acetonitrile's solvation frequency $\tau_{1/e}$ is ~ 90 fs, therefore the inertial relaxation is missed. The use of time zero analysis allows the SRF to be correctly normalized and aids in predicting the effectiveness of the inertial relaxation. The results of the time zero analysis are given in table 3.1. For the $X_b = 0.50$ and $X_b = 0.80$, the inertial time constants for the SRF's exponential fits were set to 90 fs. Due to the fast inertial response of acetonitrile and the inadequate time resolution, the data can be fit well with time constants as low as 70 fs, but 90 fs was chosen based on the response of pure acetonitrile.

Following the procedure used in the chapter 2 we examine the solvation frequency under the approximation of linear response for a neutral solute, taking into account only solvent rotations [18]. The neglect of translations is less appropriate for quadrupolar solvents, but lends insight into the solvation frequency. If we express the solvation velocity correlation function as G(t), then

$$C(t) = \exp\{-(\tfrac{1}{2} t^2)\ [\,(G(0)_{bz} + G(0)_{acn}) / \langle \delta\Delta E^2 \rangle\,]\,\} \qquad 3.3$$

$$= \exp\{-(\tfrac{1}{2} t^2)\,(1/\langle \delta\Delta E^2 \rangle)\,(\langle \Delta \dot{E}_{bz}^2 \rangle + \langle \Delta \dot{E}_{acn}^2 \rangle)\} \qquad 3.4$$

From equation 3.4 we identify

$$\omega_z^2 = (1/\langle\delta\Delta E^2\rangle)(\langle\Delta \dot{E}_{bz}^2\rangle + \langle\Delta\dot{E}_{acn}^2\rangle) \quad 3.5$$

Considering ion-dipole and ion-quadrupole interactions,

$$E_{ion\text{-}dipole} = \sum_i q(\mu\cdot r_i)/4\pi\varepsilon_0 r_i^3 = q\mu \sum_i \mu_{ir}/4\pi\varepsilon_0 r_i^2 \quad 3.6$$

$$E_{ion\text{-}Qpole} = \sum_i q(r_i\cdot Q\cdot r_i)/4\pi\varepsilon_0 r_i^5 = qQ\sum_i (Q_{ir})/4\pi\varepsilon_0 r_i^3 \quad 3.7$$

$$E_{total} = q\mu \sum_i (\mu_{ir})/4\pi\varepsilon_0 r_i^2 + qQ \sum_i (Q_{ir})/4\pi\varepsilon_0 r_i^3 \quad 3.8$$

where r_i = the center of mass distance between the solute and solvent i, μ is the dipole moment, Q is the quadrupole moment, the angular dependence of $\mu\cdot r_i$ is given by $\mu_{ir} = \cos\theta$, with θ equal to the angle between r_i and μ, and $Q_{ir} = (3\cos^2\theta-1)/2$, and ε_0 is the permittivity of free space. For a neutral solute where $\langle\Delta E\rangle = 0$,

$$\langle\delta\Delta E^2\rangle = \langle\Delta E^2\rangle - \langle\Delta E\rangle^2 = \langle\Delta E^2\rangle \quad 3.9$$

$$= \langle[q\mu\sum_i (\mu_{ir})/4\pi\varepsilon_0 r^2 + qQ\sum_i (Q_{ir})/4\pi\varepsilon_0 r^3]^2\rangle \quad 3.10$$

$$= (q/4\pi\varepsilon_0)^2\langle \mu^2 \sum_i\sum_j (\mu_{ir}\mu_{jr})/(r_i^2 r_j^2) + Q^2\sum_i\sum_j (Q_{ir}Q_{jr})/(r_i^3 r_j^3) + \mu Q\sum_i\sum_j (\mu_{ir}Q_{jr})/(r_i^2 r_j^3)$$

$$+ Q\mu\sum_i\sum_j (Q_{ir}\mu_{jr})/(r_i^3 r_j^2)\rangle \quad 3.11$$

The velocity correlation function includes no correlation of velocities between unlike molecules, so cross terms can be ignored. This yields,

$$\langle \Delta \dot{E}_{0z}^2 \rangle = (q/4\pi\varepsilon_0)^2 \langle \mu^2 \sum_i (\dot{\mu}_{ir})^2/(r_i^4) + Q^2 \sum_i (\dot{Q}_{ir}/dt)^2/(r_i^6) \rangle \qquad 3.12$$

Following the method of Maroncelli *et al.*,[18] we replace $\langle \mu_{ir}^2 \rangle$ and $\langle Q_{ir}^2 \rangle$ with $\langle w_l^2 \rangle$, the average squared rotational frequency in a direction perpendicular to the multipole moment.

$$\omega_s^2 = [\langle \mu^2 \sum_i \langle w_{la}^2 \rangle/(r_i^4) + Q^2 \sum_i \langle w_{lb}^2 \rangle/(r_i^6) \rangle] \; /$$

$$[\langle \mu^2 \sum_i (\mu_{ir})^2/(r_i^4) + Q^2 \sum_i (Q_{ir})^2/(r_i^6) + \mu Q \sum_i \sum_j (\mu_{ir} Q_{jr})/(r_i^2 r_j^3)$$

$$+ Q\mu \sum_i \sum_j (Q_{ir} \mu_{jr})/(r_i^3 r_j^2) \rangle] \qquad 3.13$$

This expression shows the contributions to the solvation frequency explicitly. That is the inertial rotational frequencies of acetonitrile and benzene are weighted by the magnitude of their multipole moments and their respective r dependence. This expression is then normalized by the magnitude of an average fluctuation (given in the denominator). A continuum prediction is not available because the denominator includes terms for a nonpolar solvent. The inertial rotational frequency, $\langle w_l \rangle$, favors acetonitrile ($\langle w_l \rangle$ = 3.14 ps^{-1}), compared to the rotation of benzene perpendicular to the plane ($\langle w_l \rangle$ =2.4 ps^{-1}). Acetonitrile is also favored by its r dependence. This agrees with the experimental results that show an increased inertial response with the addition of acetonitrile. Unfortunately, not

knowing the magnitude of the denominator makes it impossible to predict the magnitude of the solvation frequencies.

C. Diffusional Relaxation

The values for $\tau_{1/e}$ and $\langle\tau\rangle$ versus mole fraction are shown in figure 3.9. The values for $\langle\tau\rangle$ are more strongly influenced by the long time dynamics and display a slight increase with the initial addition of acetonitrile, followed by a decrease with additional acetonitrile. The $\tau_{1/e}$ values show a monotonic decrease as acetonitrile is added.

Unfortunately the usual dependence of the diffusional portion of the SRF on the dielectric relaxation time does not hold here due to the nonpolar nature of benzene. However the acetonitrile response should be well represented by the dielectric relaxation response for acetonitrile in benzene, given by Subramanian *et al* [15] and shown in figure 3.2. The increase in the dielectric relaxation with X_b scales with the mixture viscosity until the acetonitrile clusters begin to break up at $X_b = 0.80$. The breaking of the clusters results in a rapid increase in the dielectric relaxation, which is about twice as fast as neat acetonitrile at $X_b = 0.95$,due to decreased acetonitrile interaction. The pure benzene response is not present, but will likely become slower with acetonitrile addition due to the more compact structure upon mixing [5,6]. Therefore the single particle relaxation times of benzene and acetonitrile will be slower in mixtures, with the exception of acetonitrile at in mixtures over $X_B = 0.80$. Examination of figure 3.8 shows that the addition of a small amount of acetonitrile to benzene results in a large change in $\tau_{1/e}$. This is consistent with acetonitrile's fast inertial response. The increases in $\langle\tau\rangle$ for high benzene concentrations

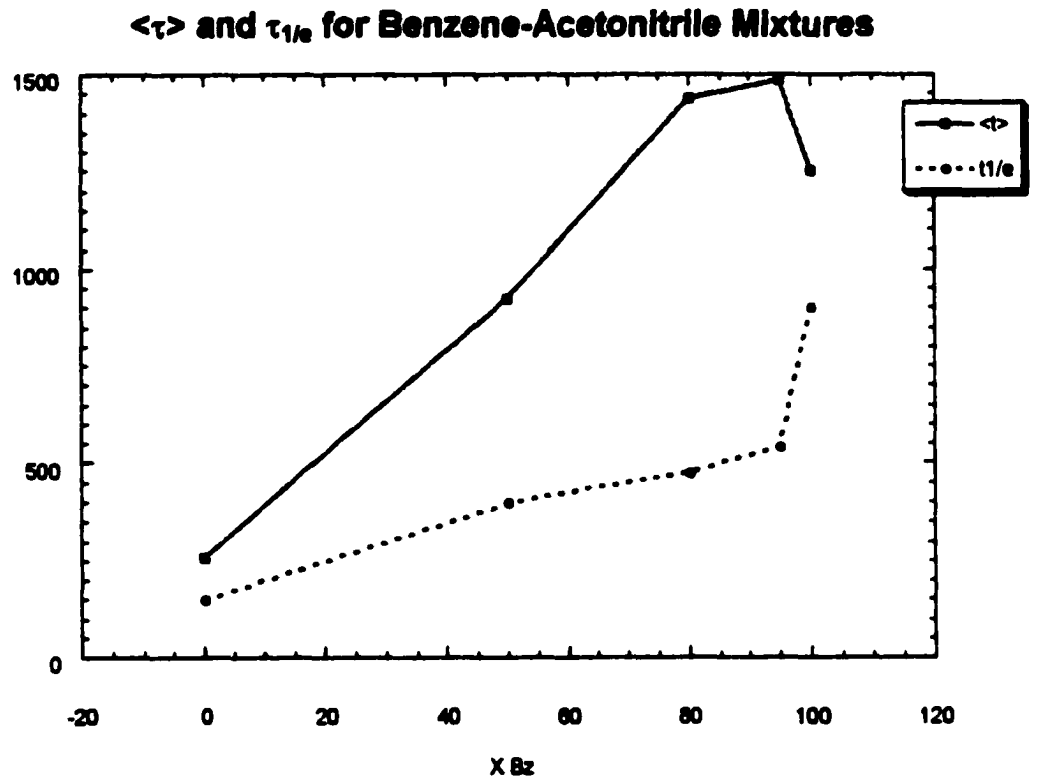

Figure 3.9
Average and 1/e times for benzene-acetonitrile mixtures from table 3.2

are consistent with the slowing of the benzene response, and with acetonitrile translational diffusion (preferential solvation) [35].

Within linear response the SRF for the benzene- acetonitrile mixture is given by

$$C(t) = (1/\langle\delta\Delta E^2\rangle)\{\langle\delta\Delta E(0)\delta\Delta E(t)\rangle_{bzs} + \langle\delta\Delta E(0)\delta\Delta E(t)\rangle_{acns} + \langle\delta\Delta E(0)\delta\Delta E(t)\rangle_{bzp} + \langle\delta\Delta E(0)\delta\Delta E(t)\rangle_{acnp} + \langle\delta\Delta E(0)\delta\Delta E(t)\rangle_{bz\text{-}acn} + \langle\delta\Delta E(0)\delta\Delta E(t)\rangle_{acn\text{-}bz}\} \quad 3.14$$

$$= (1/\langle\delta\Delta E^2\rangle)\{\text{term } b^s + \text{term } a^s + \text{term } b^p + \text{term } a^p + \text{term } x^1 + \text{term } x^2\} \quad 3.15$$

$$\langle\delta\Delta E\rangle = \Delta E - \langle\Delta E\rangle, \quad \Delta E = \Sigma\, \Delta w_{0j} \quad 3.16$$

where the s and p subscripts refer to single and pair contributions respectively, Δw_{0j} is the solute-solvent interaction for solvent j. From the above equations, it is apparent that the SRF is a sum over all solvent molecules, and therefore the time correlation functions are double summations. For a mixture, this results in a total of six terms for the overall time correlation function, two single particle terms and the four pair functions. When the SRF is analyzed in this fashion the result is positive single particle terms and negative pair terms. The size of the negative pair contributions, and their effectiveness in canceling the single particle terms reflects the degree of solvent-solvent correlations. Analysis of the acetonitrile SRF in this manner shows that the pair cancellation is very effective [19]. Benzene has not been analyzed in this fashion, but the quadrupolar solvent CO_2 has [19].

The results show that pair cancellation is very important and substantial even for this nonpolar solvent, but the effectiveness of the cancellation is much smaller than for acetonitrile. It should be noted that the structural correlations are larger for benzene than for CO_2 in simulations of the longitudinal charge density relaxation.

Not knowing the values of the terms in equation 3.14 prevents an evaluation of the acetonitrile versus benzene contributions. However, the addition of acetonitrile to benzene will likely increase the degree of solvent correlations and therefore increase the magnitude of cancellation for the mixture. This is due to the longer ranged dipole interactions of acetonitrile. This would be consistent with the experimental results for $\tau_{1/e}$ shown in figure 3.8. On the other hand, the increases in $\langle\tau\rangle$ at low acetonitrile concentration is less obvious. Simulation results show this to be related to translational diffusion of acetonitrile towards the solute [35], which is consistent with other experiments on polar-nonpolar mixtures [26].

IV Summary and Conclusions

This chapter has presented SRF's for benzene-acetonitrile mixtures. To our knowledge this is the first investigation of the solvation dynamics of a quadrupole-dipole mixture. The SRF's show interesting behavior in that the 1/e times show a rapid decrease with the initial addition of acetonitrile to benzene, while $\langle\tau\rangle$ increases with the addition of small amounts of acetonitrile. The results have been described in terms of the solvation frequency and the diffusive response.

For the inertial response the solvation frequency is of interest. For these mixtures the solute-solvent interaction energies for the dipolar and quadrupolar solvents favor the dipolar solute. The contribution to the solvation frequency from each solvent is

proportional to its inertial rotational frequency, which again favors the dipolar solvent, acetonitrile.

The diffusive response is more complicated involving two single particle terms, and four pair terms. The SRF is very sensitive to the partial cancellation of the single particle and pair terms, with effective cancellation resulting in faster decays of the SRF. The cancellation is most effective for solvents where solvent-solvent correlations are large. The diffusive response is therefore a complicated combination of terms. These terms differ in their r dependence, their interaction energies, the degree of correlation between the particles in the double summation, and their rates of decay. This makes analysis of the SRF in terms of individual contributions difficult. The addition of acetonitrile to benzene involves the addition of a solvent with a faster single particle relaxation and more effective pair cancellation. Acetonitrile may also increase the effectiveness of the pair cancellation in the mixtures by introducing longer ranged solvent-solvent correlations in benzene, as well as acetonitrile-benzene correlations. On the other hand, the addition of benzene to acetonitrile will result in the addition of a slower single particle response, and a decrease in the very effective pair cancellation of acetonitrile.

The solvation dynamics of quadrupole-dipole mixtures are therefore strongly effected by the differences in interaction energies, and relaxation rates of the individual components. At the same time the nature of the SRF is very sensitive to cancellation effects, which are sensitive to the nature of the mixture. Finally the presence of translational diffusion can affect the average relaxation times substantially.

References for Chapter 3

1. M. Barrow, Acta. Crystallogr. B. 37, 2239 (1981).
2. J. Reimers, L. Hall, J. Am. Chem. Soc. 121, 3730 (1999)
3. G. Smith, and R. Jaffe, J. Phys. Chem, 100, 9624 (1996).
4. S. Miyanaga, K. Tamura, and S. Mura Kami, J. Thermal. Analysis, 38, 1767 (1992).
5. A. Colin, S. Concho, R. Rubio, and A. Compostizo, J. Phys. Chem. 97, 10796 (1993).
6. P. Torongey, T. Ramanjappa, and N. Murthy, Ind. J. Pure and Applied Phys. 36, 26 (1998).
7. W. Schneidier, Can. J. Chem. 66, 2653 (1962).
8. R. Yadava, and S. Yadava, Revue Roumaine de Chimie, 36, 11 (1991).
9. P. Mosier-Boss, and A. Popov, J. Am. Chem. Soc. 107, 6168 (1985).
10. K Jackowski, J. Mol. Liqs. 45, 109 (1990).
11. M. Evans, J. Mol. Liqs. 25, 149 (1988)
12. E. Knozinger, D. Leutloff, and R. Wittenbeck, J. Mol. Structure, 60, 115 (1980).
13. A. A. Stolov, D. I. Kamalova, M. D. Borisover and B.N. Solomonov, Spectrochemica Acta 50A, 145(1994)
14. A. Laaksonen, P. Stilbs, and R. Wasylishen, J. Chem. Phys. 108, 455 (1998).
15. V. Subramanian, B. Bellubbi, and J. Sobhandri, Prama, 41, 9 (1993).
16. B. Tiffon, B. Ancian, and J. E. Dubois, J.Chem. Phys. 74, 6981 (1981)

17. M. L. Horng, J. A. Gardecki, A. Papazyan, and M. Maroncelli, J. Phys. Chem. 99, 17311 (1995).

18. M. Maroncelli, V. Kumar, and A. Papazayan, J. Phys. Chem. 97, 13 (1993).

19. B. M. Ladanyi, *Electron Transfer in Condensed Media*, edited by A. A. Kornyshev, M. Tosi, and J. Ulstrup (World Scientific, Singapore, 1997).

20. B.M.Ladanyi, R. Stratt, J. Phys. Chem. 99, 2502, (1995)

21. J. Gardecki, M. Horng, A. Papazyan, and M. Maroncelli, J. Mol. Liqs. 65-6, 48 (1995).

22. L. Reynolds, J. Gardecki, S. Frankland, M. Horng, and M. Maroncelli, J. Phys. Chem. 100, 10337 (1996).

23. B. C. Perng, and B. M. Ladanyi, J. Chem. Phys. 110, 6389 (1999).

24. J. A. Gardecki, and M. Maroncelli, Chem. Phys. Lett. 301, 571 (1999).

25. N. Petrov, A. Wiessner, and H. Staerk, J. Chem. Phys. 108, 2326 (1998).

26. F. Cichos, A. Willert, U. Rempel, and C. von Borczyshowski, J. Chem Phys. 108, 2326 (1998).

27. T. J. F. Day, and G. N. Patey, J. Chem. Phys. 106, 2782 (1997).

28. W. Acree, S. Tucker, and D. Wilkins, J. Phys. Chem. 97, 11199 (1993).

29. A. Chandra, and B. Bagchi, J. Chem. Phys. 94, 8367 (1991).

30. W. Zarawsky, and S. Scarlata, Photochemistry and Photobiology, 60, 343 (1994).

31. T. Swinney, and D. Kelly, J. Chem. Phys. 99, 211 (1993).

32. Y. J. Ooshika, J. Phys. Soc. Jpn. 9, 594 (1954).

33. E. G. McRae, J. Phys. Chem. 61, 562 (1957).

34. M. Skaf, and B. M. Ladanyi, J. Phys. Chem. 100, 18258 (1996).

35. B.M. Ladanyi private communication.